Assessing Chemokine Delivery Strategies for Neural Regenerative Medicine

by

Kassondra Nicole Hickey

A Dissertation Presented in Partial Fulfillment
of the Requirements for the Degree
Doctor of Philosophy

Approved November 2021 by the
Graduate Supervisory Committee:

Sarah Stabenfeldt, Chair
Julianne Holloway
David Brafman
Michael Caplan
Jason Newbern

ARIZONA STATE UNIVERSITY

December 2021

ABSTRACT

Annually, approximately 1.7 million people suffer a traumatic brain injury (TBI) in the United States. After initial insult, a TBI persists as a series of molecular and cellular events that lead to cognitive and motor deficits which have no treatment. In addition, the injured brain activates the regenerative niches of the adult brain presumably to reduce damage. The subventricular zone (SVZ) niche contains neural progenitor cells (NPCs) that generate astrocytes, oligodendrocyte, and neuroblasts. Following TBI, the injury microenvironment secretes signaling molecules like stromal cell derived factor-1a (SDF-1a). SDF-1a gradients from the injury contribute to the redirection of neuroblasts from the SVZ towards the lesion which may differentiate into neurons and integrate into existing circuitry. This repair mechanism is transient and does not lead to complete recovery of damaged tissue. Further, the mechanism by which SDF-1a gradients reach SVZ cells is not fully understood.

To prolong NPC recruitment to the injured brain, exogenous SDF-1a delivery strategies have been employed. Increases in cell recruitment following stroke, spinal cord injury, and TBI have been demonstrated following SDF-1a delivery. Exogenous delivery of SDF-1a is limited by its 28-minute half-life and clearance from the injury microenvironment. Biomaterials-based delivery improves stability of molecules like SDF-1a and offer control of its release.

This dissertation investigates SDF-1a delivery strategies for neural regeneration in three ways: 1) elucidating the mechanisms of spatiotemporal SDF-1a signaling across the brain, 2) developing a tunable biomaterials system for SDF-1a delivery to the brain, 3) investigating SDF-1a delivery on SVZ-derived cell migration following TBI. Using *in vitro*, *in vivo*, and *in silico* analyses, autocrine/paracrine signaling was necessary to produce SDF-1a gradients in the brain. Native cell types engaged in autocrine/paracrine

signaling. A microfluidics device generated injectable hyaluronic-based microgels that released SDF-1a peptide via enzymatic cleavage. Microgels (±SDF-1a peptide) were injected 7 days post-TBI in a mouse model and evaluated for NPC migration 7 days later using immunohistochemistry. Initial staining suggested complex presence of astrocytes, NPCs, and neuroblasts throughout the frontoparietal cortex.

Advancement of chemokine delivery was demonstrated by uncovering endogenous chemokine propagation in the brain, generating new approaches to maximize chemokine-based neural regeneration.

DEDICATION

In loving memory of Joshua Edward Norman. Thank you for your never-ending support and encouragement. I'll never forget the lessons you taught me and the way you helped me be a better person.

"Friends stay side by side,
In life and death you've always stole my heart,
You've always meant so much to me, it's hard to believe this."
-Bayside "Winter"

ACKNOWLEDGMENTS

I would first like to thank my advisor Sarah Stabenfeldt for pushing me to be the best I can be and for allowing me to pursue so many opportunities within the scientific community. I appreciate the significant amount of time you gave to answer questions, give feedback, and provide insight. I am stronger both in my scientific abilities and mental fortitude through your mentorship. I would also like to thank my committee, Michael Caplan, Jason Newbern, Julianne Holloway, and David Brafman for their support and guidance.

Thank you to the various mentees I've had the opportunity to work with over the years and the hard work and dedication they have given me. I'd like to thank Shannon Grassi for the countless hours spent isolating and culturing cells for this project and your overall support and friendship. I'd like to thank Lydan McLaws for helping in any way I needed during the last push of this project. Thank you to Amanda Witten for the illustrations curated for this research.

Thank you to my fellow graduate students and lab members who always listened to me when I needed an ear and made me laugh when I needed it most.

Thank you to my brother, Alec, for keeping me motivated and laughing throughout this journey. Thank you for the countless hours on the phone checking in on me and encouraging me. The trips you generously took out to Arizona helped provide breaks to look forward to between all the hard work. I appreciate you more than you will ever know.

Thank you to my best friend and partner, Adam, for being by my side no matter how miserable and difficult I was during this process. These years have been some of the hardest to endure but you made it all okay. I am forever grateful for your love and belief in me.

This work would not have been possible without the support and funding of the ARCS foundation, the School of Biological and Health Systems Engineering, and the Graduate and Professional Student Association.

TABLE OF CONTENTS

LIST OF TABLES

LIST OF FIGURES

CHAPTER 1

Goals of this Dissertation

Traumatic brain injury (TBI) is a contributing factor in over 30% of injury related deaths in the United States[1]. Following an initial mechanical insult to the brain, primary and secondary injuries lead to cell death, inflammation, edema, coagulopathy and in turn cognitive and motor disabilities[2, 3]. Simultaneously, the injury also initiates cellular and molecular processes that aim to attenuate the injury and initiate repair[4, 5]. For example, neural progenitor cells (NPCs) residing in the subventricular zone (SVZ) migrate outside of their traditional route to the olfactory bulb and redirect themselves towards TBI lesions via injury-induced chemotactic molecular gradients such as stromal cell-derived factor-1a (SDF-1a; also known as CXCL12)[6, 7]. These SDF-1a driven phenomena may contribute to the repair of damaged tissue as SVZ-derived cells may infiltrate the injury region, differentiate into neurons, and integrate into remaining neural circuitry. However, this endogenic response results in a transient increase in the number of NPCs arriving at the injured tissue, peaking at 3-7 days post-injury in a TBI model[8, 9]. Exogenous delivery of SDF-1a aims to maximize the endogenous repair time course, but efforts have not yet led to complete restoration of the damaged tissue [10, 11]. Therefore, our overarching goal is to promote endogenous NPC migration after TBI via improved SDF-1a delivery strategies.

A major limitation in maximizing the endogenic NPC response to SDF-1a is that the mechanism of SDF-1a gradient propagation across large distances such as the cortex is not fully understood. Limited research has considered the role of autocrine/paracrine signaling on endogenous production of SDF-1a and how this mechanism modulates total SDF-1a levels across brain tissue. Without incorporating the endogenous production and regulation of proteins following their delivery, new delivery strategies may not increase

NPC infiltration to its potential. Therefore, maximizing signal propagation for endogenous NPC repair requires improved knowledge of SDF-1a signaling in the brain. Prior literature on SDF-1a and its receptor CXCR4 elsewhere in the body is known to promote cell invasion due to cell autocrine/paracrine signaling[12, 13]. This gap in knowledge on SDF-1a propagation within the brain is addressed in Specific Aim 1.

Aim 1. Identify and model cellular responses to exogenous SDF-1a

To accomplish Aim 1, we perform a series of *in vivo*, *in vitro*, and *in silico* experiments to establish a model of SDF-1a propagation. We describe these experiments in detail in Chapter 2. Briefly, we assess differences in spatiotemporal SDF-1a signal in brain tissue after administering exogenous SDF-1a via bolus injection or PLGA nanoparticles. We then generate a mathematical model using COMSOL Multiphysics® that recapitulates the SDF-1a spatiotemporal patterns observed *in vivo*. The model determined that autocrine/paracrine signaling dynamics were required to generate the signal pattern from the *in vivo* trends. We then asked which cells within brain tissue participate in SDF-1a autocrine/paracrine signaling. To test this, we perform *in vitro* experiments to determine if astrocytes, endothelial cells, or microglia engage in SDF-1a autocrine/paracrine signaling. By using RT-qPCR, we measure upregulation of SDF-1a and CXCR4 following exposure to exogenous SDF-1a. By determining cell engagement in SDF-1a autocrine/paracrine signaling, we may better use this innate tool to maximize SDF-1a spatiotemporal presence and therefore NPC recruitment and TBI repair. In addition, our mathematical model may be used by the scientific community to test hypotheses regarding exogenous SDF-1a delivery and SDF-1a/CXCR4 signal propagation.

In Chapter 2, we detail the contribution of autocrine/paracrine signaling to SDF-1a signal propagation. Autocrine/paracrine loops are precisely regulated by cells, where

threshold amounts of molecules are required to start the signal propagation, yet large amounts may prevent further signaling through downregulation of receptors[14]. Taking this into consideration, a tunable SDF-1a delivery system would allow for tailored release that may overcome the short half-life of SDF-1a and CXCR4 desensitization. Further, a tunable delivery system allows for more complicated release (i.e., pulsatile) to be achieved to work in conjunction with autocrine/paracrine dynamics. Current neural protein delivery strategies with traditional polyester cores have drawbacks due to inciting inflammation and mechanical mismatch with native brain tissue. Hydrogels provide increased tissue compatibility and a large range of tunable features such as stiffness, loading capacity, degradation, and release profile. The native extracellular matrix component hyaluronic acid (HA) has been used extensively in the nervous system and can be chemically modified with high precision to achieve target drug release profiles[15–17]. When HA is functionalized with norbornene groups and reacted with di-thiols, the resulting hydrogel is non-toxic and can be tuned precisely for drug release. HA has been noted as one of the key components of the tissue regeneration process and has been shown to modulate inflammation, cellular migration, and angiogenesis[18]. Beyond innate regenerative properties, HA can be chemically modified with functional groups to tether molecules with high specificity. Another approach to control delivery of therapeutic molecules is injury-induced release mechanisms. Matrix metalloproteinases (MMPs) are known to be upregulated following traumatic brain injury and can serve as a cleavage domain for drug release[19, 20]. Coupling these technologies together may allow for sustained drug delivery and elimination of adverse effects incited by alternative materials. To examine tailored SDF-1a release in a TBI environment, we generated Specific Aim 2 which was divided into two Sub-Aims.

Aim 2.1. Develop a customizable HA microgel platform for SDF-1a delivery

To accomplish Aim 2.1, we develop a microgel drug delivery platform using microfluidics that builds upon the SDF-1a signaling kinetics elucidated in the previous chapter. In Chapter 3, we use a microfluidic system to create monodisperse microgels that overcome particle size variation found in bulk methods. In addition, we create microgels that can be designed for specific size, stiffness, and drug release kinetics. We use soft lithography to create flow focusing microfluidic devices that produce uniform microgels from polymer precursor solution. We use norbornene-modified hyaluronic acid (NorHA) polymer due to its high biocompatibility and ability to precisely tether bioactive molecules. We incorporate a truncated SDF-1a peptide that has been shown to incite a migratory response in NPCs and allows for further modification to extend the release duration.[21] To aid in longer release, we add a cysteine modified MMP cleavable domain to the SDF-1a peptide. This domain (VPMSMRGG) was chosen for the sensitivity it has for both MMP-2 and MMP-9, both which are upregulated following TBI.[19, 22] We then characterize the chemical and physical properties of the microgel delivery system and validate the function of the system to deliver SDF-1a peptide in response to MMPs. This microgel system provides a customizable platform for small molecule delivery that can be adjusted to interventions throughout the CNS and beyond. To test the application of our microgel system *in vivo*, we identify Specific Aim 2.2.

Aim 2.2. Assess migration of NPCs in vivo with SDF-1a release

In Chapter 3, we test the application of the SDF-1a microgels in a TBI model. We hypothesize that SDF-1a microgels will enhance the migratory response of NPCs compared to control groups (blank microgels, vehicle, naïve). We first created NorHA microgels to release SDF-1a peptide following exposure to the TBI microenvironment

using a MMP cleavable domain. Since NPC migration peaks 7 days post-injury in TBI models and exogenous SDF-1a delivery kicks off autocrine/paracrine signaling, we delivered SDF-1a microgels 7 days post-CCI to restimulate SDF-1a propagation. Injections of either saline, blank microgels, or SDF-1a microgels were made into the perilesional tissue to provide SDF-1a to viable cells near the injury region. Lastly, we assessed recruitment of NPCs and other SVZ-derived cells using immunohistochemistry 14 days post-CCI. Our preliminary data found neuroblast and NPC presence in the corpus callosum and cortical tissue following CCI in all groups examined. We also found a complex astrocyte presence that required further assessment. We determine additional sample processing, immunostaining, and image processing is needed to draw final conclusions. Once thorough analysis is completed, this study will reveal the impact of exogenous SDF-1a peptide on SVZ-derived cell migration 14 days after brain injury. Lastly, Chapter 4 discusses the described work and future implications.

Using Biomaterials to Modulate Chemotactic Signaling for Central Nervous System Repair

K.N. Hickey, S.E. Stabenfeldt

Presented as published in *Biomedical Materials*. 2018; 13(4): 044106. DOI: 10.1088/1748-605X/aaad82.

Chemotaxis enables cellular communication and movement within the body. This review focuses on exploiting chemotaxis as a tool for repair of the central nervous system (CNS) damaged from injury and/or degenerative diseases. Chemokines and factors alone may initiate repair following CNS injury/disease, but exogenous administration may enhance repair and promote regeneration. This review will discuss critical chemotactic molecules and factors that may promote neural regeneration. Additionally, this review highlights

how biomaterials can impact the presentation and delivery of chemokines and growth factors to alter the regenerative response.

Chemotaxis: Basic Overview

Dating back to 1891, Theodor Leber first observed the prominent leukocyte migration from the blood vessels in response to certain chemical substances. These seminal experiments discovered active, directed leukocyte migration through the vasculature towards the location where certain chemical substances were introduced [23]. For example, rabbits exposure to mercury at finite locations intravascularly yielded infiltration of leukocytes, yet such response was completely absent with saline exposures [23]. In a follow-up experiment, researchers injected various chemicals intra-abdominally in frogs and observed selective leukocyte infiltration with alkali albuminate, but not with urea [23]. Leber first coined this selective migration phenomena as chemotaxis [23]. Since these seminal experiments, chemotaxis has been implicated in several biological processes such as inflammation, stem cell recruitment, development, and tumor progression. Admittedly, we cannot cover all aspects of chemotaxis thoroughly and therefore the focus of our review centers on chemotactic cell recruitment in the context of central nervous system (CNS) injury repair. More in-depth overview on other chemotaxis processes can be found in previously published reviews [24–27].

Chemokines, or chemoattractant ligands, are small proteins that bind to G-protein coupled receptors (GPCR; also known as seven-transmembrane domain receptors) and activate the phosphatidylinositol 3-kinase (PIP3) and phospholipase A_2 (PLA_2), or rapamycin complex 2 (TorC2) intracellular signaling pathways to subsequently induce cellular movement [24]. Chemokines are divided into four groups based upon their structure. The four groups are named C, CC, CXC, CX_3C. Classification of a specific receptor or ligand is based upon which group or family it belongs followed by the letter L

or R, denoting ligand or receptor, and lastly a unique number [25]. It is important to note that one chemokine receptor may engage different chemotactic ligands, for example CXCL12 binds to both CXCR4 and CXCR7 [25, 26]. The binding of these ligands to their receptors leads to movement via directed cell migration along a chemical concentration gradient. Although not labeled as classic chemokines, neurotrophic factors and growth factors may also employ a gradient mechanism to direct cell migration and thus will be included in this review [27–30]. Cells use temporal and/or spatial sensing to determine a chemical gradient and the direction/location to migrate [31, 32]. Temporal sensing describes the method whereby the cell compares the number of bound receptors over time as the cell moves in any direction. In contrast, spatial sensing utilizes receptors distributed across the cell perimeter and correlates bound receptor location on the cell body to movement in a particular direction [33]. Temporal sensing tells the cell whether or not it is moving with a concentration gradient as it travels while spatial sensing allows for the cell to compare concentrations of ligands around the cell body and have a more directed movement towards the gradient [33]. These mechanisms allow directed cellular recruitment to discrete regions facilitating development, repair, inflammation, or disease processes [31, 34–37].

Engagement of a chemokine ligand with its corresponding GPCR leads to a conformational change and activation of a G protein subunit [34]. Once bound, intracellular signaling cascades induce F-actin polymerization and activation of phosphatidylinositol 3-kinase (PI3K) [35, 37]. The newly created F-actin helps guide PI3K and its products, PIP3, to the cell membrane, or leading edge, of where the chemoattractant has bound [35, 38]. The local accumulation of PIP3 amplifies the chemoattractant signal intracellularly by creating a steep gradient of PI3Ks to one region of the cell based upon the small difference in bound receptors around the cell body [35,

37, 38]. The F-actin concentrated to the leading edge then protrudes and creates a polarized cell [37]. Rho family proteins then tune the migration by controlling protrusion and adhesion of the leading edge, and detachment of the non-leading portions [37]. Ras family proteins are able to initiate a positive feedback loop through PI3K activation directly at the leading edge upon receptor binding and further enhance the PIP3 gradient intracellularly (Fig. 1A) [37]. In addition to this dominate pathway, two other intracellular pathways, TorC2 and PLA_2, elicit cytoskeletal rearrangement and chemotactic cell migration. While additional studies are needed to fully elucidate these pathways, evidence supports the notion that the TorC2 pathway (Fig. 1B) works independently of PIP3, whereas the PLA_2 pathway works in parallel to PIP3 [35, 36]. In summary, the GPCR transmembrane receptor binds chemokines to initiate multiple signaling pathways that result in directed cytoskeletal reorganization in response to a chemotactic gradient.

Chemotaxis in the Central Nervous System.

Chemokine ligands, growth factors, and their receptors are a critical part of the development, maintenance, and repair process of the CNS. Developmental events mediated by chemokine ligand and receptors include formation of the cerebellum [39–41], spinal cord [42], cortical layers [43], and hippocampus [44]. For example, developing cortical interneuron migration is regulated by CXCL12 and receptor CXCR4 [45]. A CXCL12 gradient attracts interneurons to form a migratory stream traveling to the marginal zone (MZ) [45]. In addition, the tangential migration of interneurons out of the MZ and into the appropriate cortical layer during development coincides with the loss of responsiveness to CXCL12 [45]. Exit of interneurons from the MZ can be replicated *in vivo* by elimination of CXCR4 expression on interneurons, suggesting the ligand-receptor interaction strongly regulates interneuron placement [45]. Further

examination of the chemoattractant effects of CXCL12 on interneurons has shown that CXCL12, when ectopically expressed in the cortex during development, leads to the irregular interneuron distribution due to local accumulation at the region of expression [45]. The role of chemotaxis during development is also apparent in other CNS regions. Specifically, secretion of the chemokine CXCL12 by meningeal cells during cerebellar layer development guides neural stem cells to the external granule layer (EGL), while no effect on internal granule cells is observed (Fig. 2A) [40]. This selective response is due to CXCL12 secretion by the meningeal cells in the EGL and homing of neural stem cells expressing the corresponding receptor (CXCR4) while the subpopulation of post-mitotic granule cells that lie below the proliferative region of the EGL do not express CXCR4 and remain in the internal granule cell layer [40]. Further, mice deficient of CXCL12 have abnormal cerebellar layers with reduced thickness of the EGL [39]. Additional studies have suggested that brain derived neurotrophic factor (BDNF) also mediates cerebellar granule cell layer development as migration of cerebellar granule cells out of the EGL is significantly reduced in BDNF knockout mice [41, 46]. Altogether, these developmental events demonstrate the necessity for growth factors and chemokines to direct cellular organization and maturation during development in the CNS.

Secreted factors and chemokines not only attribute to development, but also play a major role in the maintenance of the CNS. For example, the subventricular zone (SVZ) of the adult brain contains progenitor cells that migrate along the rostral migratory stream (RMS) to the olfactory bulb to create new interneurons (Fig. 2B) [47]. While several migratory cues work together to direct the movement of the neural progenitor cells, we will only touch on two prominent molecules as they have direct roles in chemotaxis. In rodents, a concentration gradient of the protein Slit acts as a chemorepulsive, repelling neural progenitor cells from its area of highest concentration,

the SVZ, to the olfactory bulb along the RMS [48]. In addition, vascular endothelial growth factor (VEGF) secretion from the olfactory bulb has been reported as a chemoattractant that further enables homing of neural progenitor cells to the olfactory bulb [49]. The Slit and VEGF directed migration of progenitor cells through the RMS exemplifies the ability chemokines possess in replenishing cells of the CNS. Interestingly, these progenitor cells of the RMS also express CXCR4 and thus are capable of directional migration outside of the RMS in response to the chemotactic ligand, CXCL12 [20, 50]. Neural progenitor populations may be able to respond to other chemokines as Tran et al. reported the expression of multiple chemokine receptors that correspond to CXCL12, CCL25, CCL27, CCL5, and CCL8.[51] As eluded to above, SVZ progenitor cells use similar chemotactic mechanisms to respond to injury-induced chemotactic signals [52]. Gordon et al. used retroviral labeling techniques to eloquently demonstrate that quinolinic acid-induced striatal loss led to an increase in neural progenitor cell proliferation in the SVZ followed by cell migration to the striatum [53]. The migration of SVZ cells to the lesion area was suggested to be due to microglial secretion of CXCL12 and CCL2, as previous studies showed that quinolinic acid upregulated expression in astrocytes [53, 54]. These results are supported by another study, where a cortical lesion led to increased proliferation of SVZ cells and increased expression of CXCL12 near the lesion followed by migration of SVZ cells to the lesion area (Fig 1C) [55]. When CXCR4 was blocked by AMD3100 antagonist, there was a significant reduction in the number of neural progenitor cells that migrated to the lesion alongside astrocytes [55]. Collectively, these examples begin to reveal the critical importance of chemotaxis in the CNS for controlled and coordinated cellular proliferation, migration, and differentiation during development, maintenance, and injury.

In the context of CNS injury or disease processes, many studies have reported transient and insufficient effects of secreted chemokines within an injury or that a diseased microenvironment may inhibit chemotactic repair [53, 55–58]. Therefore, it is not surprising that researchers have turned to tuning chemotactic signaling mechanisms to control the recruitment of cellular players for CNS repair. Here in this review, we will take the opportunity to first highlight discovered chemokines and factors essential for CNS repair. Then, we will discuss biomaterials-based strategies employed to tune different chemotactic signals.

Chemokines for CNS Repair

CXCL12/Stromal Cell Derived Factor-1α (SDF-1α).

CXCL12, SDF-1α, is a chemokine that plays pivotal roles in neural development, induction of stem cells to neuronal fate [59], neural progenitor cell migration [21, 51], initiation of neurite growth and neurogenesis [60, 61], inflammation [62], and cancer cell migration and tumor growth [63]. In the context of CNS injury, CXCL12 is upregulated suggesting a key function in neural repair [56, 60]. Specifically, CXCL12 has been directly correlated to chemotactic migration of neural progenitor cells (NPCs) from neurogenic niches *in vivo* [21, 64]. This chemotactic response has been confirmed with controlled *in vitro* experiments demonstrating that NPCs increase proliferation and chemotaxis in a dose-dependent manner when exposed to CXCL12 gradients [65–67]. Additionally, Barkho et al. reported that CXCL12 significantly increased neuronal and astrocyte differentiation of adult neural progenitor cells *in vitro* [68]. Based on these studies that demonstrate CXCL12 as a potent chemotactic signal, it is not surprising that CXCL12 is a target therapeutic mechanism for promoting CNS repair and regeneration.

Recent therapies utilizing CXCL12 include both direct exogenous delivery of CXCL12 and also exploiting endogenous secretion of CXCL12 within regions of neural

injury as a homing mechanism for transplanted cells. For example, Filippo et al. demonstrated that intracortical administration of an N-terminal CXCL12 peptide increased SVZ neuroblast migration from the SVZ niche towards regions of neural injury following traumatic brain injury in mice [21]. The CXCL12/CXCR4 signaling axis has been used as a homing mechanism for a number of transplantation studies. Our group reported an increased chemotactic response to CXCL12 when neural progenitor cells were transplanted within hyaluronic-acid (HA) hydrogel that increased CXCR4 expression [69]. In a mouse kainic acid seizure model, Hartman et al. demonstrated that there was upregulated CXCL12 in the dentate gyrus. Subsequent, transplantation of CXCR4+ embryonic stem cell derived-neural progenitors (ESNPs) following kainic acid induced seizure led to ESNP migration to the upper blade of the dentate gyrus, a response that was abolished with administration of the CXCR4 antagonist, AMD3100 [70]. Similarly, i*n vivo* studies in CNS injury models (ischemia and traumatic brain injury) have demonstrated that injury-induced upregulation of CXCL12 promotes chemotaxis of transplanted immature cells towards injury sites [56, 71]. Wang et al. found that elevated CXCL12 levels following middle cerebral artery occlusion correlated with migration of transplanted bone marrow stromal cells (BMSCs) to the ischemic penumbra [56]. The role of CXCL12 was confirmed as incubation of the BMSCs with the CXCR4 antagonist, AMD3100, prior to transplantation markedly decreased directed migration to the ischemic penumbra compared to native non-treated BMSCs [56]. These results indicate that chemotaxis promoted by CXCL12 and its receptor is a viable mechanism to increase cell recruitment to injury areas in the CNS.

Beyond endogenous progenitor cell and transplanted stem cell recruitment, CXCL12 also appears to influence angiogenesis *in vivo* [71]. CXCL12 intracortical injection following a brain injury in the rat resulted in increased microvessel density

compared to vehicle injection, which was abolished in the presence of a CXCL12 function blocking antibody [71]. The microvessels in the injury area were both positive for CD34 and CXCR4, suggesting recruitment of immature endothelial cells via CXCL12 [71]. Spatial learning via a Morris water maze and probe trial kept the same trend as the microvessel density assessment, where administration of CXCL12 led to the best outcome and blocking antibody administration, the lowest [71]. Overall, these studies indicate not only that CXCL12 can promote chemotaxis within the CNS during injury, but also exogenous application leads to enhanced functional outcomes.

CCL2/Monocyte Chemoattractant Protein-1 (MCP-1).

CCL2, also known as MCP-1is produced by astrocytes, microglia, and neurons of the CNS under various pathological conditions [58, 72]. Particularly, CCL2 expression increases in astrocytes following traumatic brain injury [73] and spinal cord contusion injury [74]. Previous in vitro characterization of Nestin+ and Notch-2+ neural stem/progenitor cells isolated from the SVZ of adults rats migrate towards CCL2 via expression of CCR2 [58, 75]. The ability of CCL2 to attract SVZ cells has led to the investigation of CCL2 levels and effects after CNS injury. Yan et al. examined the role of CCL2 in recruiting neuroblasts from the SVZ following middle cerebral artery occlusion in rats [58]. Results indicated that increased CCL2 expression in the ipsilateral cortex and striatum within the first 7 days post-injury in concert with increased doublecortin positive (Dcx+) neuroblasts within these regions [58]. This study further probed this chemotactic response by infusing CCL2 into the striatum of injured animals for 7 days via an osmotic minipump [58]. CCL2 treatment markedly increased the number of Dcx+/CCR2+ neuroblasts that migrated to the infused striatum [58]. Moreover, mice deficient for the ligand or receptor significantly reduced the number of cells in the ischemic striatum [58]. This study demonstrated the chemotactic potential of CCL2 with

respect to SVZ cells during injury and highlighted how exogenous administration may enhance the cellular recruitment to sites of injury.

CX3CL1/Fractalkine.

CX3CL1, commonly referred to as fractalkine, is expressed by neurons of the CNS and interacts primarily with CX3CR1 positive microglia and astrocytes [76, 77]. Regionally, fractalkine is expressed most prominently in the cortex, hippocampus, caudate putamen, thalamus, and olfactory bulb [76]. In the context of injury, CX3CL1 is upregulated after stroke [78] and experimental autoimmune encephalomyelitis, suggesting involvement in the injury process [79]. In addition, *in vitro* chemotaxis assays have demonstrated microglia migration towards CX3CL1 in a dose-dependent manner. Due to upregulation during injury and chemotaxis of microglia, the broader chemotactic effect of CX3CL1 on other cells types has been explored. Zhu et al. determined that CX3CL1 directed the migration of human bone marrow stromal cells (hMSCs) to the lesion site of a middle cerebral artery occlusion rat model [80]. Subsequent knockdown of CX3CR1 on hMSCs prior to injection significantly reduced homing to the ischemic penumbra thereby implicated CX3CL1 as a potent cell recruiting tool for CNS repair [80]. Exogenous administration of CX3CL1 to enhance endogenous repair has also been examined following neural injury. Qin et al. administered exogenous CX3CL1 following the middle cerebral artery occlusion in the rat and reported a significant increase in the number of endothelial progenitor cells at the infarct region [81]. Moreover, the measured infarct area and modified neurological severity score were also significantly lower [81]. These studies suggest that CX3CL1 can promote the migration of progenitor cells after injury and enhance repair through supplemental exogenous administration.

Vascular Endothelial Growth Factor (VEGF).

VEGF is a neurotrophic factor that is involved in development, cell proliferation, injury repair, and most notably, angiogenesis [27, 82–85]. Developmental angiogenesis of the RMS is mediated by VEGF secreting astrocytes [86]. Bozoyan et al. illustrated that downregulation of VEGF leads to significant decrease in blood vessel density on the outer border of the RMS (evaluated in P14 mice) [86]. Moreover, VEGF-mediated angiogenesis may also directly impact neurogenesis in neural progenitor cell niches of the CNS [84, 87]. Sun et al. identified a direct relationship between VEGF expression and angiogenesis in the SVZ of the rat brain, but also noted a relationship between VEGF levels and the organization of SVZ neural progenitor cells located in close proximity to blood vessels [87]. Additionally, immature neuronal doublecortin cells of the subgranular zone (SGZ) and SVZ of the rat brain express VEGF receptor 2, suggesting that VEGF stimulation is not solely implicated in angiogenesis and plays a role in the development and organization of the neurogenic niches [84]. As mentioned previously, VEGF does play a chemotactic role in the migration of SVZ cells to the olfactory bulb for neuronal replenishment in rodent models [49]. These migratory effects are not limited to development and maintenance of proliferative CNS niches, but have been examined during CNS injury as well. For instance, Wang et al. evaluated neurogenesis following a middle cerebral artery occlusion induced cerebral ischemia in conjunction with injection of VEGF expressing plasmids in the lateral ventricle of the rat brain. The upregulated expression of VEGF began in the lateral ventricle and traveled to the cortex [82]. The presence of VEGF in these areas significantly reduced infarct volume in the ipsilateral hemisphere and increased the number of proliferative cells in the cortex that ultimately stained positive for immature neuronal markers (Tuj1) two weeks after injury [82]. Although the origin of the increased neuronal population was not determined, this study provides evidence that enhanced VEGF presence in the CNS can increase proliferative

cells near sites of injury. Similar outcomes have been discovered when exogenous VEGF is infused into the lateral ventricle of mice for 7 days after traumatic brain injury [88]. Like the previous study, administration of VEGF in the ventricles led to a significant increase in the number of proliferative cells in the SVZ and the injured cortex compared to vehicle infusion [88]. After 90 days, the TBI lesion volume of mice infused with VEGF was half the volume of the control group, suggesting VEGF had a protective and/or regenerative role [88]. Again, the origin of the cells that were more populated around the injury in the VEGF group and labeled with neuronal marker NeuN, was not determined [88]. The authors however speculate that the elevated population of proliferative cells in the VEGF group across the SVZ, corpus callosum, and injured cortex suggest VEGF may promote migration through white matter to the injured region [88]. The capability of VEGF to incite cell migration *in vitro* combined with the known protective and regenerative effects *in vivo* makes VEGF a factor to be further investigated in the context of CNS repair.

Brain-derived Neurotrophic Factor (BDNF).

BDNF is a neurotrophic factor secreted by neurons and endothelial cells of the brain that has roles in development, maintenance, and injury repair [41, 89, 90]. BDNF is essential for proper development of cerebellar granule cell neurons and like CXCL12, is also needed for proper cerebral granule cell migration to the internal layer through chemotaxis [46]. Furthermore, Bath et al. examined the effects of BDNF haploinsufficient mice by injecting BrdU to track proliferative cells and found a significant reduction in the density of BrdU labeled cells in the olfactory bulb granule cell layer after 28 days, suggesting BDNF haploinsufficient mice may have a reduced chemotactic cue needed for proper migration or survival [91]. BDNF has also been investigated for its role in axon formation in hippocampal neurons, where neurons

secrete BDNF locally to initiate a positive feedback loop to enhance axon growth and differentiation [89]. Outside of these roles, BDNF is a critical chemotactic signal during CNS injury with transient secretion of BDNF from endothelial cells and neurons [90, 92]. Grade et al. labeled SVZ cells prior to induction of ischemia in mice and used time-lapse imaging of *ex vivo* brain slices to measure SVZ progenitor cell migration toward ischemic tissue. The results demonstrated a direct relationship between SVZ progenitor cell migration and BDNF expression from the ischemic tissue as the application of a BDNF scavenging molecule markedly decreased migration relative to the control [92]. Similarly, Cook et al. examined the injection of soluble BDNF compared to BDNF released slowly from an injected hydrogel following induced striatal stroke in mice [93]. Nine weeks after stroke, then number of recruited neuroblasts was significantly increased only when BDNF was released slowly from an injected hydrogel, suggesting BDNF is capable of recruiting neuroblasts to the injury region when presented appropriately [93]. Therefore, it may be beneficial to sustain BDNF in the injury area in order to enhance the functional outcome. Together, these studies suggest BDNF is not only involved in directing developmental migration, but also initiating CNS injury repair and chemotaxis.

Challenges and Biomaterial-Based Opportunities in Chemokine Delivery

While chemokines initiate robust cellular recruitment responses inherently in the body, harnessing that process as a repair tool has proved challenging. Previous studies exploring administration of chemokines have reported transient and insufficient therapeutic outcome [94, 95]. We have highlighted several studies that make use of chemotactic molecules for CNS repair in the section above and in Table 1. Short half-life [96], rapid clearance *in vivo*, proteolytic degradation [97, 98], and receptor internalization [99] all limit the therapeutic potential of delivered chemokines.

Moreover, a better understanding of how the body responds to administration of exogenous chemokines is necessary to elicit desired cellular response for repair and regeneration. This section will focus on the challenges of chemokine and growth factor delivery and how biomaterials-based strategies may address some of these challenges. Although we cannot discuss all biomaterials-based strategies for maximizing chemotaxis and repair, we summarized seminal studies in Table 2 that demonstrate key findings within the field. Finally, we highlight the additional benefits of biomaterials in CNS repair beyond serving as carriers for chemotactic factors.

Half-life and Clearance.

One key limitation in delivering any biological molecule, including chemokines, is the maximizing the bioactivity lifespan. Once delivered, proteins are susceptible to a myriad of degradation and clearance mechanisms, including proteolytic degradation and endocytosis. Together, these processes result in rapid clearance of bioactive chemokines or the loss of bioactivity. For instance, Emerich et al. reported that VEGF bolus administration into the rat striatum had a half-life of about 90 minutes and was not able to be detected between 4-8 hours after injection [100]. Adding further complexities, the injury microenvironment exacerbates degradation with increased expression of proteases from activated inflammatory cells. Proteases break down chemokines via N-terminal processing, which truncates the chemokine and can alter bioactivity (Fig. 3A) [101]. One subset of proteases, matrix metalloproteinases (MMPs), are found throughout the CNS and are markedly elevated following traumatic brain injury, stroke, spinal cord injury, and CNS diseases [102–105]. Adelita et al. reported that MMPs cleave CXCL12, leading to both a loss of chemotactic potential to adult neural stem cells isolated from the mouse SVZs and induction of neural stem cell apoptosis by activating the intrinsic caspase 9 pathway when treated with the truncated form *in vitro* [97]. Moreover, MMPs

actions are not limited to degradation, some MMPs such as MMP-1 are capable of breaking down ligands and producing chemokine receptor antagonists [98]. Serine proteases such as cathepsin G [106] and neutrophil elastase [107] also contribute to cleavage of chemokines. For example, Delgado et al. found that cathepsin G, which is produced by neutrophils and monocytes, was able to cleave CXCL12 thereby eliminating chemotaxis of T lymphocytes *in vitro* [106]. Alternatively, cleavage of certain ligands such as CCL15 and CCL23 by several MMPs can, in fact, increase chemotaxis [108]. While these chemokines are not known to be expressed in the CNS, MMP processing is very potent during CNS injury and should be considered when developing a chemotaxis strategy [108]. From a therapeutic delivery standpoint, one obvious mechanism to compensate for rapid proteolytic breakdown is to deliver a larger amount of the chemoattractant at one time; however, specific gradients are required for optimal effect as chemotaxis often exhibits a biphasic dose-dependent response [21, 59]. For example, Widera et al. examined neural stem cell migration *in vitro* toward a CCL2 gradient and discovered the optimal chemotactic response was at a moderate level of CCL2 both above and below that amount resulted in a much muted chemotactic response [75]. These results have also been demonstrated by our lab with NPCs response to CXCL12 and further suggest optimal chemokine concentration gradients are necessary to produce maximal chemotaxis [67, 109]. The invasive nature of osmotic pumps, the lack of control over bolus delivery combined with the specific concentration gradients required for chemotaxis and their rapid inactivation demands better more controlled delivery mechanisms. Therefore, biomaterials have emerged as a means to sustain controlled therapeutic levels of chemokines in the CNS following injury all the while also preventing and/or protecting chemokines from rapid inactivation and elimination from prominent degradation mechanisms.

Receptor Internalization.

Receptor internalization may decrease the sensitivity of cells to respond to ligand presence. Depending upon the cell type, specific receptor, and surrounding ligand concentration, the internalization half-life of chemokine receptors varies between 10 minutes to 8 hours [110–112]. In addition, different chemokine receptors have different pathways and therefore rates of internalization. For example, CXCR4 is more rapidly internalized when compared to CCR5 due to CCR5 containing fatty acids bound to its cysteine residues [97]. Due to variable receptor half-lives, a single ligand delivery rate may not be beneficial to all chemokine receptors and modification of the release profile may reduce receptor internalization. Ligands bind to their receptor to initiate the signaling pathways associated with chemotaxis. However, overstimulation by ligands may desensitize this process via internalization and lysosomal receptor degradation (Fig. 3B) [29]. Upon ligand binding to receptors, the receptors internalize and may follow a pathway to be either recycled to the surface or degraded [113]. Studies have shown that prolonged exposure time to ligands increases receptor degradation compared to shorter term administration [110, 114]. Studies have also shown that the dose of chemokines and factors significantly impacts receptor presence [29, 110, 112]. For example, Lopez et al. studied ligand induced endocytosis and reported a ligand dose-dependence on the percentage of receptor endocytosis [29]. This study suggests that smaller, controlled amounts of ligand over time may have the ability to reduce receptor internalization and increase intracellular signaling, chemotaxis, and ultimately repair. Biomaterials can generate slow and concentration-controlled release rates that reduce the possibility for receptor overstimulation.

Biomaterials for Altered Presentation and Release of Chemokines

Inherent differences in chemokine half-life, internalization rates, host microenvironment, and pathology-specific demands implies the need to tune delivery systems/approaches for each specific application. Below we outline various approaches that researchers have used to address this need through distinct biomaterials systems. We note that only a handful of neural biomaterial approaches have directly measured chemotaxis as an outcome, therefore the following sections will include seminal biomaterial examples that may serve as platforms for future chemokine delivery systems.

Physical Encapsulation within Biomaterials for Sustained Release.

Many diffusion-based systems have been created to release chemokine over a prolonged period. Hydrogels are a prominent materials approach to encapsulate chemotactic molecules within their porous network [115]. The encapsulated molecules are then free to diffuse throughout the gel matrix to provide a sustained release rather than single bolus injection. The hydrogel composition may be tuned by modifying many different properties (e.g. blends of multiple polymers, varying extents of crosslinking, charged sidechains) to ultimately influence the release rate [116, 117]. Examples of using hydrogel platforms for prolonging chemotactic factor release include an injectable gelatin-hydroxyphenylpropionic acid hydrogel containing polyelectrolyte nanoparticles sequestering CXCL12 [118]. This complex platform prolonged the release such that less than 10% was delivered over 7 days and resulted in significantly enhanced chemotactic *in vitro* migration of adult neural stem cells when compared to CXCL12 alone [118]. In a similar fashion, Silva and Mooney compared bolus delivery of the chemokine VEGF versus VEGF delivered in an injectable alginate hydrogel in an ischemic hindlimb mouse model. The study found that while bolus delivery of VEGF persisted for 72 hours *in vivo*, hydrogel delivery enabled VEGF detection for 15 days leading to significantly increased blood vessel density [119]. This approach has also proved successful for VEGF delivery to

the CNS, where alginate hydrogel sustained levels of VEGF contributed to reduced lesion volume and neurologic impairment score in a rat cerebral ischemia model [100]. While these studies did not measure chemotaxis, the ability for the hydrogel systems to sustain VEGF delivery and lead to increased CNS repair may be applied to future chemotaxis studies. Altogether, these studies highlight the impact hydrogel-based delivery systems can have on preventing rapid clearance of bioactive factors *in vivo* thereby enhancing their therapeutic effect. We emphasized that the optimal hydrogel design varies according to the application as many different gels have shown positive outcomes for different CNS applications. Some studies focus on in situ gelling to allow for hydrogels to fill an irregularly shaped injury cavity [120], while others have developed fast-gelling blends that remain able to be injected due to their shear-thinning properties [121]. Similarly, hydrogel platforms range in composition including chitosan [122], hyaluronan-methylcellulose blends [123], poly(ethylene glycol) diacrylate [124], and agarose [120]. Overall, the simplistic but effective means by which hydrogels sustain molecule delivery *in vivo* lends them to be one of the most well studied biomaterial systems for chemotactic repair.

Nanoparticles and microspheres also enable sustained delivery of chemotactic molecules through diffusion and degradation. The release of chemotactic molecules from biodegradable polyester-based particles differs from hydrogels in that the particles encapsulate the molecules thereby enabling a more complex release profile. Diffusion of the payload molecule through the polymer matrix is followed by degradation of the particle itself, leading to sustained diffusion over a longer period of time [125]. Nanoparticles are desirable for CNS applications due to their size and potential for systemic delivery. For instance, our lab has established the feasibility for systemic nanoparticle delivery to the injured brain following a traumatic brain injury. We found

that 20nm and 40nm nanoparticles crossed a dysfunctional blood-brain-barrier for up to 13 hours after injury (controlled cortical impact mouse model) [126]. Moreover, nano- and microparticles also have facile, minimally invasive local tissue delivery for CNS applications [127]. For example, our lab recently demonstrated significantly increased and sustained presence of CXCL12 when encapsulated within poly(lactic-co-glycolic) acid nanoparticles (PLGA NPs) compared to bolus presentation following intracortical injections in adult mice [127]. Furthermore, this sustained exposure to bioactive CXCL12 lead to upregulation of endogenous CXCL12 expression across the cortex, indicating the presentation of chemokines impacted endogenous chemotactic signaling as shown previously by Enam et al. [124, 127]. Additional examples include Cao and Shoichet demonstrating the release of bioactive nerve growth factor (NGF) from PLGA microspheres up to 91 days [128]. While the sustained release profiles may achieve prolonged delivery windows with polymeric particles, the disadvantages of using biodegradable thermoplastic or elastomeric polymers include low encapsulation efficiency[128] and potential to denature biomolecules during the synthesis process as harsh organic solvents are typically required. To address these shortcomings, recent studies have shifted to composite hydrogel/particle platforms to exploit the positive attributes of each component [129, 130]. For instance, a hyaluronan-methylcellulose hydrogel containing fibroblast growth factor 2 (FGF-2) loaded PLGA NPs stimulated increased blood vessel density in a spinal cord injury model compared to controls [130]. A later study by Khaing et al. used a similar composite delivery system to provide sustained and localized BDNF delivery following spinal cord injury [129]. The study found a significant effect on spinal mediated learning when the composite system was applied [129]. Again, chemotaxis was not directly measured in both of these studies, yet sustained delivery and positive outcomes demonstrate the feasibility of such systems to

enable complex chemokine delivery and enhanced CNS repair. Interestingly, particle-based delivery approaches alone are less common than hydrogels or composites for CNS repair, their utility as a chemotactic delivery tool has been well characterized for other physiologic applications. Huang and Liu demonstrated enhanced migration of mesenchymal stem cells (MSCs) *in vitro* when CXCL12 was delivered via chitosan/tripolyphosphate/fucoidan NPs versus CXCL12 alone [131]. In the same fashion, a study by Popova et al. revealed the effects of chemokine loaded NPs *in vivo* on neutrophil infiltration in the lymph nodes of mice [132]. Poly(N-isopropylacrylamide) NPs loaded with both CXCL8 (interleukin-8) and CCL3 (macrophage inflammatory protein 1-alpha) injected into the footpads of mice [132]. The cell counts of neutrophils in the subcapsular region were significantly higher 24 hours post injection with animals receiving NPs compared to bolus [132]. Altogether, employing a solely particle-based strategy may be sufficient to induce enhanced chemotactic responses in CNS applications.

Electrostatic/Affinity/Immobilization-based Biomaterial Strategies.

Electrostatic, affinity, and immobilization-based biomaterial systems are complementary to physical entrapment strategies for providing sustained release profiles. Such systems deviate from primary physical entrapment to exploit electrostatic or affinity-based interactions to control the adsorption and release of chemotactic molecules [123, 133, 134]. These methods result in high protein loading efficiency, often above 90% [135, 136]. Wang and Irvine created anionic alginate microspheres loaded with cationic CCL21 via electrostatic adsorption that successfully stimulated dose-dependent T-cell chemotaxis [137]. Similarly, Gonçalves et al. examined the ability of chitosan/poly(γ-glutamic acid) films to release CXCL12 through electrostatic adsorption and recruit human MSCs [138]. When CXCL12 was incorporated in between the film

layers or adsorbed to the final film layer MSCs were readily recruited compared to the negative control [138]. These studies demonstrate the feasibility and utility for electrostatic-based delivery to provide sustained chemokine release. More recently, researchers have utilized affinity bound CXCL12 to induce myoblast migration *in vitro* [139]. Specifically, Thakar et al. found that heparin sulfate bound CXCL12 induced myoblast movement at a significantly higher velocity compared to biotin immobilized presentation on a gold-supported oligoethylene glycol surface over 4 hours [139]. A study by Lee et al. found that controlled release of affinity bound nerve growth factor (NGF) resulted in enhanced peripheral nerve regeneration [140]. Although we did not highlight NGF in our section discussing relevant chemokines, NGF reportedly stimulates potent chemotactic migration of spinal neuroblasts [141]. While immobilized presentation did not prove superior to affinity-based in the previous study, other studies have found immobilization successful in promoting chemotaxis [142]. A study by DeLong et al. showed that a polyethylene glycol (PEG) immobilized basic fibroblast growth factor (bFGF) gradient resulted in increased migration of smooth muscle cells, which are known to respond chemotactically to bFGF [142].

Similar to the gradient created by immobilized bFGF in the previous study and endogenous chemotactic gradients, more sophisticated presentation of factors may be necessary to initiate specific cell recruitment. A recent novel approach to mimic endogenous gradient spatial complexities is to employ patterning techniques for immobilizing varying concentrations of factors within a material [143, 144]. Specifically, Wylie et al. developed a three-dimensional protein patterned scaffold that immobilized multiple growth factors using two photon patterning of two complementary peptide binding pairs [143]. A barstar-sonic hedgehog (SHH) fusion protein gradient was patterned into the gel using immobilized barnase and neural progenitor stem cells

(NPSCs) migrated a greater distance into the gradient gel *in vitro* compared to the gel without SHH, showing that the pattern may have initiated movement along the gradient like native migration [143]. In summary, electrostatic, affinity, and immobilization-based biomaterial strategies are capable of inciting chemotaxis and repair in the CNS and may overcome the limited protein loading of other deliver methods. Further, spatially controlled immobilized factors may allow for fine tuning of chemotactic molecule delivery and recapitulation of complex chemokine niches.

Conclusion

Chemotaxis-based repair remains relevant, as it exists as an inherent tool used throughout CNS development, replenishment, and repair. Here we summarized key molecules relevant to CNS repair, the outcome of their direct application during injury, and the limitations that can be addressed through the use of biomaterials. Chemokines and factors have the potent ability to attract transplanted and endogenous immature cells to sites of injury within the CNS, although that is not their only role. It is necessary to consider that while chemokines and factors can be manipulated in favor of CNS repair, chemokines also regulate inflammatory cell migration and cancer progression [63, 145]. The complex involvement of chemokines and factors in homing cells from various microenvironments further illustrates that tuned delivery through biomaterials may help advance chemotactic repair in the CNS by reducing chemokine clearance, creating tailored release profiles, and decreasing ligand induced receptor internalization. Finally, we find biomaterial-based chemokine delivery is an area of CNS regenerative research that has yet to be explored to its full potential.

Figures

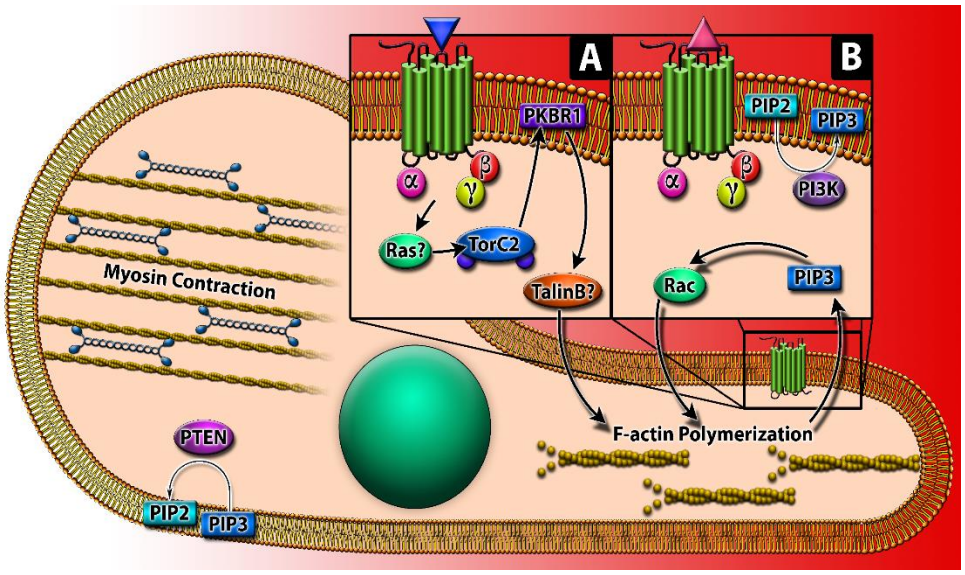

Figure 1.1. Chemotactic Signaling Cascades. The leading edge of a migratory cell (right side) responds to chemotactic molecules initiating intracellular signaling that culminates in F-actin polymerization to protrude the cell towards the source. The trailing edge of the cell (left side) responds with myosin contraction pulling the cell off the substrate with PIP3-phosphatases (PTEN) dephosphorylating PIP3 to PIP2. (A) TorC2 pathway (PI3K independent): A chemotactic ligand binds to the GPCR activating an intermediate G-protein and subsequently the Tor Complex 2 (TorC2). The complex then phosphorylates protein kinase B related kinase (PKBR1) at the membrane leading to phosphorylation of several cytoskeletal proteins including TalinB. (B) The PIP3/PI3K pathway: A chemotactic ligand binds to the GPCR leading to recruitment of PI3K to the membrane. PI3K phosphorylates PIP2 to PIP3, PIP3 then activates Rac initiating F-actin polymerization. The F-actin polymerization stimulates additional recruitment of PIP3 and Rac creating a positive feedback loop at the cell's leading edge.

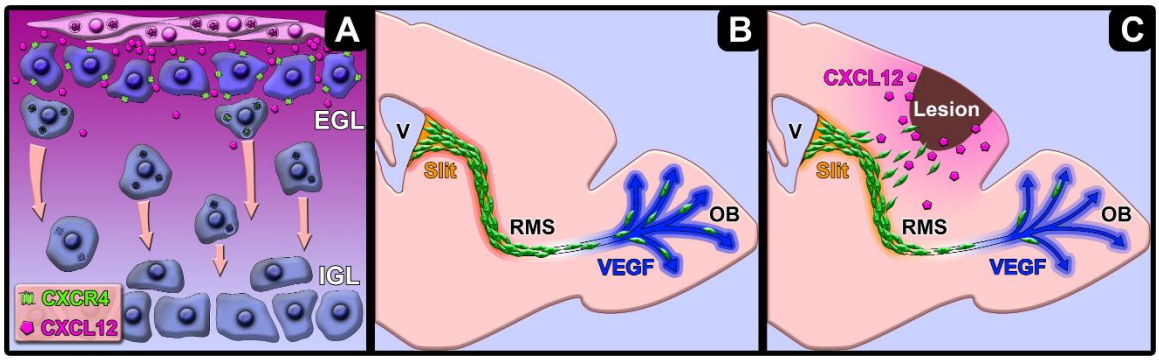

Figure 1.2. Chemotaxis during CNS Development, Replenishment, and Repair. (A) Granule cell migration during development where CXCL12 secretion by the meninges homes CXCR4+ granule cells to the external granule layer (EGL) and CXCR4- cells migrate to the internal granule layer (IGL). (B) Interneuron replenishment to the

olfactory bulb(OB) is mediated by chemorepulsive protein Slit originating from the subventricular zone (SVZ) and VEGF chemoattractant originating from the olfactory bulb, directing immature cells to the olfactory bulb along the rostral migratory stream(RMS). (C) CXCL12 induces CNS repair by local secretion near the cortical lesion, causing directed migration of CXCR4+ SVZ cells to the injury site.

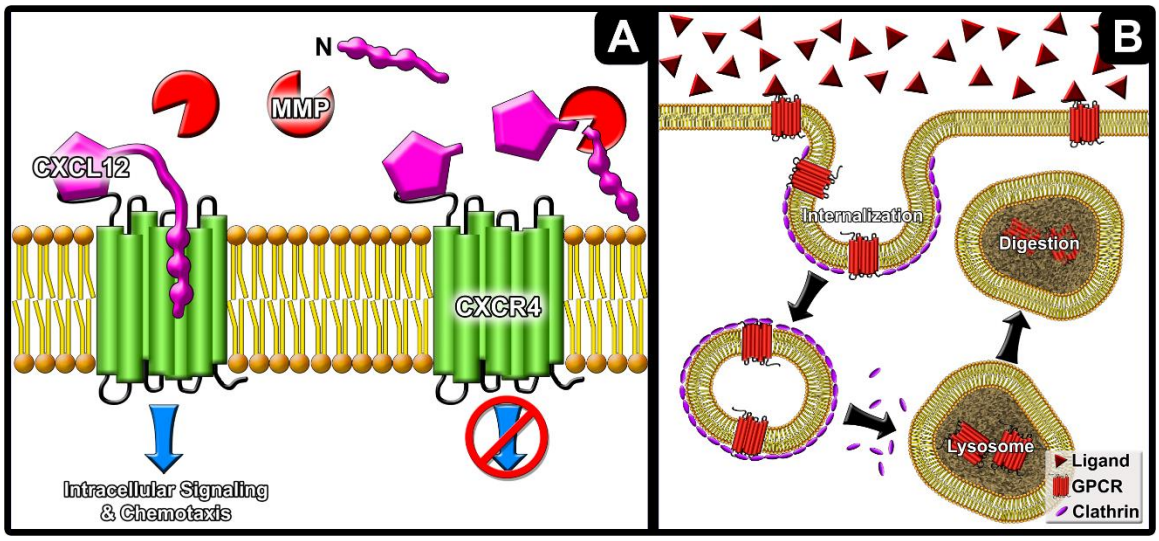

Figure 1.3. Chemokine Inactivation by MMPs and Ligand Induced Receptor Internalization. (A) N-terminal processing by MMPs inactivates CXCL12 by preventing N-terminal binding to CXCR4 and subsequent intracellular signaling. (B) Overstimulation by large concentrations of chemokine ligands induces receptor internalization and degradation.

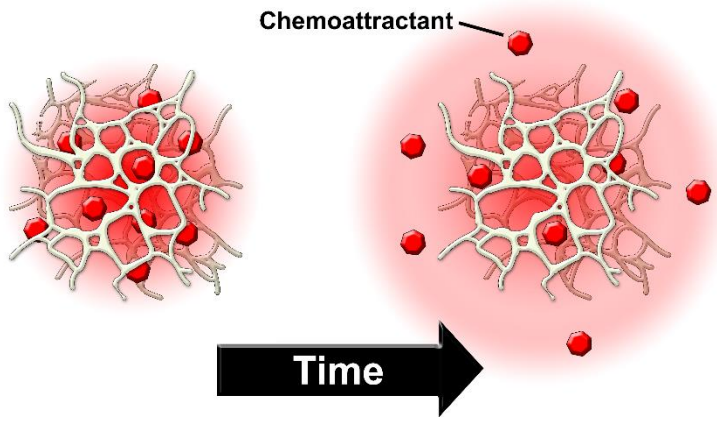

Figure 1.4. Hydrogel releasing chemoattractant sustains delivery over time.

Table 1.1

Chemokine Delivery and Outcomes

Ligand/Factor	Associated Receptor	Delivery Method	Injury Model	Outcomes	Reference
CCL2	CCR2	Striatal infusion for 7 days, osmotic pump	Focal cerebral ischemia, rat	↑Migration of Dcx+ neuroblasts to infusion	[58]
CX3CL1	CX3CR1	Intracerebroventricular injection	Middle cerebral artery occlusion, rat	↓ Infarct Volume ↑Endothelial progenitor cells in infarct area	[81]
VEGF	VEGFR	Intraventricular infusion for 7 days, mini-osmotic pump	Close head traumatic brain injury, mouse	↓ Lesion Volume ↑ SVZ cell migration to lesion	[88]
BDNF	trkB	Transplanted BDNF secreting fibroblasts	Spinal segment lesion, rat	↑ Forelimb usage ↑ Axonal regeneration	[95]
EGF	EGFR	Intraventricular infusion for 7 days, mini-osmotic pump	Lateral fluid percussion brain injury, rat	↑ SVZ cell proliferation at 7 days	[146]
CXCL12	CXCR4	Cortical injection	Lateral fluid percussion brain injury, rat	↑ Increase in microvessel density at 14 days	[71]
VEGF	VEGFR	Bolus injection into subconjunctival space	PNS corneal injury model, mouse	↑ Increase in central & peripheral nerve regeneration	[147]
CXCL12	CXCR4	28-day intrathecal osmotic pump	Spinal cord contusion injury, rat	↑ Motor function test ↑ Number of Neurons	[148]
CXCL12	CXCR4	Intracranial injection	Weight drop traumatic brain injury model	↓ Cerebral edema ↑Cortical cell number	[7]
BDNF	trkB	Intraventricular injection	Streptococcus pneumoniae meningitis	↑ Number of Dcx+ neuroblasts at 14 days	[149]

Table 1.2

Biomaterial Based Approaches to Chemotaxis and Outcomes

Ligand/Factor	Associated Receptor	Delivery Method	Injury Model	Outcomes	Reference
BDNF	trkB	Hyaluronic acid hydrogel	Focal stroke, mouse	↑ Migrated BrdU/NeuN cells[a]	[93]
BDNF-mimetic	trkB	Nanofibrous scaffold implant	Implant only, rat	↑ Dcx+ neuroblast migration from SVZ to implant	[150]
BDNF	trkB	In situ gelling hydrogel implant	Hemisection, spinal cord injury, rat	↑ Spinal neurofilament intensity	[120]
CXCL12	CXCR4	Injected polymer microspheres	Traumatic brain injury, mouse	↑ Dcx+ neuroblast migration to lesion area[a]	[10]
VEGF	VEGFR	Injected alginate hydrogels	Vessel ligation ischemic hindlimb, mouse	↑Angiogenesis in limbs[a]	[119]
CXCL12	CXCR4	Striatal infusion of polymeric micelles	Focal cerebral ischemia, rat	↑ Number of BrdU/Dcx+ SVZ cells[a] ↑ vWF+ cells in ischemic border[a]	[151]
VEGF	VEGFR	Striatal injection of alginate	Middle cerebral artery occlusion, rat	↓ Motor asymmetry[a] ↓ Neurologic severity score[a] ↓ Lesion volume[a]	[100]
CXCL12	CXCR4	Gelatin-hydroxyphenylpropionic acid hydrogel containing polyelectrolyte complex NPs	Neural Stem Cells[b]	↑ Migration of cells[a]	[118]
CXCL12	CXCR4	Chitosan/tripolyphosphate /fucoidan NPs	Mesenchmyal Stem Cells[b]	↑ Migration of cells[a]	[131]
CXCL8 CCL3	CXCR1 CXCR2 CCR1 CCR4 CCR5	Poly(N-isopropylacrylamide) NPs	Restoration of immune cell chemotaxis, mouse	↑ Migration of neutrophils into lymph nodes[a]	[132]
CCL21	CCR7	Alginate microspheres – electrostatic adsorption	T-Cells[b]	Dose-dependent T-cell migration	[137]
CXCL12	CXCR4	Poly(γ-glutamic acid) to create multilayered films – electrostatic adsorption	Mesenchymal stem cells[b]	↑ Migration of cells	[138]
CXCL12	CXCR4	Poly(lactic-co-glycolic) acid NPs	Traumatic brain injury, mouse	↑ Number of CXCR4+ cells[a] ↑ Endogenous CXCL12 expression	[127]

[a]Increased/decreased compared to bolus delivery
[b]*In vitro* study

CHAPTER 2

Stromal Cell-Derived Factor-1a Autocrine/Paracrine Signaling Contributes to Spatiotemporal Gradients in the Brain

Presented as published in:

Hickey, K, Grassi, S, Caplan, MR, Stabenfeldt, SE. Stromal Cell-Derived Factor-1a Autocrine/Paracrine Signaling Contributes to Spatiotemporal Gradients in the Brain. *Cellular and Molecular Bioengineering*. 2021; 14: 75-87. DOI: 10.1007/s12195-020-00643-y

Stromal cell-derived factor-1a (SDF-1a)/chemokine receptor 4 (CXCR4) is a chemokine/receptor pair responsible for the migration of various cell types[50, 152, 153]. SDF-1a induces migration by binding to its receptor CXCR4. Cells detect gradients of SDF-1a through spatial and temporal sensing of occupied receptors thereby guiding cells along the gradient[33]. For example, neural stem cells (NPCs) migrate large distances towards locally secreted SDF-1a *in vivo* following multiple sclerosis inflammation, hypoxic-ischemic cerebral injury, and traumatic brain injury[6, 57, 154]. However, injury-induced migration is transient where the number of immature cells present in the lesion area drops off around 14 days in a TBI model[9]. We and others are interested in exploiting this signaling cascade via controlled release biomaterial devices to modulate/tune NPC recruitment for maximal regenerative capacity. The mechanism that the SDF-1a/CXCR4 cascade guides cells across large distances is not fully understood, particularly considering that the half-life of SDF-1a is 26 minutes[155]. Therefore, understanding how SDF-1a chemotactic gradients are created in complex tissue microenvironments is critical for successful drug carrier designs.

One mechanism cells use to generate far-reaching chemotactic gradients is autocrine/paracrine signaling[12, 13, 156, 157]. This cell signaling loop stimulates cells to

secrete additional signal locally and to pass that signal along to neighboring cells who in turn engage in the same process. SDF-1a/CXCR4 autocrine/paracrine signaling contributes to the long-distance migration of numerous cell types outside the central nervous system. For example, metastatic cancer cell migration of skin, breast, and ovarian cancers are dependent upon SDF-1a/CXCR4 autocrine/paracrine signaling[12, 13, 157]. Further, studies are beginning to elucidate the role of SDF-1a autocrine/paracrine signaling in the peripheral nervous system. A recent study by Gao et al. showed that the SDF-1a/CXCR4 autocrine loop promotes Schwann cell migration *in vitro*[156]. Specifically, SDF-1a administration led to significantly increased Schwann cell migration and upregulation of SDF-1a compared to non-treated controls[156]. Therefore, SDF-1a/CXCR4 may act in a similar autocrine/paracrine fashion in the central nervous system to establish chemotactic gradients that contribute NPC migration.

We hypothesize that autocrine/paracrine signaling is a critical component of SDF-1a gradient formation in the brain. We used *in vivo* and *in vitro* signaling assays in combination with *in silico* modeling to elucidate and model the kinetics of SDF-1a propagation following exogenous SDF-1a delivery. In doing so, we may better exploit SDF-1a signal dynamics to control cell recruitment. We addressed our hypothesis in three ways: 1) by comparing different SDF-1a delivery strategies *in vivo* via bolus injection or sustained release nanoparticles (NPs) over 7 days, 2) by investigating SDF-1a autocrine/paracrine signaling *in vitro* through exogenous application of SDF-1a on neural cell cultures and measuring changes in gene expression, 3) by creating a mathematical model to study SDF-1a spatiotemporal dynamics using COMSOL Multiphysics®.

Materials and Methods

Intracortical Injection of AFSDF-1a and AFSDF-1a Loaded NPs.

We fabricated poly(lactic-co-glycolic) acid NPs to deliver SDF-1a using a previously established water/oil/water emulsion technique[109]. Recombinant SDF-1a conjugated with AlexaFluor647 (AFSDF-1a; Almac, Craigavon, United Kingdom) was used for exogenous SDF-1a delivery to distinguish between delivered SDF-1a and total SDF-1a levels. PLGA NPs were fabricated to release approximately 30ng of AFSDF-1a in the first 24 hours followed by 9ng over the next 6 days. To best match this expected release, the bolus injections contained 30ng of AFSDF-1a. All animal procedures were approved by Arizona State University's Institute of Animal Use and Care Committee (IACUC) with previously published protocols[127]. Briefly, 3µL injections were performed centered over 1.5mm anterior of bregma and 1.5mm lateral of midline at a depth of 0.8mm into the cortical tissue of adult CXCR4-EGFP transgenic mice, n = 4-5 animals (kindly donated by Dr. Richard Miller)[127].

Immunohistochemistry and Image Processing.

Immunohistochemistry was used to detect total SDF-1a levels following 1, 3, and 7 days post-injection as previously described[127]. Acute time points were selected based upon both the 26 minute half-life of SDF-1a and the NP burst release of SDF-1a occurring within 24 hours. Animals were euthanized and perfused following specified time points with cold phosphate buffer followed by 4% paraformaldehyde. Brains were extracted and fixed in 4% paraformaldehyde followed by incubation in 30% sucrose. Brains were embedded in OCT and stored at -80°C until cryo-sectioning was performed. 25µm sections were blocked, permeabilized, and incubated with rabbit polyclonal anti-SDF-1a (Abcam, Cambridge, MA) overnight at 4°C followed by a 2 hr incubation with goat anti-Rabbit IgG Alexa Fluor555 (Thermo Fisher Scientific, Waltham, MA) at room temperature. Stained sections were visualized using fluorescence microscopy

(DMI6000B, Leica). Tile scans of each brain slice were prepared for further analysis with consistent acquisition settings. ImageJ (National Institutes of Health, Bethesda, MD) was used to quantify the percent immunopositive area of total SDF-1a (exogenous + endogenous) surrounding the injection. The region of interest quantified was 1200μm on each side of the injection by 1200μm deep. Each image was thresholded using the tissue's contralateral signal, and threshold values were used to calculate the area fraction of SDF-1a positive stain. For each group/time point, 4-5 animals with 3-5 tissue sections per animal were quantified.

Primary Cell Cultures.

Primary glial cell cultures were obtained based on established protocols and in accordance with Arizona State University's IACUC approved protocol[158, 159]. Neonatal CXCR4-EGFP mice (aged P0-P2) were collected, anesthetized, and sacrificed via rapid decapitation. Tail clips were obtained for genotyping. Brains were dissected out in cold Hank's Balanced Salt Solution (HBSS) using super fine forceps and micro dissecting knives. The meninges, cerebellum, and midbrain were removed and both hemispheres from each pup were placed in fresh HBSS at 4°C for temporary storage. Briefly, each tube containing dissected brain hemispheres was triturated 3 times and centrifuged. Supernatant was aspirated and 0.25% Trypsin (0.1% EDTA) was added to each tube and incubated at 37°C for 20 minutes. Equal amounts growth media (Dulbecco's Modified Eagle Medium: Nutrient Mixture F-12 (DMEM/F-12) with 10% Fetal bovine serum (FBS)) were added to neutralize suspensions. Suspensions were then washed, DNAse was added, and tubes were vortexed briefly to break up any large tissue fragments. Cells were washed 2 more times and resuspended in fresh growth media. Suspensions were filtered through a 70μm cell strainer and then plated at a concentration of 1 T75 flasks per hemisphere. Mixed glial cultures were grown for 3 days

before receiving a media change and then allowed to grow for 11 more days without a media change to enrich microglia in the cultures. On day 14, cultures were harvested with trypsin and magnetic bead separation was performed according to manufacturer's instructions for either CD11b (microglia) or Glast (astrocytes) (Miltenyi Biotec, Bergisch Gladbach, Germany).

Reverse Transcription Quantitative Real Time Polymerase Chain Reaction (RT-qPCR).

Sorted primary microglia and astrocyte cultures as well as a bEnd.3 cell line (ATCC CRL-2299, kindly donated by Dr. Rachel Sirianni) were used to evaluate the effects of exogenous SDF-1a application on expression of SDF-1a and CXCR4 (Fig. 2.7). Each cell type was plated in a 6-well plate, n=3-6 for both control and experimental samples for each time point. Exogenous murine recombinant SDF-1a (Peprotech, Rocky Hill, NJ) treated cultures were exposed at 400ng/ml for 30 minute intervals up to 120 minutes. Control cultures were not exposed to SDF-1a. At each time interval after SDF-1a application, media was removed and cells were washed before performing RNA isolation using the RNeasy Plus Kit (Qiagen, Hilden, Germany). Isolated RNA was tested for quality using the Agilent Bioanalyzer and RNA concentration was determined using the Thermo Fisher Scientific Nanodrop. RNA was converted to cDNA (Bio-rad S1000 thermo cycler) using the SuperScript™ IV VILO™ Master Mix (Invitrogen, Carlsbad, CA) and included a reverse transcriptase (RT) negative control. Primers for SDF-1a (forward: 5'-CGCCAGAGCCAACGTCAAGC-3', reverse: 5'-TTCGGGTCAATGCACACTTG-3'), CXCR4 (forward: 5'- CGGTACCTCGCTATTGTCCA-3', reverse: 5'-CTGTCATCCCCCTGACTGA-3'), and GAPDH (reference gene, forward: 5'-AATGTGTCCGTCGTGGATCTG-3', reverse: 5'- CAACCTGGTCCTCAGTGTAGC-3') were designed using the National Center for Biotechnology Information (NCBI) Primer Blast

tool and purchased as custom oligonucleotides (IDT, Newark, NJ). The qPCR reaction was carried out using Luminaris Color HiGreen qPCR Master Mix (Thermo Fisher Scientific, Waltham, MA) on the Analytik Jena Qtower 2.0. The thermal cycling protocol consisted of denaturation at 95°C for 15 seconds, annealing at 60°C for 30 seconds, and extension at 72°C for 30 seconds (40 cycles). Genomic DNA contamination was assessed by using a RT negative control, where acceptable samples had at least 10 quantification cycles (Cq) smaller than the RT negative sample. Primer efficiency was calculated by creating a standard curve. To account for variations in primer efficiencies, the Pfaffl method was used to quantify relative expression ratios between cultures ± SDF-1a[160]. Specificity of the primers was confirmed by running PCR products against a ladder on gels and by confirming single products via the melting profile.

Mathematical Modeling.

Two principle models were created using COMSOL Multiphysics software to reproduce the spatiotemporal patterns of total SDF-1a and CXCR4 from the immunohistochemistry experiments. All models contained three equations describing the mass transport of 3 dilute species: soluble SDF-1a, SDF-1a/CXCR4 complexes, and unbound CXCR4. This transport is governed by the following mass balance equation:

$$\frac{\partial c_i}{\partial t} + \nabla \cdot (-D_i \nabla c_i) = R_i \quad (1)$$

where dc_i/dt represents the accumulation of the species. The diffusive transport of the species is represented by $\nabla \cdot (-D_i \nabla c_i)$ where D_i is the diffusion coefficient and c_i is the concentration of the species. The last term needed is the reaction term, R_i, which is used to model the rate of production and removal of the species. All models used the same 2D geometry that represented a tissue section with a centered injection site. The first model was based upon diffusion only, which assumed that no autocrine/paracrine signaling was taking place. The second model incorporated production of SDF-1a by cells; the

production rate was modeled using Michaelis-Menten kinetics so that SDF-1a production was linearly proportional to the concentration of SDF-1a/CXCR4 complexes when there are few complexes but there is a maximum SDF-1a production rate when there are many complexes. This method has been previously established for modeling autocrine signaling[161]. The reaction term for soluble SDF-1a included this SDF-1a induced production and loss of soluble SDF-1a due to degradation. The reaction term of unbound CXCR4 included a constant basal production rate, an endocytosis rate, association with SDF-1a (as a loss term because then this becomes a complex rather than unbound), and an additional production rate modeled in Michaelis-Menten form based on the number of complexes. The reaction term of SDF-1a/CXCR4 complexes included association of soluble SDF-1a and unbound CXCR4 and loss of complex (to receptor-mediated endocytosis). A detailed outline of model equations and terms can be found in Table 2.1. A corresponding parameter list was generated (Table 2.2) that includes transport properties, Michaelis-Menten constants, and baseline concentration values. For each of the diffusion and autocrine models, 2 sub-models were created: bolus injected SDF-1a and SDF-1a loaded NPs (Fig 2.8). The NP model was created by fitting SDF-1a release data to the Korsmeyer-Peppas equation and taking the derivative to provide the rate of change in SDF-1a over time (Fig 2.9)[162]. All models were computed over the course of 7 days to compare against the experimental data. Cross-section plots were created to visualize the amount of total soluble SDF-1a present over time as computed by each model. These plots were compared against the immunohistochemistry trends.

Sensitivity Analysis.

To examine model sensitivity, we adjusted parameter values for all four models and visualized the output plots for SDF-1a (diffusion and autocrine models) and CXCR4

(autocrine models only). Increases/decreases were made to each parameter value, and results were plotted alongside the results using the original parameter value. Lines representing a 10% increase and 10% decrease in the baseline results were plotted to visualize if the tested parameter values were within a 10% tolerance of the original data. This process was repeated until the changed parameter resulted in plots that fell within 10% of the standard results. Exceptions were used when baseline values were less than 10^{-13} mol/m^3. These values were considered zero and any plots where values fell below this due to parameter changes were also considered zero and acceptable. Amount of change in each parameter value was recorded for each model.

Statistical Analysis.

All quantitative results were analyzed using GraphPad Prism software Version 8.4.3 (GraphPad Software, Inc., La Jolla, CA). Statistical analysis of differences between groups were performed by one-way analysis of variance with Tukey post-hoc testing where $p<0.05$ was considered significant. Logarithmic transformation was performed on the SDF-1a immunopositivity and CXCR4+ cell density data prior to one-way analysis of variance with Tukey post-hoc testing (Fig. 2.1). All data were graphed as the mean ± standard deviation or standard error of the mean.

Results

Sustained SDF-1 immunostaining suggests autocrine/paracrine signaling.

We first studied the impact of exogenous SDF-1a delivery on local SDF-1a and CXCR4 levels via bolus injection or injection of SDF-1a loaded NPs over 7 days, first reported in Dutta et al.[127]. We utilized fluorescent labeled exogenous SDF-1a and compared against total SDF-1a immunostaining to uncover differences that may be attributed to autocrine/paracrine signaling. Here, we focused on the temporal and

spatial trends of total SDF-1a quantification and CXCR4+ cell density following exogenous delivery first identified in our prior publication[127]. Visually, we reported higher levels of total SDF-1a immunostaining and CXCR4+ cell density in the NP group on day 1 than the bolus group (Fig. 2.1). Additionally, the pattern of immunostaining for the NP group on day 1 showed sustained levels across the tissue sections. Quantitation of both total SDF-1a and CXCR4+ surrounding the injection site showed distinct temporal trends between the bolus injected SDF-1a and NP delivered SDF-1a. Levels of total SDF-1a immunopositivity were highest at day 1 and significantly decreased between day 1 and day 7 following bolus SDF-1a delivery (Fig. 2.2a, $p=0.0469$). In contrast, more total SDF-1a was detected in the NP group across all time points and did not exhibit any significant changes over 7 days (Fig. 2.2b). Likewise, CXCR4+ cell density was higher in the NP group than the bolus group, suggesting that the presentation of SDF-1a impacts cell response and potential recruitment (Fig. 2.2). Specifically, significant decreases in CXCR4+ cell density occurred between 1 and 7 days and 3 and 7 days in the bolus group ($p=0.0115$ and $p=0.0067$, respectively) and between 1 and 7 days in the NP group ($p=0.0052$). We then analyzed the total SDF-1a immunopositivity and CXCR4+ density spatially across the 7 days. On day 1, the NP group exhibited near constant levels of both SDF-1a and CXCR4+ density out to 1600μm from the injection site, where the only statistical difference found was between 0-400μm and 1200-1600μm for SDF-1a (Fig. 2.3b, $p=<0.05$). In contrast, the bolus group immunostaining and cell density declined across the tissue on day 1 with significant differences between 0-400μm and all subsequent tissue sections (Fig. 2.3a, $p<0.05$). On day 3, the trends remained the same for both groups where the NP group remained higher and more sustained in both SDF-1a immunostaining and CXCR4+ cell density (Fig. 2.3c,d). By day 7 the SDF-1a area and CXCR4+ cell density diminished for the bolus group (Fig. 2.3e). However, the NP group

exhibited sustained levels to that of day 1 and day 3 immediate to the injection site (Fig. 2.3f). Both the bolus and NP group exhibited significant differences in immunostaining and cell density between the 0-400μm region and all other regions ($p<0.05$). In summary, the NP group showed spatially constant levels of SDF-1a and CXCR4+ cell density on days 1 and 3 whereas the bolus group exhibited a decline.

Brain Microglia, Astrocytes and Endothelial Cells Respond Dynamically to Exogenous SDF-1a in vitro.

To determine whether autocrine/paracrine signaling is induced by SDF-1a in the brain we examined microglia, endothelial cells, and astrocytes response to exogenous SDF-1a. Each cell type responded in a unique, dynamic manner to exogenous SDF-1a stimulation. Microglia expressed higher levels of SDF-1a over the time course but never reached statistical significance perturbation (Fig. 2.4a). Microglia CXCR4 gene expression was significantly different between 30 and 90 minutes, suggesting its role in the autocrine/paracrine loop. In comparison to the upregulation of SDF-1a in microglia at 30 minutes, brain endothelial cell upregulation of SDF-1a occurred later at 60 minutes and was significantly higher than the 30 minute level (Fig. 2.4b). Endothelial cells exhibited the largest reduction in expression of CXCR4 amongst all cell types at 60 minutes, which was significantly lower than expression levels at 90 minutes. This result suggests endothelial cells may be more sensitive to ligand-induced desensitization. Astrocytes exhibited the largest changes in gene expression amongst the three cell types (Fig. 2.4c). SDF-1a expression increased at 30 minutes compared to baseline and subsequently significantly decreased by 120 minutes. CXCR4 expression mirrored this trend with increased expression at 30 minutes then significantly declined by 90 and 120 minutes. Collectively, each of the cell types increased SDF-1a expression in response to exogenous SDF-1a, demonstrating participation in autocrine/paracrine signaling.

Increases in SDF-1a expression coincided with changes in CXCR4 expression, confirming CXCR4 is part of the autocrine/paracrine loop. Suggestion of both ligand induced activation and delayed negative feedback of CXCR4 were observed across all cell types.

In silico Model of Diffusion only Predicts Undetectable SDF-1a after One Hour.

We next created mathematical models that were representative of the SDF-1a temporal trends observed *in vivo*. The first models included diffusion only kinetics and could not recapitulate sustained levels of SDF-1a over the period of days. Instead, both the bolus delivery and NP delivery model predicted undetectable levels of SDF-1a for after the 1-hour time period (Fig. 2.5a,b). The SDF-1a concentration profiles depicted by the diffusion only models are consistent with the very short half-life of SDF-1a reported in the literature.

In silico Model with Autocrine/Paracrine Signaling Predicts Persistent SDF-1a Levels Over Time.

Our *in vitro* and *in vivo* analyses indicated presence of autocrine/paracrine signaling. Therefore, we developed models that included autocrine/paracrine signaling kinetics. By fitting values for Michaelis-Menten reaction rates and constants, we created a model for bolus delivery of SDF-1a that was consistent with our *in vivo* results. The bolus delivered SDF-1a model with autocrine/paracrine kinetics showed SDF-1a levels sustained for 3 days like that of our immunohistochemistry results (Fig. 2.6a). In the same fashion, our autocrine/paracrine model of NP delivered SDF-1a resulted in SDF-1a levels sustained for 7 days (Fig. 2.6b). Further, the overall trends showed that bolus delivered SDF-1a gradually decreased over the 7 days whereas the NP delivered SDF-1a remained at the same level over the 7 days, like that of the *in vivo* trends. We also examined our models against the *in vivo* CXCR4 data. For the bolus CXCR4 data the

model accurately represented the *in vivo* trends where CXCR4 activation occurs out to 500μm at day 1 and decreases one-tenth by 1000μm (Fig. 2.6c). Day 3 was also represented where CXCR4 levels drop off after 300μm. Day 7 was not predicted by our model as the *in vivo* data show CXCR4 activity near the injection but our model predicts a lack of activity. For the NP group, the CXCR4 trends resulting from our model at day 1 appear like the bolus model, where CXCR4 declined around 500μm (Fig. 2.6d). However, the *in vivo* data showed sustained levels further from the injection which was not predicted. The model also calculated that CXCR4 levels will drop off around 500μm from the injection at both day 3 and day 7. This prediction matched day 7 *in vivo* data, but under predicted day 3. Overall our models predicted the *in vivo* observations for both SDF-1a and CXCR4 to a degree that discerned differences between the exogenous delivery methods.

Parameter Sensitivity.

To test the robustness of each of our models, parameter sensitivity was performed. Parameter sensitivity analysis measured maximal changes in parameter values that did not affect the outcome significantly (±10% of original results). As expected, the diffusion only models were not impacted by changes in parameters km, ka, ke, Vr, kr, Vrc, and crt since upstream signaling parameter Vmax was set to zero for these models (Table 2.2). Further, the diffusion only models allowed for larger changes in the diffusion coefficient, degradation rate, and delivered amount of SDF-1a than the autocrine models. This can be explained by the fine-tuned dynamics of autocrine systems[161]. The autocrine models were the most sensitive to changes in soluble SDF-1a degradation and complex endocytosis, where rate adjustments of less than ±0.005% would significantly impact the model predictions. Likewise, this is representative of the

highly regulated nature of autocrine/paracrine biological systems. All other parameters could be adjusted between ±0.005% and 5% without changing the resulting plots ±10%.

Discussion

The results of our previously published *in vivo* study demonstrated that sustained exogenous SDF-1a therapy elicits an endogenous SDF-1a response.[127] Considering the 26-minute half-life of SDF-1a, the immunohistochemistry results analyzed here suggests autocrine/paracrine signaling prolongs SDF-1a presence following exogenous administration. Further, we showed that sustained release of exogenous SDF-1a from degradable NPs engages autocrine/paracrine signaling longer resulting in higher, constant levels of SDF-1a across the cortex compared to bolus delivery. The differences between these two delivery strategies indicated that the presentation of SDF-1a is critical to the duration of endogenous signaling and therapeutic potential. These results align with other studies where controlled release of SDF-1a prolonged SDF-1a gradients and subsequently stem cell recruitment[163].

We demonstrated that autocrine/paracrine signaling contributes to establishing SDF-1a gradients. Microglia, astrocytes, and endothelial cells significantly modulate both endogenous SDF-1a and CXCR4 levels as a result of exogenous administration. These results were consistent to SDF-1a/CXCR4 signaling in cancer progression where SDF-1a autocrine loops contribute to cell migration and invasion[13, 157, 164]. Our identification of cell types engaging SDF-1a/CXCR4 autocrine/paracrine signaling in the brain justify the need to further utilize this cascade as a tool for repair. SDF-1a is a known stimulator of astrocyte proliferation[165, 166]. A recent study by Mao et al. suggests that SDF-1a delivery increases radial glial cell proliferation following traumatic brain injury and that these cells may act as a cellular scaffold to aid in the migration of immature neurons[167]. Here, we are the first, to our knowledge, to confirm that astrocytes

participate in SDF-1a/CXCR4 autocrine/paracrine signaling that may be tuned for maximal endogenous repair. Future studies should investigate ways to best modify this signaling loop for increased cell recruitment. If we can further understand SDF-1a/CXCR4 gene regulation, we may design a better delivery strategy to increase spatiotemporal presence of SDF-1a for enhanced signaling and repair.

While our results show CXCR4 cell density and gene expression coinciding with changes in SDF-1a, we cannot neglect the potential implications of CXCR7. CXCR7 was first identified as a cognate receptor to SDF-1a in T lymphocytes 15 years ago[26]. While relatively new, research on the role of CXCR7 in the brain is being established. Liu et al. found CXCR7 is a functional receptor for SDF-1a in brain endothelial cells and modulates their migration *in vitro*[168]. Therefore, it is possible that the changes we found in SDF-1a expression were due in part to CXCR7. Moreover, CXCR7 can also be a negative regulator for SDF-1a where CXCR7 activation reduces levels of CXCR4 and downstream SDF-1a induced cellular events[169, 170]. The extent to which CXCR7 impacts spatiotemporal levels of SDF-1a in the brain and its role in SDF-1a autocrine/paracrine dynamics requires further investigation.

To validate our findings and create a representative model of SDF-1a levels following exogenous SDF-1a delivery, we evaluated two different mathematical model types. We found that the model that only incorporated diffusion was not able to reproduce the spatiotemporal trends observed *in vivo*. This result suggests that diffusion only is not responsible for sustained gradients of SDF-1a and there must be another mechanism involved. The lack of sustained gradients based on diffusion only is predictable based upon the short half-life of SDF-1a and transport via diffusion. As suggested by our gene expression results, inclusion of autocrine/paracrine kinetics in the models were required to achieve the same SDF-1a levels observed *in vivo*. Specifically,

constant levels of SDF-1a across large sections of tissue were indicative of endogenous SDF-1a production. The only way constant levels could be achieved is through production of the molecule in conjunction with degradation and diffusion. Adding molecule production to our models allowed for SDF-1a curves to flatten (decreased slope), which would not be possible in a diffusion-only model where SDF-1a levels could only decline over time at a steady rate.SDF-1a constant levels were demonstrated by adding autocrine/paracrine kinetics to our models where flat curves of SDF-1a and CXCR4 were achieved.

We found that the parameters for soluble SDF-1a degradation rate constant and the SDF-1a/CXCR4 complex endocytosis rate constant were sensitive to less than ±0.005% change. This behavior seems to be a product of the cellular machinery rather than model limitations as cells are known to tightly regulate chemokine signaling through endocytosis[171, 172]. In the same fashion, others have noted that epidermal growth factor receptor (EGFR) system signaling requires threshold amounts of ligand to trigger downstream signaling, yet, EGFR overstimulation shuts off signal propagation through endocytic control[173]. If a similar phenomenon is at play for SDF-1a/CXCR4, one can postulate that if the rates of SDF-1a degradation or receptor endocytosis could be physically adjusted then autocrine/paracrine signals could be reduced or extended experimentally.

Current SDF-1a release systems focus primarily on extending the overall duration of exogenous SDF-1a activity. Sustained release platforms such as hydrogels, scaffolds, particles, and particle composite systems have been utilized to extend SDF-1a release for cell recruitment[174–177]. Sustained release platforms are limited in their efficacy since they do not account for autocrine/paracrine engagement and desensitization. There is a lack of systems that work to alter the presentation of SDF-1a such that it is informed by

the cellular machinery. Our model allows for experimentally testable predictions to be made and includes these dynamics. Our model results will inform next generation release systems by providing a platform to test SDF-1a release strategies for maximal SDF-1a/CXCR4 output and therefore cell recruitment.

Conclusion

The SDF-1a/CXCR4 signaling axis remains a promising tool for increasing cell recruitment following injury and disease. SDF-1a autocrine/paracrine kinetics and their impact on overall sustainment of SDF-1a was investigated here. We identified cell types that contribute to SDF-1a autocrine/paracrine signaling within the brain, the extent to which they impact SDF-1a levels and validated that this signaling is required to create sustained gradients for cellular migration. Knowing that autocrine/paracrine dynamics play a role in brain cell responses, the future of SDF-1a/CXCR4 based therapies should work to best control this signaling mechanism for specific outputs and improved therapies.

FIGURES

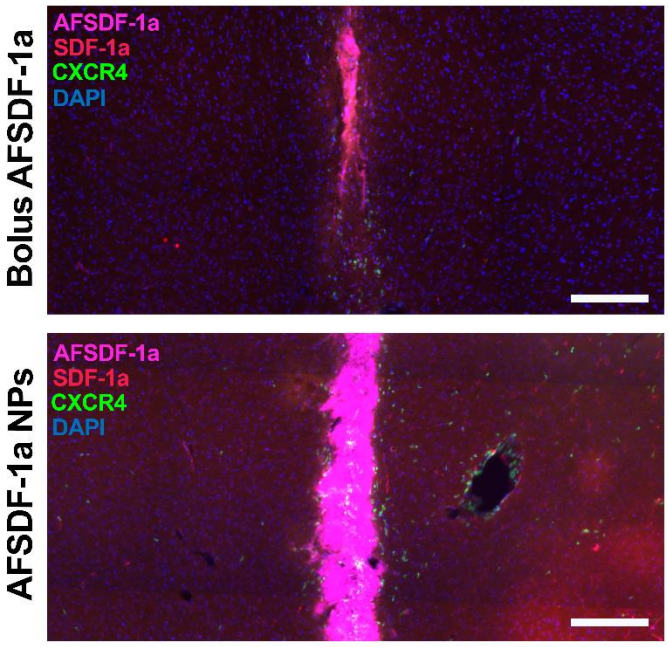

Figure 2.1. Spatial distribution of total SDF-1a 1 day after exogenous delivery. Representative cortical tissue sections from bolus delivered AFSDF-1a (top) and AFSDF-1a loaded NPs (bottom) stained for cell nuclei (DAPI, blue) and total SDF-1a (red), with EGFP-CXCR4 (green) and exogenous AFSDF-1a (pink). Increased levels of total SDF-1a immunostaining and CXCR4 are present visually across the cortex for the NP group. Immunostaining reveals steady levels of total SDF-1a across the cortex for the NP group in contrast to the spatially decreasing pattern for the bolus group. Consistent spatial levels of total SDF-1a suggest autocrine/paracrine signaling is occurring. Figure is adapted from Dutta et al. with copyright permissions.*[127]* Scale bar = 200μm

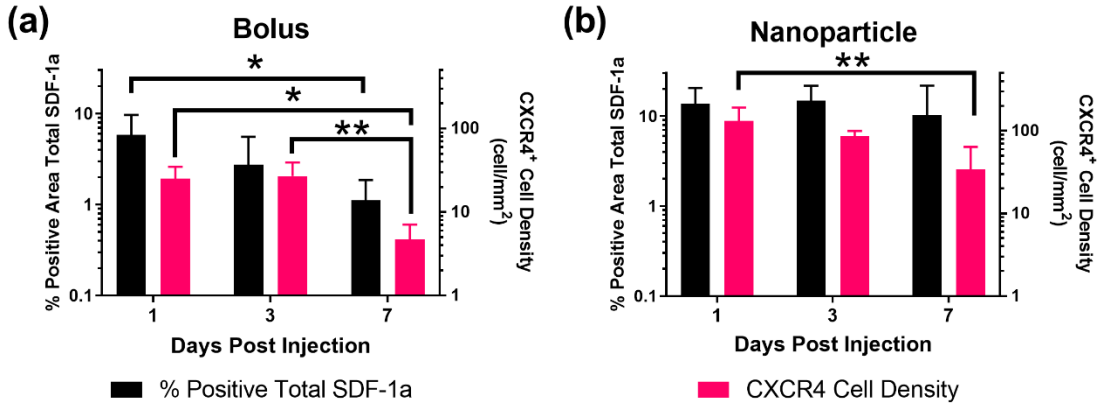

Figure 2.2. Temporal trends of total SDF-1a immunostaining and CXCR4 cell density 1, 3, and 7 days post injection. Total SDF-1a (black) and CXCR4 (pink) immunopositivity was persistent across 7 days for the NP group (b) and gradually

declined over 7 days for the bolus group (a). Overall sustainment of total SDF-1a immunopositivity and CXCR4 activity across the 7 day time window suggests autocrine/paracrine signaling. Mean ± SEM. n = 4-5 animals per group. *p<0.05, **p<0.01

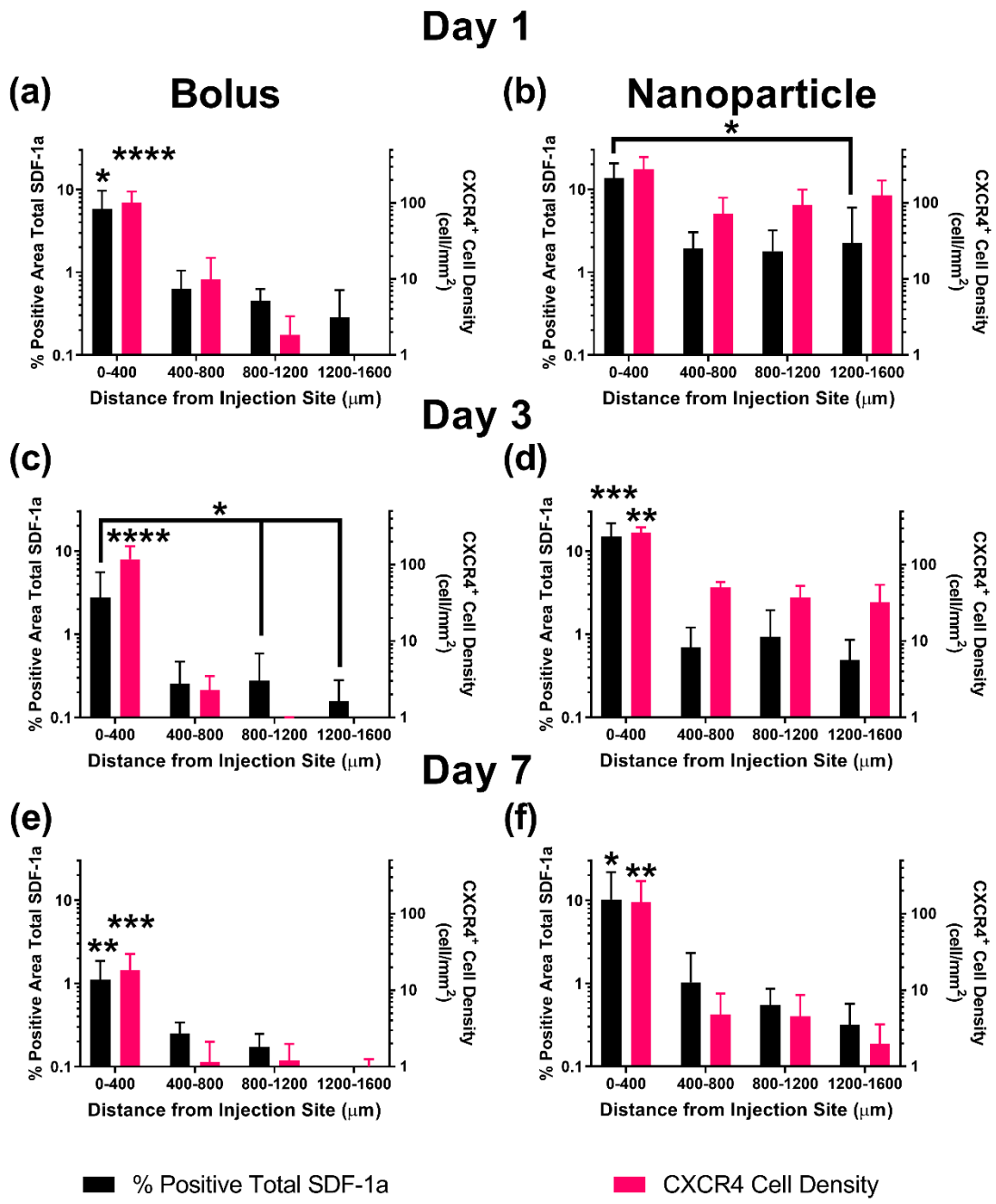

Figure 2.3. Spatial trends of total SDF-1a (black) immunostaining and CXCR4 (pink) cell density 1, 3, and 7 days post injection. Day 1 and day 3 bolus (a, c) spatial distribution of SDF-1a and CXCR4 declines steadily across the tissue. Day 1 and day 3 NP (b, d) spatial distribution reveals sustained levels of SDF-1a and CXCR4

across 1600μm of tissue, suggesting production of SDF-1a must be occurring endogenously. Spatial levels diminish on day 7 for the bolus group (e) and remain persistent immediate to the injection for the NP group (f). Mean ± SEM. n = 4-5 animals per group. Single asterisks above error bars indicate significance compared to all groups within data set where *p<0.05, **p<0.01

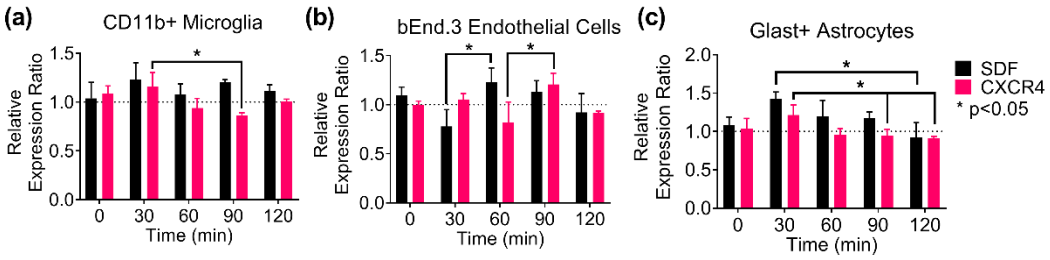

Figure 2.4. Microglia (a), brain endothelial cells (b), and astrocytes (c) engage autocrine/paracrine signaling via dynamic response to exogenous SDF-1a. Significant changes in SDF-1a (black) and/or CXCR4 (pink) mRNA expression were found across all cell types. Changes in expression are dynamic and distinct over time for each cell type. n = 3-6 cultures per cell type. Mean ± SEM. *p<0.05

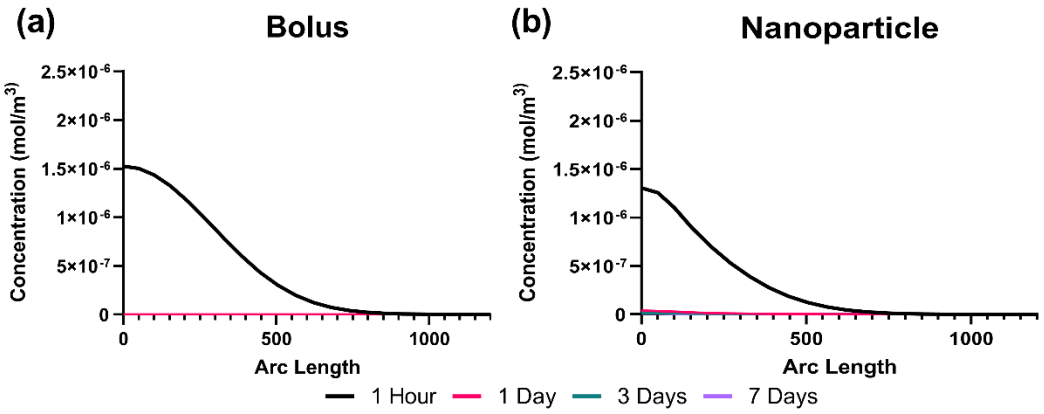

Figure 2.5. Diffusion only model predicts undetectable SDF-1a after 1 hour. Diffusion-only model concentration plots of soluble SDF-1a for bolus (a) and NP (b) delivered SDF-1a across 1 hour, 1 day, 3 days, and 7 days. Arc length represents equidistant space from the injection. Separate colors/line styles used to distinguish between time points (1 hour, 1 day, 3 days, 7 days). Lack of concentration plot lines indicates undetectable soluble SDF-1a present at corresponding time points. Both bolus (a) and NP (b) trends are not consistent with in vivo data, suggesting another mechanism is required to sustain SDF-1a signal spatiotemporally.

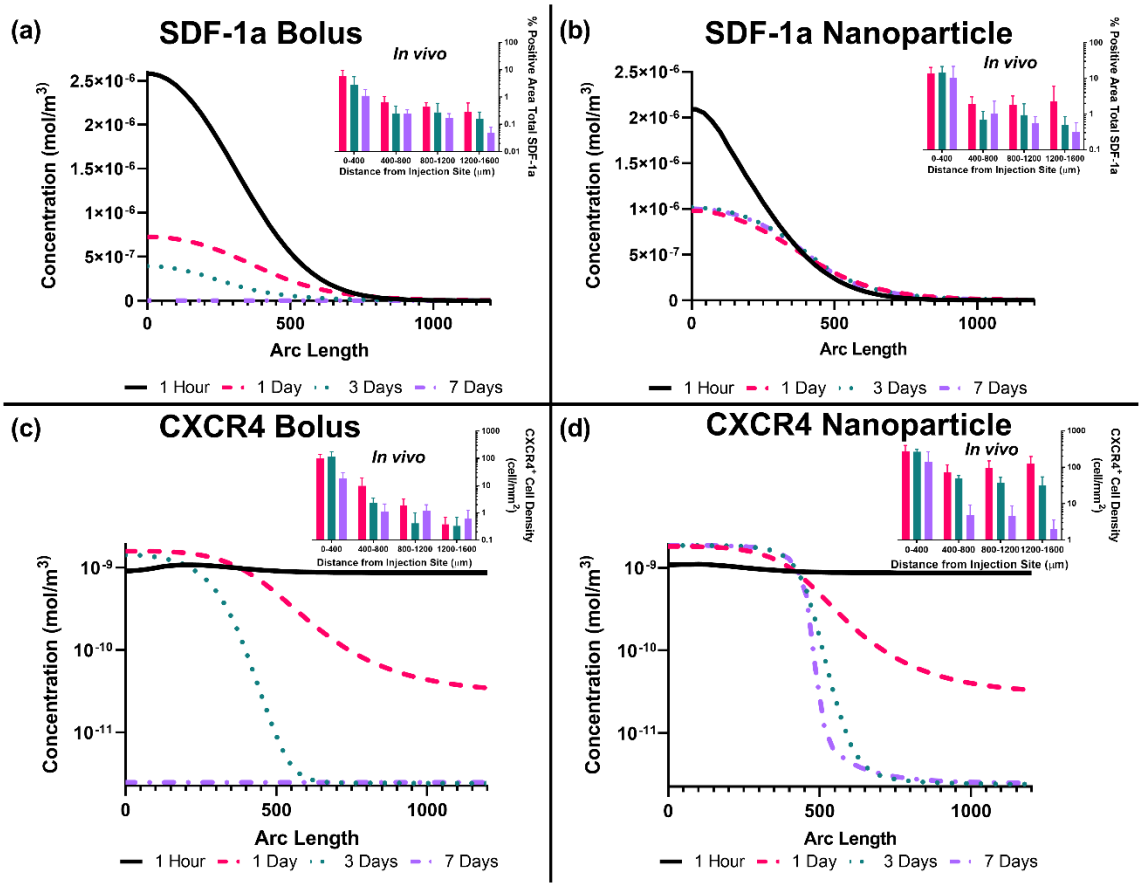

Figure 2.6. Autocrine/paracrine model replicates in vivo results. Autocrine/paracrine model concentration plots of soluble SDF-1a for bolus (a, c) and NP (b, d) delivered SDF-1a across 1 hour (black), 1 day (pink), 3 days (teal), and 7 days (purple). Arc length represents equidistant space from the injection. Addition of autocrine/paracrine kinetics flattens concentration curves of both SDF-1a and CXCR4, yielding spatiotemporal sustainment and matching most *in vivo* results.

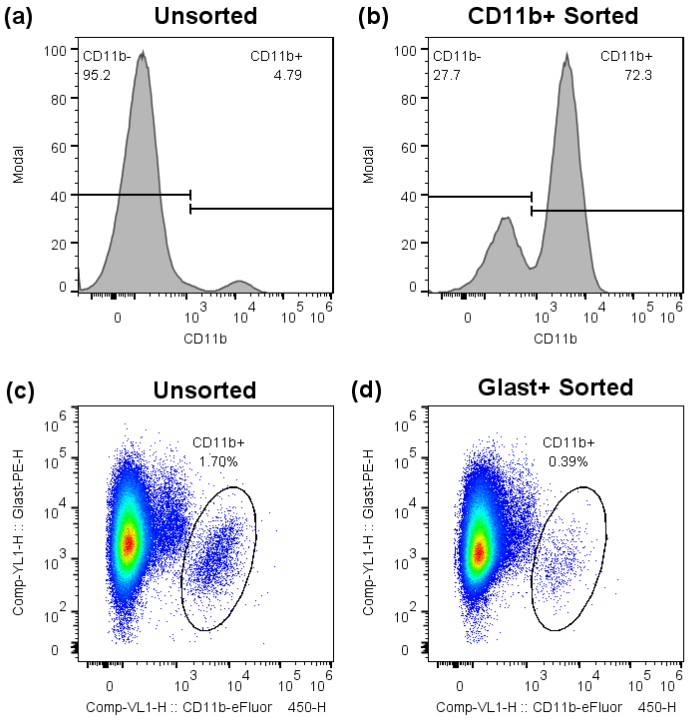

Figure 2.7. Flow cytometry enrichment of CD11b+ microglia (a,b) and Glast+ astrocytes (c,d). Histogram plots of cell population before (a) and after (b) magnetic activated bead sorting for CD11b+ cells. Cell population increases from 4.79% CD11b+ to 72.3% CD11b+ prior to RT-qPCR. X-axis = CD11b-e450 intensity. Dot plots of cell population before (c) and after (d) magnetic activated bead sorting for Glast+ cells. Gated cells show a decrease from 1.7% to 0.39% CD11b+ cells present in the Glast+ cells prior to RT-qPCR.

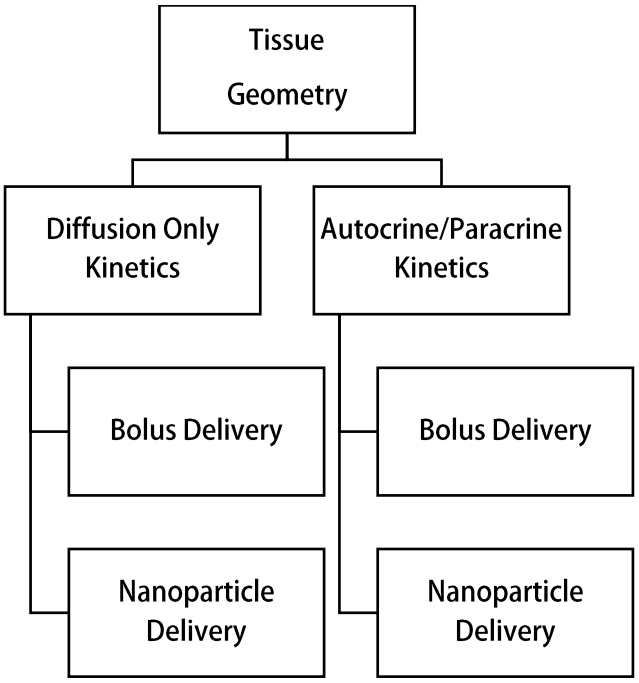

Figure 2.8. Overview of mathematical models and submodels.

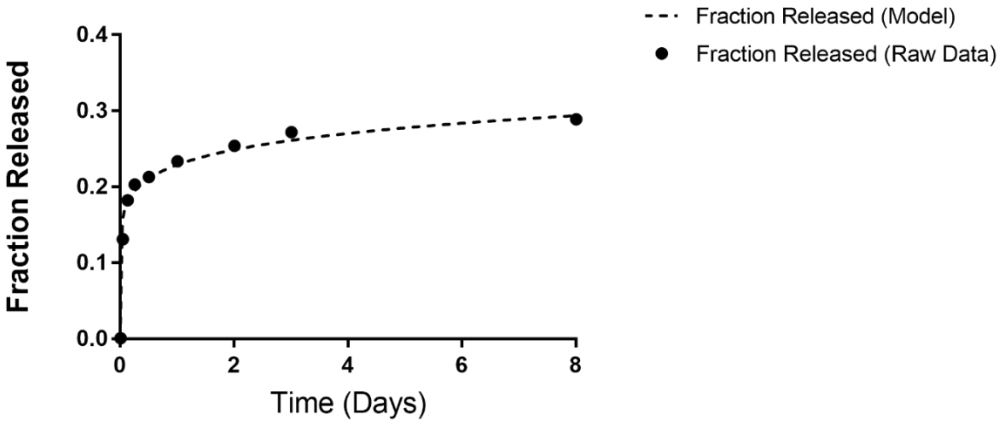

Figure 2.9. Nanoparticle release data fitted to Korsmeyer-Peppas model.
Fraction of drug released = Kt^n. For our release data, K = 0.0585 n = 0.12.

Table 2.1

COMSOL Parameters

Name	Value	Description
Vmax	1e-9[mol/(s*m^3)]	Max Reaction Rate, Soluble SDF-1a
Km	1e-10[mol/m^3]	Substrate Concentration for half-maximal SDF-1a Reaction
Dc	1e-11[m^2/s][178]	Diffusion Coefficient, SDF-1a
kdeg	0.000406[1/s]	Degradation Rate of SDF-1a
ka	50[1/((mol/m^3)*s)]	Association Rate Constant, SDF-1a with CXCR4
ke	0.00105[1/s][179]	Endocytosis Rate Constant of complex
Vr	0.35e-12[mol/(s*m^3)]	Max Reaction Rate, CXCR4
Kr	1e-10[mol/m^3]	Substrate Concentration for half-maximal CXCR4 Reaction
Vrc	1e-16[mol/(s*m^3)]	Baseline Production Rate of CXCR4
crt	1e-9[mol/(m^3)]	Initial Concentration of CXCR4
blc	1e-6[mol/(m^3)]	Baseline Concentration of Soluble SDF-1a

Table 2.2

Parameter Sensitivity Values

Parameter	Original	Bolus Autocrine	NP Autocrine	Bolus Diffusion	NP Diffusion
Vmax	1.00E-09	0.004%	0.004%	N/A*	N/A*
km	1.00E-10	0.01%	0.01%	No impact**	No impact**
Dc	1.00E-11	0.10%	0.10%	10.00%	10.00%
kdeg	0.000406	0.002%	0.002%	5.00%	5.00%
ka	50	0.008%	0.008%	No impact**	No impact**
ke	0.00105	0.005%	0.005%	No impact**	No impact**
Vr	3.50E-13	0.006%	0.006%	No impact**	No impact**
kr	1.00E-10	0.009%	0.009%	No impact**	No impact**
vrc	1.00E-16	5.00%	5.00%	No impact**	No impact**
crt	1.00E-09	0.01%	0.01%	No impact**	No impact**
blc	1.00E-06	0.10%	0.10%	5.00%	5.00%

*Parameter is set to zero for model
**Parameter is multiplied by zero or dependent on unchanging parameter

CHAPTER 3

Changes in the Migratory Response of Neural Progenitor Cells Following TBI and SDF-1a Delivery

Traumatic brain injury (TBI) is a contributing factor in over 30% of injury related deaths in the United States [1]. Following an initial mechanical insult to the brain, primary and secondary injuries lead to cell death, inflammation, edema, coagulopathy and in turn cognitive and motor disabilities [2, 3]. TBI incites an array of cellular processes that include necrosis, apoptosis, and inflammation that aim to attenuate the injury and initiate repair [4, 5]. Efforts to mitigate this cell loss include both administration of exogenous stem cells and recruitment of endogenous neural progenitor cells from the prolific niches of the adult brain (i.e., subgranular zone, SGZ, and subventricular zone, SVZ). Each of these strategies has limited success due to different challenges. For example, exogenous stem cell transplant approaches are limited by poor survival and engraftment rates; whereas endogenous cell recruitment is limited by the number of cells that arrive at lesions as well as their cell phenotype favoring an astrocytic path [4, 180, 181]. Here, we will focus on developing strategies to promote endogenous NPC recruitment, while recognizing how the knowledge gained with these approaches may contribute to future cell transplant technologies. Limitations for endogenous NPC recruitment may be addressed via two key strategies. First, introducing biomaterials to improve the injury microenvironment to maximize NPC recruitment and promote regenerative processes. Second, incorporating biomolecules that readily incite cell migration, promote cell survival, and modulate differentiation into a neural phenotype. With these biomaterial-based tools in hand, we can develop combinatorial approaches to tune brain repair processes that contribute to improved functional cognitive and motor abilities.

Stromal cell derived factor 1-a (SDF-1a) is one prominent signaling molecule that contributes to the migration of NPCs from the SVZ of the adult brain towards brain injuries. Our prior work (Chapter 2, [182]) indicates that in the injured brain, SDF-1a chemoattractant gradients are generated via endogenous expression and secretion in part from astrocytes, microglia, and endothelial cells local to the brain injury. In a preclinical model of TBI, upregulation of SDF-1a lasts only 7 days before returning to baseline levels (unpublished data) and the molecule itself has a short half-life of 28 minutes [155]. Coincidentally, reported endogenous NPC arrival to brain lesions also peaks at 7 days and then returns to minimal levels[9]. Based on our prior findings that autocrine/paracrine signaling contributes to SDF-1a secretion and that sustained release aids this response, we may use this mechanism to our advantage. Here, we aim to stimulate autocrine/paracrine signal propagation using a SDF-1a delivery system to increase endogenous NPC arrival towards TBI lesions. We hypothesize that stimulating a second wave of SDF-1a endogenous signaling via controlled release of SDF-1a 7 days after TBI may initiate increased NPC migration from the SVZ to the cortical lesion. Increasing endogenous NPC recruitment has the potential to improve functional outcomes following TBI. Prior studies have tested whether small molecules or growth factors could increase endogenous neurogenesis to a level of functional recovery and significance. The majority of studies have examined local neurogenesis, where delivery of bioactive molecules after brain injury demonstrated increases in SVZ and SGZ cell proliferation, local neurogenesis, and ultimately cognitive improvements via morris water maze [146, 183–185]. However, studies have also demonstrated that SVZ-derived cells are capable of maturing into neurons and integrating into the striatum and damaged cortex following stroke [186, 187]. These studies warrant further investigation of endogenous neurogenesis as a potential source for TBI repair.

Many materials and drug delivery systems have been designed to deliver molecules to the brain following TBI. Most common are either polyester-based systems with long-term sustained release of biomolecules or hydrogel systems that release at a faster rate but offer improved biocompatibility [188, 189]. Biomolecules like SDF-1a require increased protection and prolonged release to overcome rapid clearance from the injury environment. There are two main approaches to extending the hydrogel drug release period. The first is to increase the overall crosslinking density of the hydrogel thereby delaying the release to physical entrapment. However, altering the degree of polymer crosslinking increases the mechanical stiffness of the hydrogel, a parameter that is critical for neural and other soft tissue applications. The second approach is to chemically modify the polymer network to covalently tether desired biomolecules within the network thereby stabilizing the biomolecule and extending release kinetics. In this approach, the tethering scheme may include enzymatically sensitive peptide sequences to enable enzyme mediated controlled release [190, 191]. Here, we employed such a tethering approach to prolong SDF-1a release to initiate autocrine/paracrine SDF-1a signal propagation. We developed a hyaluronic acid (HA) microgel system that allows for the release of SDF-1a peptide upon exposure to matrix metalloproteinases (MMPs). MMPs are upregulated locally following TBI and hyaluronic acid is a native extracellular matrix protein that has been used extensively in the central nervous system for tissue repair. This system allows for both the protection and release of SDF-1a peptide *in vivo* through anti-inflammatory and synergistic HA.

In this study, we developed and characterized a HA microgel system with MMP mediated release of SDF-1a peptide. We first characterize the microgel size and tunability, degradation properties, loading capacity, and SDF-1a peptide sensitivity and release to MMPs. We then use this system in a mouse TBI model (controlled cortical

impact; CCI) to determine the impact of SDF-1a peptide microgels on NPC migration. We show preliminary data of migratory neuroblast marker doublecortin and immature progenitor marker nestin presence ectopically from the SVZ in all injured groups. We also present patterns of astrocytosis (glial fibrillary acidic protein; GFAP) and present the complex immunostaining imaged thus far. Lastly, we outline our experimental approach for completing the data acquisition and analysis to determine the differences in cellular migration and localization between the experimental groups.

Materials and Methods

Microfluidic Device Fabrication.

PDMS microfluidic devices were fabricated via soft lithography from a master silicon wafer using established protocols [192, 193]. Briefly, SU8 2075 was spin-coated to a 25µm thickness on a 4 inch silicon wafer. The wafer was exposed to ultraviolet light through a transparent mask containing the design for 18 microfluidic devices (created in Solidworks). The SU8 was developed and the wafer was prepared for polydimethylsiloxane (Sylgard 184; Electron Microscopy Sciences) via silanization using methyltri-chlorosilane (MTCS; Sigma). The PDMS was cured in an 80°C oven for 1 hour and then carefully removed from the wafer. Individual devices were cut apart, inlet and outlet holes were created with a 1mm biopsy punch, and devices were exposed to plasma treatment (PDC-32G; Harrick Plasma) and bonded to glass slides. Bonded devices were cured in an 80°C oven overnight and were then subject to a dry sterilization cycle in the autoclave. Aquapel treatment was performed to make the channels hydrophobic.

Norbornene Hyaluronic Acid Microgel Generation.

Norbornene functionalized hyaluronic acid (NorHA) was generated using established protocols and nuclear magnetic resonance (NMR) to confirm degree of functionalization[194]. NorHA microgels were generated with a microfluidic flow-

focusing device equipped with a UV light source downstream to crosslink microgels and encapsulate thiol-containing biomolecules (Figure 3.). A dual syringe pump (Chemyx) was used to deliver controlled flow rates of oil and aqueous phase solutions. The oil phase consisted of light mineral oil (Sigma) supplemented with Span80 (2% v/v; Sigma). The aqueous phase was comprised of NorHA (0.1% w/v), Lithium phenyl-2,4,6-trimethylbenzoylphosphinate (0.05% w/v LAP; Sigma), matrix metalloproteinase (MMP) cleavable SDF-1α peptide (KPVSLSYRCPCRFFESHIARAGVPMSMRGGDRCG, 200ng/μl; Watson Bio), and dithiol (0.4 stoichiometric ratio to Norbornene; Sigma). Sulfo-Cy3 tetrazine (100uM; Fisher) was incorporated into the aqueous phase to visualize microgels and measure their size distribution. The flow rates for the oil and aqueous phase were 0.5ul/min and 0.25ul/min respectively. Microgels were generated within the devices and then traveled to outlet tubing where they were exposed to 365nm light to crosslink them and collected in microcentrifuge tubes for analysis and use. Microgels prepared for *in vivo* use were prepared aseptically and sterile filtered.

Microgel Size Distribution.

Microgel size analysis was conducted on single batches generated from four microfluidic devices with a minimum of 50 microgels per device/batch. Each batch contained 10μM sulfo-Cy3 tetrazine (Lumiprobe) fluorescent dye. Fluorescent microscopy images were obtained with a Leica DMI 6000B microscope, imported into ImageJ, converted to greyscale, and threshold adjusted for ease of measurement. ImageJ was used for automated size analysis using the 'analyze particles' feature.

Microgel Degradation.

Collected microgels were prepared for assays by removing the upper layer of oil and adding 200 proof ethanol. Suspensions were lightly vortexed and then centrifuged for 5

min at 10,000rcf. The supernatant was removed, distilled water was added, and microgels were vortexed lightly. Microgel suspensions were combined from three separate batches and trypan blue (0.04%; Gibco) and a hemocytometer was used to approximate their density. A microgel suspension (50 μL of ~2000 microgels/μL) was added to microcentrifuge tubes with 60 μL of either hyaluronidase (0.01mg/ml; Sigma) in TTC buffer (0.05% Triton-X 100, 50mM Tris Hydrochloride, 1mM $CaCl_2$) or TTC buffer alone. At 1, 7, and 14 days the microgel suspensions were centrifuged, supernatant collected, and replaced with the appropriate buffer. After 14 days, 45 μL of 5mg/ml hyaluronidase was added to all samples to degrade and quantify any remaining hyaluronic acid. A carbazole assay was used to quantify the amount of NorHA in each supernatant by measuring absorbance at 530nm. The absorbance values were transformed to mass based on a NorHA standard curve. Data were presented as the cumulative total amount of hyaluronic acid in each sample with 3 replicates per group.

SDF-1a Peptide Bioactivity.

SDF-1a peptide bioactivity was assessed using a neurosphere outgrowth assay. Animal studies were approved by Arizona State University's Institutional Animal Use and Care Committee (IACUC) and were performed in accordance with the relevant guidelines. Neurospheres were obtained through an established protocol by primary harvest from E13.5 time pregnant rats [195]. Briefly, rats were anesthetized and underwent rapid decapitation. The abdomen was opened and the uterine tissue containing the embryos were removed. Fine forceps were used to isolate the brain of each embryo and dissect out the ganglionic eminences containing neural progenitor cells (NPCs). The tissue was dissociated and placed in media for at least one week to allow for neurosphere formation. To assess neurosphere outgrowth, cultures were moved from their initial plates to new plates with modified growth media (no EGF or FGF added) to encourage attachment to

the plate surface. Culture wells (n=3 per group) were supplemented according the following experimental groups: media only, murine SDF-1a (1.25e-10M; Peprotech), or SDF-1a peptide (3e-8M, 3e-7M, 3e-6M; WatsonBio). After 24 hours, each of the neurospheres were imaged using a compound microscope at 10x magnification and exported with a scale bar for subsequent measurements. NPC outgrowth was calculated by quantifying the longest outer diameter of the neurosphere growth and normalizing it to the inner sphere core diameter (ImageJ; NIH).

Microgel Release Kinetics and Loading Capacity.

Collected microgels were prepared using the same methodology as the degradation experiments. The MMP cleavable peptide (KPVSLSYRCPCRFFESHIARA-K(Acp-Biotin)-VPMSMRGGDRCG; Watson Bio) contained a biotin molecule for quantification of peptide release from the microgels. To induce microgel peptide release, microgels were incubated with 250U/ml collagenase (MP Biomedicals) in 0.1M CaCl2 buffer at 0, 6, and 13 days for 24 hours. An equal amount of microgels were incubated in buffer without collagenase to serve as control. At each time point, microgels were centrifuged at 10,000g for 5 minutes and the supernatants were collection for biotin quantification. First, a fluorescence biotin quantification kit (Invitrogen) was used to generate a standard curve of biocytin. The standard curve was then used to interpolate the amount of biotin released into the supernatants on day 1, 7 and 14 (n=3 per group/time point). A paired t-test was conducted for each time point where a p value of <0.05 was considered significant. To assess total possible release, an additional group of microgels were incubated with 1500U/ml collagenase for 24 hours. The supernatants were collected and quantified using the same technique as the time course experiments (n=3).

Subventricular Zone Lentiviral Injections.

Animal studies were approved by Arizona State University's Institutional Animal Use and Care Committee (IACUC) and were performed in accordance with the relevant guidelines. To determine accuracy and reproducibility of SVZ injections, 2.5% fast green dye or lipophilic dye (Vybrant Dil; Invitrogen) was injected stereotactically into lateral ventricle using the following coordinates: A/P -0.3mm, M/L +1.00mm, D/V -2.6mm from the skull surface. Within an hour, mice were euthanized via pentobarbital overdose (150 mg/kg intraperitoneal injection) and brains were extracted. Coarse sections were made using a brain matrix and visualized for presence and location of dye. For subsequent studies, 1μL of fluorescent lentiviral particles driven by the constitutive promotor EF1α (rLV.EF1.tdTomato-9; Vectalys) were injected into the same coordinates as the dye. After visualization of the initial particle injections, the coordinates were adjusted to the following: A/P -0.6mm, M/L +1.20mm, D/V -3.0mm from the skull surface. Three days after lentiviral particle injection, mice were perfused and prepared for sagittal or coronal sectioning and immunohistochemistry.

Controlled Cortical Impact (CCI) and Microgel Injections.

Animal studies were approved by Arizona State University's Institutional Animal Use and Care Committee (IACUC) and were performed in accordance with the relevant guidelines. Adult C57BL/6 mice (Jackson Laboratory) aged 8-10 weeks were anesthetized via isoflurane inhalation and mounted to a stereotaxic instrument. An incision was made along the top of the head and a 3mm craniotomy was performed over the frontoparietal cortex. A stereotaxic frame (Leica Microsystems) was used to center a 2mm impactor over the craniectomy and the impact was performed at a velocity of 6m/s and a depth of 1mm. The skull piece was placed back over the craniotomy site and secured using dental cement. The incision was sutured, and animals were provided (0.05mg/kg buprenorphine) and 500μL saline subcutaneously. Animals were monitored

in a recovery cage until consciousness and movement was regained. Animals were subject to HA microgel-SDF-1a intervention or control injections 7 days following the CCI. Animals were anesthetized and the initial incision was re-opened. A total of four 0.5 μL injections were positioned in the peripheral tissue of the damaged cortex using the stereotaxic frame and needle holder. The skull piece and dental cement from the craniotomy was removed. Burr holes were created on the border of the craniotomy using a rotary drill and animals received injections from one of the following groups: saline, SDF-1a peptide microgel (100ng/0.5 μL; 1000 microgels/injection), or blank microgel (1,000 microgels/injection). A 27g needle was lowered into the tissue to a depth of 0.8mm, retracted to 0.6mm to allow space for the injection, and performed at a rate of 0.5 μL /min. The needle was left in place for 1 min before removal. The skull piece was repositioned and secured in place with dental cement. The incision was sutured, animals were given analgesics, saline, and monitored in a recovery cage. Mice were euthanized via pentobarbital overdose (150 mg/kg intraperitoneal injection) 7 days after injection (14 days after CCI). One additional set of age matched naïve animals were sacrificed to serve as a control group. Four animals for the saline group and five animals for all other groups were used for subsequent immunohistochemical analysis.

Immunohistochemistry and Image Analysis.

Following euthanasia, mice were subject to transcardial perfusion with phosphate buffered saline and 4% paraformaldehyde (Sigma). Brains were then extracted and placed in 4% paraformaldehyde, 15% sucrose (Sigma), and 30% sucrose at 4°C consecutively until saturation. Brains were dried of excess sucrose and placed into embedding molds (Electron Microscopy Sciences) and covered with O.C.T. compound (Electron Microscopy Sciences). The embedding mold was then placed into a slurry of dry ice and 200 proof ethanol until the compound was opaque and the block was frozen.

Frozen embedded brains were stored at -80°C until cryosectioning. Coronal sections (30 μm) or sagittal sections (50 μm) were obtained with a cryostat (Cryostar NX70; Thermo Scientific) and placed into phosphate buffer saline supplemented with 0.01% sodium azide and stored at 4°C until staining. Primary antibodies were selected for astrocytes (GFAP; Abcam ab53554 1:500), neural progenitor cells (Nestin; Novus Biologicals, NB100-1604, 1:250), neuroblasts (Doublecortin; Abcam, ab18723, 1:1000), and oligodendrocytes (Olig2; R&D Systems AF2418, 1:50) and paired with secondary antibodies. An inverted microscope (DMI6000B; Leica) was used to capture fluorescent images of stained sections for downstream analysis (ImageJ; NIH).

Statistical Analysis.

All quantitative results were analyzed using GraphPad Prism software (GraphPad Software, Inc., La Jolla, CA). Statistical analysis of differences between groups were performed by one-way analysis of variance with Tukey post-hoc testing or a paired t-test where $p<0.05$ was considered significant. All data were graphed as the mean ± standard deviation or standard error of the mean.

Results

Microfluidic Flow Focusing Device Creation and Iterations.

We determined two necessary features for the microgels to be used for our TBI applications: 1) microgels must be injectable (i.e., below 100μm in diameter to flow through 27g needle) and 2) monodisperse. Monodispersity reduces batch to batch variation and ultimately reduces variation in drug release kinetics and rate of particle degradation. After evaluating a number of fabrication methods, we chose to develop a microfluidic flow focusing system based on this system's reproducibility and tunability in particle generation. Specifically, we employed a previously published microfluidic flow focusing system where a dispersed phase flows perpendicular into a continuous phase

and then through an orifice (Fig. 3.5) [196, 197]. Capillary instability leads to droplet formation and the addition of surfactant to the continuous phase stabilizes the droplets in solution. Microfluidic devices were created using soft lithography; we went through 6 major design iterations to optimize the device for our use (Fig. 3.1). In addition to changes to the microfluidic base device design, system parameters were also tuned to achieve a functional system included syringe size (for injecting fluid into the system), surfactant concentration, flow rate of the continuous phase, flow rate of the dispersed phase, irradiation time, distance from irradiation source, and polymer concentration. A few system parameter choices were key in creating stable HA microgels. For example, photo-initiator selection was critical where switching from Irgacure2959 (I2959) to Lithium phenyl-2,4,6-trimethylbenzoylphosphinate (LAP) significantly impacted microgels crosslinking consistently. We determined that LAP is less soluble in oil than I2959 and therefore was able to remain in the dispersed phase whereas I2959 moved to the continuous phase (HA polymer phase). Another major device design challenge to overcome was that a small orifice size was needed to generate microgels within our design constraints (i.e., less than 100μm in diameter). A basic equation to estimate the output microgel diameter is twice that of the orifice diameter. Therefore, the orifice size needed to be 25μm across to ensure the microgels would be less than 100μm in diameter and led to the device clogging frequently. Therefore, we designed "particle traps" to address this issue (Fig. 3.1; device 6). These 25μm traps were upstream of the microgel-generating orifice and allowed for any particulates to be trapped with flow diverted around them before reaching the orifice. This device design change led to more consistent and efficient production of microgel batches.

Monodisperse Microgels with Tunable Size are Generated using Flow Focusing Microfluidics.

We adapted published protocols to design and fabricate flow focusing microfluidic devices for the generation of NorHA microgels[198–200]. Thiol-ene chemistry was used to make non-degradable crosslinked microgels with MMP cleavable linkages to an SDF-1a peptide (Fig. 3.3). To determine the size distribution of microgels, the diameter of microgels were measured from four different devices and solution batches while maintaining a constant flow rate and aqueous/oil ratio. Microgel size analysis across devices illustrated that microgel size remained monodisperse where 88% of all microgels measured fell within a 20μm size range (Fig. 3.4). These results indicate minimal variability in the size of microgels when generated with different microfluidic devices and are therefore a good platform for generating monodispersed microgels. To demonstrate the versatility of the microfluidics system, we created devices with either 25μm or 50μm orifices to tune microgel size. The average microgel diameter was significantly higher (122μm) when produced with the 50μm orifice device compared to the 25μm orifice device (73μm) (Fig. 3.6). Next, we determined the size distribution of microgels using varying flow rate ratios (Oil:Aqueous). For both 25μm and 50μm orifice devices, the microgel size was lower when the flow rate ratio was large (55μm vs. 64μm and 141μm vs. 147μm, respectively) (Fig. 3.7). The ability to tune microgel size using orifice size and flow rate allows for specific size ranges to be achieved using this microfluidic system.

Microgels Degrade upon Exposure to Hyaluronidase.

The degradation of NorHA microgels was characterized over the course of 2 weeks in presence or absence of hyaluronidase. After 24 hour incubation, NorHA microgels were sensitive to hyaluronidase mediated degradation as indicated with a significant increase in the percentage of total soluble NorHA compared to microgels incubated in PBS (20.3% vs. 30.9%) (Fig. 3.8). Note, we acknowledge limitations in our

experimental design that may have contributed to elevated NorHA levels in non-hyaluronidase group whereby the microgels did not fully pellet during the centrifugation step and therefore we cannot rule out the possible inclusion of non-degraded HA microgel contamination in the supernatants. Even with this caveat, we still observed a significant increase in the percentage of total soluble NorHA with the addition of the enzyme (Fig. 3.8a; $p=0.0291$). To further demonstrate the microgel enzyme sensitivity, we quantified NorHA released in supernatants of microgels that did not receive hyaluronidase over the course of 14 days. We performed supernatant collection and replacement on days 1, 7, and 14 for each experimental sample. We then added hyaluronidase enzyme after the final time point (day 14) to quantify any NorHA that remained in each sample tube. For each microgel sample, we calculated the total possible NorHA in each tube as the summation of the NorHA measured across the 14 days plus the NorHA measured after the addition of hyaluronidase. When normalized to the total NorHA in each sample, 18-22% of the total NorHA was quantified consistently at 1, 7, and 14 days when no hyaluronidase was present. However, the percentage increased significantly to 39.5% upon addition of hyaluronidase after day 14 (Fig. 3.8b; $p<0.0001$). Moreover, these data demonstrate that microgels remain stable and sensitive to hyaluronidase mediated degradation over 14 days.

SDF-1a Peptide has Comparable Bioactivity to Murine SDF-1a.

A murine neural progenitor cell (NPC) neurosphere assay was used to determine and validate the bioactivity of the MMP-cleavable SDF-1a peptide we designed for this study. SDF-1a stimulates prominent outgrowth from NPC neurosphere in vitro assay. Here, we assessed outgrowth in vitro over 24 hours following media supplemented with varying concentrations of the SDF-1a peptide, murine recombinant SDF-1a, or basal media. Neurosphere outgrowth was significantly higher than basal media alone when

exposed to 1.25e-10M murine SDF-1a, 3e-7M SDF-1a peptide, and 3e-6M SDF-1a peptide (Fig. 3.9). No significant difference was observed between the murine SDF-1a (1.25e-10M) and 3e-6M SDF-1a peptide. We acknowledge that the SDF-1a peptide required a significantly higher concentration than the recombinant SDF-1a to elicit a comparable response from NPCs. However, the SDF-1a peptide did induce neurosphere outgrowth compared to basal media indicating biofunctionality. It should be noted that the peptide was tested as the uncleaved form (i.e., SDF-1a peptide-MMP sensitive peptide) which may have decreased potency.

Microgels Release SDF-1a Peptide via MMP Cleavage Sites.

A critical component of this microgel system is to deliver SDF-1a peptide in response to MMPs upregulated in the TBI microenvironment. Here, we demonstrated this MMP sensitivity over 2 weeks where microgels loaded with the SDF-1a peptide were exposed to collagenase type IV for 24 hour periods. After an initial 24 hour time point, significantly higher levels of SDF-1a peptide (measured indirectly via biotin) were released from microgels exposed to collagenase compared to incubated in PBS (Fig. 3.10a; 40.4pmol vs. 19.1pmol, **p=0.022). Further, delaying the exposure of microgels to collagenase by 6 or 13 days demonstrated the retained MMP sensitivity over 2 weeks as the SDF-1a peptide levels were significantly higher following incubation with collagenase (Fig. 3.11; 10.7pmol vs. 3.9pmol after 6 days (p=0.0067), and 9.6pmol vs. 3.7pmol after 13 days (p=0.0013). These data illustrated that MMP-mediated peptide release remains stable over a 2-week period. To determine the loading capacity of the microgels, we exposed the microgel samples to highly concentrated enzyme for 24 hours (Fig. 3.10b). We calculated the microgels loading capacity to be 65% (n=3, standard deviation = 2.5%).

In vivo Labeling of Subventricular Zone Cells using Lentiviral Particles.

Confident and long-term labeling of SVZ cells is critical to measuring NPC migration after TBI and SDF-1a delivery. Here, we pursed a lentiviral labeling procedure to reliably and reproducibly label SVZ residing NPCs. To assess whether this protocol would be appropriate for our studies, we first sought to demonstrate our ability to perform accurate and consistent stereotaxic injections into the lateral ventricles of adult mice. First, we injected the lipophilic dye Vybrant Dil into the lateral ventricle of the brain. We found consistent Vybrant Dil restricted to the tissue surrounding the ventricular system (Fig. 3.12; n=4). This result indicated that we could perform consistent ventricular injections and afforded confidence to pursue lentiviral labeling assessment. Therefore, we injected 1µL of fluorescent lentiviral particles into the lateral ventricle of mice. Analysis of the tissue 3 days following injection indicated two main concerns for this approach. The injection location resulted in labeling of the dentate gyrus instead of the lateral ventricle and occurred with frequency (n = 3 out of 6 total animals) (Fig. 3.13). Injection coordinates were adjusted to A/P -0.6mm, M/L +1.20mm, D/V -3.0mm from the skull surface, and the procedures were repeated to test for improved injection accuracy. We found these injections to be much closer to the lateral ventricle but noted off-target tissue labeling (i.e., along the injection tract in 3 out of 5 total animals) (Fig. 3.14). Therefore, we did not proceed with this method for subsequent in vivo studies. Rather, we utilized immunohistochemistry to probe for makers of neuroblasts (doublecortin, Dcx) and neural progenitor cells (nestin). While we acknowledge this IHC-based approach may not capture the full breadth of chemotactic cell migration (i.e., neuroblasts that migrated and differentiated), we have full

confidence in our ability to conduct and execute such IHC analysis on relevant tissue markers.

In vivo Administration of SDF-1a Microgels Following Traumatic Brain Injury.

To assess the impact of SDF-1a peptide loaded microgels on SVZ migration following TBI, we performed CCI on mice followed by intracortical injections in the periphery of the lesion cavity at 7 days post-injury. Experimental injection groups were saline, SDF-1a peptide microgels, or blank microgels. Analysis of the tissue 7 days after peripheral injections showed a complex response. We performed initial immunostaining on a subset of tissue sections and animals (n = 3 per group). Noting the variety of cell types originating in the SVZ niche, we focused on immunostaining that would distinguish between NPCs (nestin), migratory neuroblasts (doublecortin), and astrocytes (glial fibrillary acidic protein; GFAP). Initial immunostaining observations demonstrated prominent immunopositive signal for each marker. Specifically, robust doublecortin staining was visualized in the corpus callosum above the lateral ventricle for each of the experimental groups that underwent CCI but notably not the naïve group (Fig. 3.15). This preliminary observation supports previous findings that report a CCI itself stimulates the ectopic neuroblast migration originating from the SVZ. Further, neuroblast presence was observed within the frontoparietal cortex for various experimental groups (Fig. 3.15; SDF-1a microgels). Our analyzed tissue sections thus far prove too small of a sample size for a full assessment of differences in neuroblast localization between groups. However, our initial findings warrant further quantification of doublecortin staining and localization within remaining tissue that has yet to be analyzed.

Likewise, we stained for the NPC marker nestin and found positively labeled cells in the corpus callosum and frontoparietal cortex in all groups except the naïve (Fig. 3.16). Again, our preliminary assessment confirms prominent nestin positive cells outside of the SVZ following CCI. Additional tissue staining and quantifications need to be completed to determine differences between the groups.

Lastly, we stained for GFAP to visualize the astroglial response following each condition. We found robust and complex GFAP signal patterns throughout the hippocampus, corpus callosum, and cortical tissue in all CCI groups. In contrast, significantly less GFAP signal was found in the naïve group (Fig. 3.17). This preliminary observation aligns with literature where astrogliosis is a hallmark following CCI. Further measurement and sample processing needs to be completed to determine how the hyaluronic acid microgels themselves and the SDF-1a impacted the astroglial response.

Our initial immunostaining preliminary data demonstrated prominent presence of doublecortin+, GFAP+, and nestin+ cells and near the injury cavity. To determine differences in these markers among groups, we must assess and compare the spatial distribution of these markers with respect to the injury lesion cavity and injection points – evaluate tissue spanning anterior to posterior of the peripheral injections (inclusive of injury). In addition, we will process remaining animals from each group to increase our sample size (currently processed 3 of 5 animals per group). We will assess spatial patterns of each marker across coronal sections and quantify regions of interest such as the cortex, hippocampus, corpus callosum, and subventricular zone. We will match anatomical locations between groups for quantification and normalize each tissue section to total tissue region area. Our output will be percent area of immunostaining for each group from a defined tissue region (+0.5mm to -2.0mm from bregma). A key component of this study is to determine the potential NPC migration following SDF-1a

delivery. Therefore, we will examine co-labeling of nestin and GFAP markers to distinguish between NPCs and astrocytes. Our approach will consider nestin+/GFAP- cells to be progenitor cells and nestin+/GFAP+ cells to be astrocytes. The imaging for our preliminary staining was conducted with an epifluorescence microscope. While this method provided macroscale confirmation of immunopositive staining, we recognize the limitations of this technique and acknowledge the potential need for image processing (i.e., deconvolution) or improved resolution via confocal microscopy to visualize colocalization of these markers.

Conclusion

SDF-1a delivery has been examined for several CNS interventions such as stroke, TBI, and spinal cord injury [7, 10, 148, 201]. We developed a tunable SDF-1a delivery platform using hyaluronic acid and microfluidics. We successfully generated injectable, monodisperse, and enzyme sensitive microgels to control the release of SDF-1a in a tunable manner. We began application of these SDF-1a microgels using a mouse TBI model to examine NPC recruitment. Preliminary immunohistochemistry (IHC) showed ectopically located neuroblasts, astrocytes, and possible NPCs. IHC marker validation was demonstrated by the presence of nestin, GFAP, and doublecortin surrounding the injury cavity. Further analysis of these markers, their localization, and their enumeration will be completed to determine differences between treatment groups and draw study conclusions. Prior publications have observed increased NPC recruitment following SDF-1a delivery in the injured CNS. For example, in a spinal cord injury model, delivery of SDF-1a via chondroitinase ABC led to the largest number of NPCs throughout the spinal cord compared to injury alone [133]. Another study found increased neuroblast presence in the cortical tissue following TBI and SDF-1a nanoparticle delivery [10]. Taking these results and our preliminary data into consideration, we anticipate we may

observe increased cell numbers near TBI lesions following SDF-1a microgel delivery. The long-term fate of these cells, their functional attributes, and impact on TBI functional recovery is beyond the scope of this dissertation and requires subsequent investigation.

Here, we focus on endogenous neurogenesis for TBI repair. However, NPCs may serve several pro-reparative purposes in addition to the generation of neurons following brain injury. For example, NPCs secrete many molecules that include neurotrophins and growth factors which improve cell survival and modulate the immune response [202–204]. Specifically, NPC transplantation is associated with decreased expression of pro-inflammatory molecules such as TNF-a and IL-6 following stroke [204]. NPCs also differentiate into glia which contribute to astrocytic scar formation, tissue remodeling via extracellular matrix breakdown, remyelination, and trophic support after brain injury [180, 205–207]. Altogether, increasing NPCs after TBI may result in functional improvements that are a consequence of not only newborn cell arrival and maturation to the injured tissue, but also their participation in forming a neuroprotective and reparative environment.

In the context of brain injury, SDF-1a signaling plays multiple roles. Here, we began investigating prolonging SDF-1a signaling to increase NPC arrival towards the injured cortex. However, extended SDF-1a delivery may further impact both brain repair and neuroinflammation. For instance, SDF-1a is a known chemoattractant to endothelial cells, where increasing endothelial cell recruitment may increase angiogenesis after brain injury [208]. In contrast, SDF-1a is a potent attractrant of immune cells after injury such as leukocytes which may contribute to sustained neuroinflammation [209, 210]. The multifaceted impact of SDF-1a should be considered so that the SDF-1a delivery timeline aligns with the acute phase of inflammation and does not persist to the chronic phase.

Brain injury incites a complex cascade of cellular and molecular players that participate in regeneration and degeneration processes over the course of years following initial insult [211]. Acute inflammation is necessary to remove cellular debris and separate healthy cells from the injury environment [212]. Further, complete knockout of pro-inflammatory cytokines like tumor necrosis factor lead to increased motor deficits and larger tissue loss after TBI compared to wild type counterparts [213]. This demonstrates the need for inflammation in the overall repair of TBI. However, chronic inflammation exacerbates cell death via mechanisms like metabolic dysfunction and excitotoxicity [214]. In utilizing SDF-1a delivery for increased NPC recruitment, we aim to aid the injury environment for regeneration yet acknowledge the implications it may have on neuroinflammation.

FIGURES

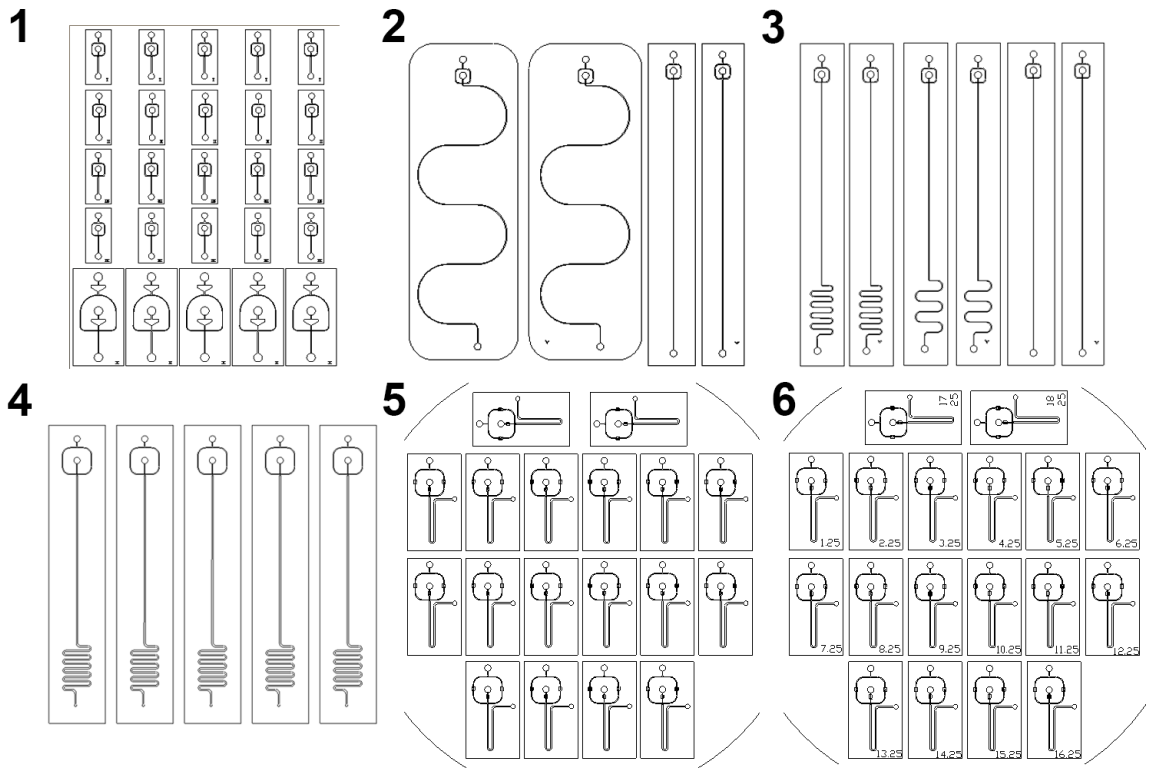

Figure 3.1. Microfluidic flow focusing design iterations. Major design iterations were made to determine the best design for microgel size, production, and stability.

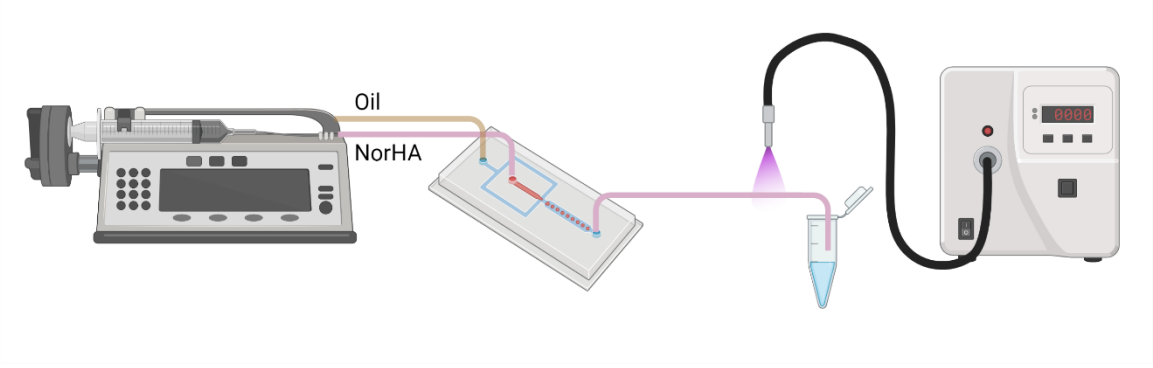

Figure 3.2. Microgel fabrication. A dual syringe pump is loaded with an oil phase and aqueous phase. The solutions are pumped simultaneously into a flow focusing microfluidics device to generate microgels. Microgels flow via outlet tubing and pass under UV light to become crosslinked prior to collection.

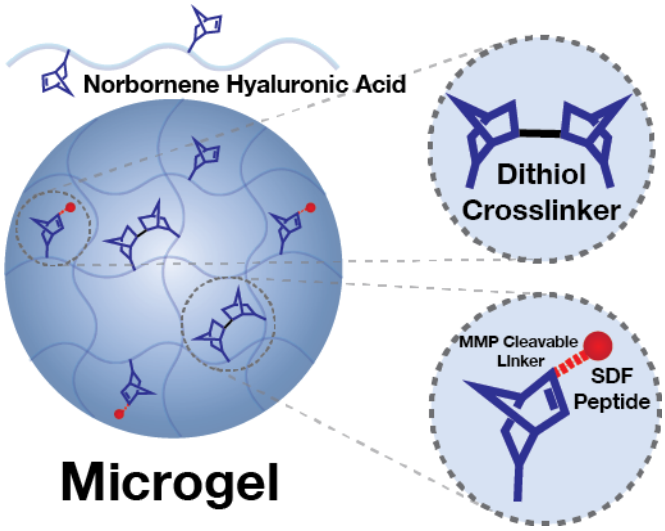

Figure 3.3. Microgel chemistry. A norbornene hyaluronic acid backbone is crosslinked by dithiol molecules. An SDF-1a peptide with a MMP cleavage site allows for controlled tethering and release of SDF-1a from remaining norbornene groups in the microgels.

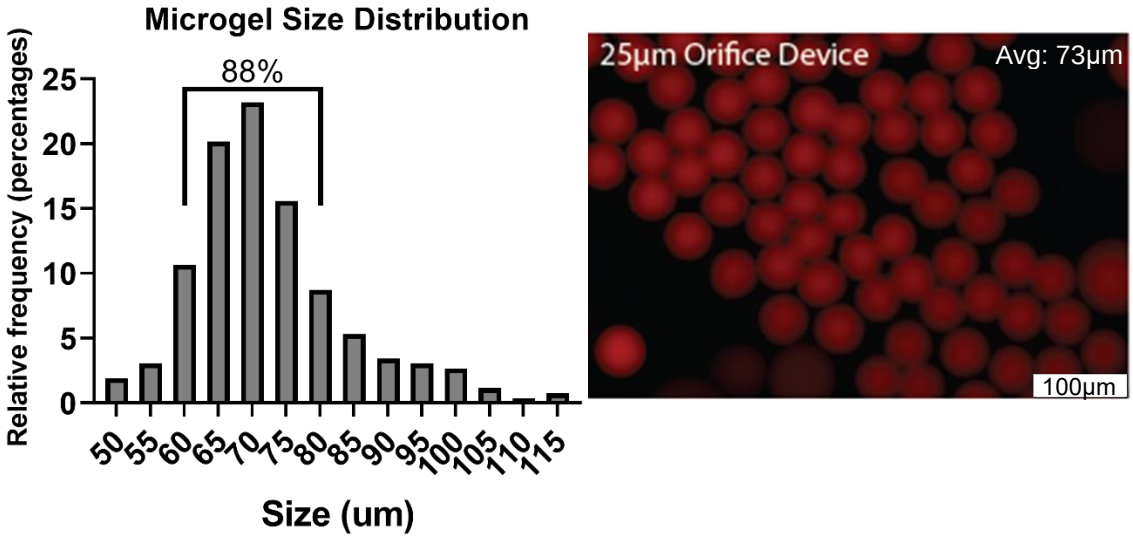

Figure 3.4. Flow focusing microfluidic devices generate monodisperse microgels. Microgels exhibit a narrow size distribution with 88% of microgels falling within 20µm size range (left). n = 263. Qualitative image of microgel monodispersity (right).

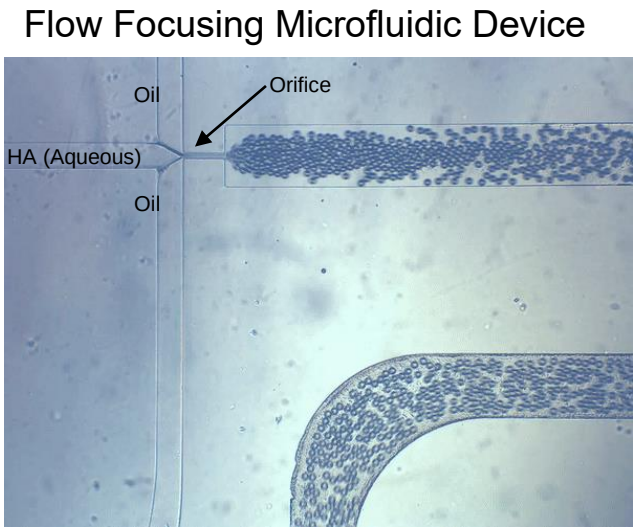

Figure 3.5. Flow focusing microfluidic device. Microgels are generated following the intersection of the oil and aqueous phase solutions. The device orifice partially dictates the overall microgel diameter.

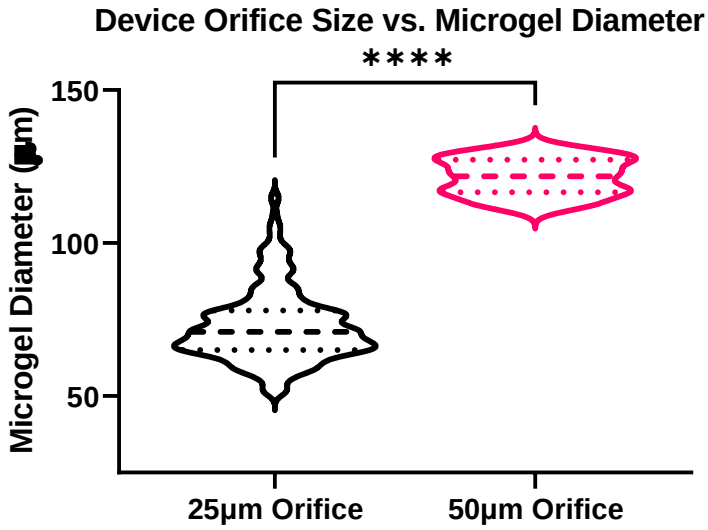

Figure 3.6. Device orifice size dictates microgel diameter. Microgel diameter increases significantly with increasing orifice size. Violin plot shows microgel size distribution where the average diameter microgels generated from the 25µm device and 50µm device are 73µm and 122µm respectively. ****p<.0001

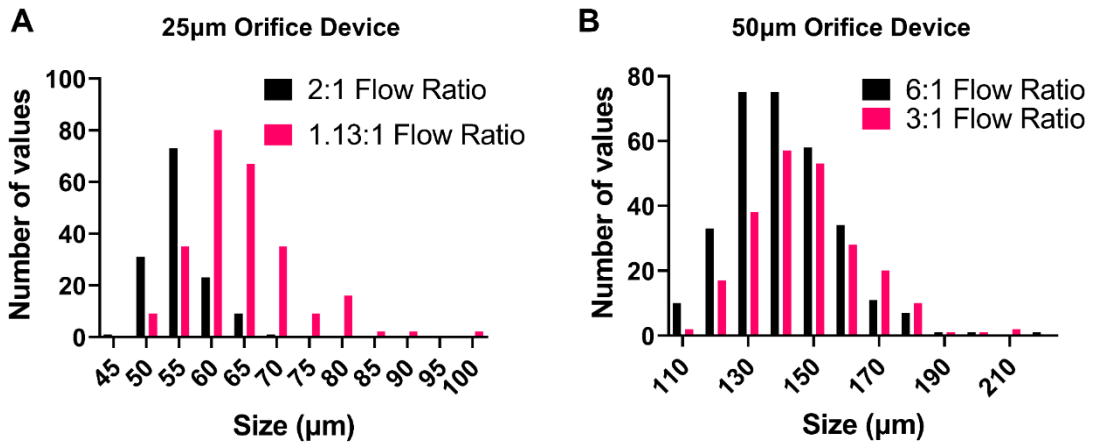

Figure 3.7. Flow rate ratio tunes microgel diameter. Microgel diameter decreases with increasing flow rate ratio (Oil:Aqueous). Microgel size distribution range decreases with increasing flow rate ratio for both the 25µm device (A) and 50µm device (B).

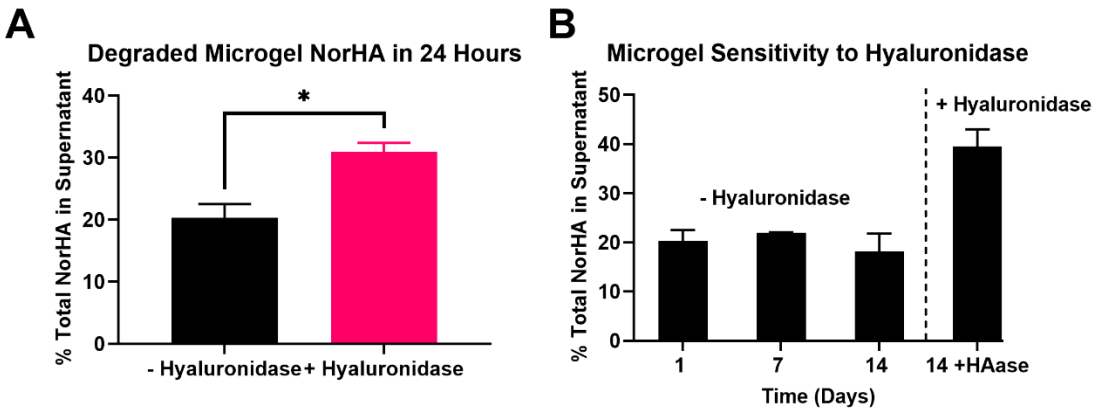

Figure 3.8. NorHA microgels degrade upon exposure to hyaluronidase. (A) The percentage of total NorHA in microgel supernatants was significantly higher in the group receiving hyaluronidase enzyme after 24 hours. (B) Microgels remain stable over 14 days without enzyme present and are degraded upon subsequent exposure to hyaluronidase. Mean ± SD, n = 3. *p<0.05

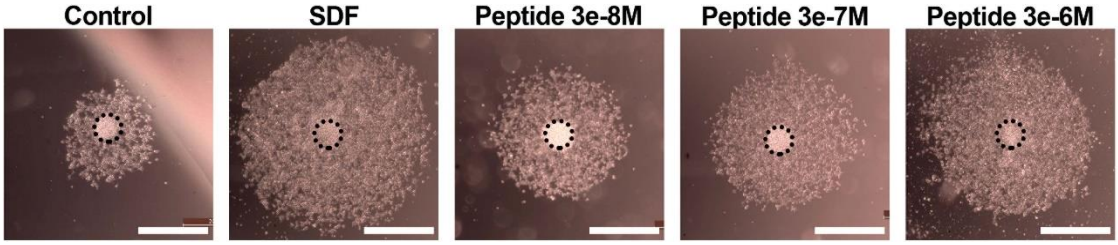

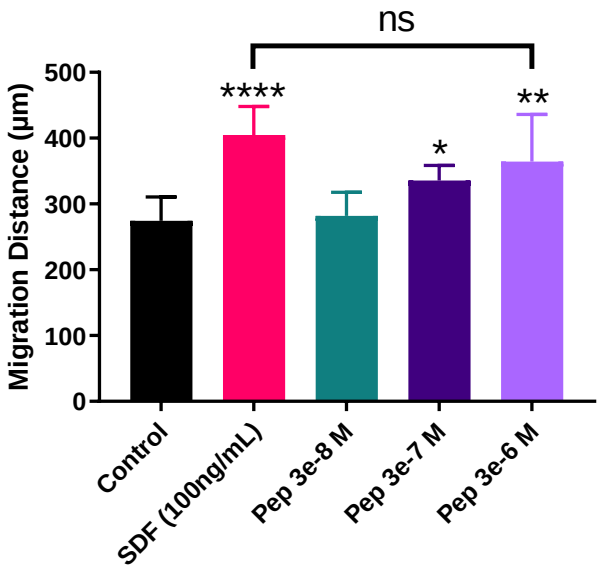

Figure 3.9. SDF-1a peptide activity is comparable to murine SDF-1a on neural stem cells. Representative images of neurosphere outgrowth following exposure to murine SDF-1a and SDF-1a peptide. Scale bar = 100µm (top). Murine SDF-1a, 3e-7M peptide, and 3e-6M peptide significantly increases outgrowth compared to control media (bottom). Mean ± SD, n = 5. *p<0.05 **p<0.01 ****p<0.0001

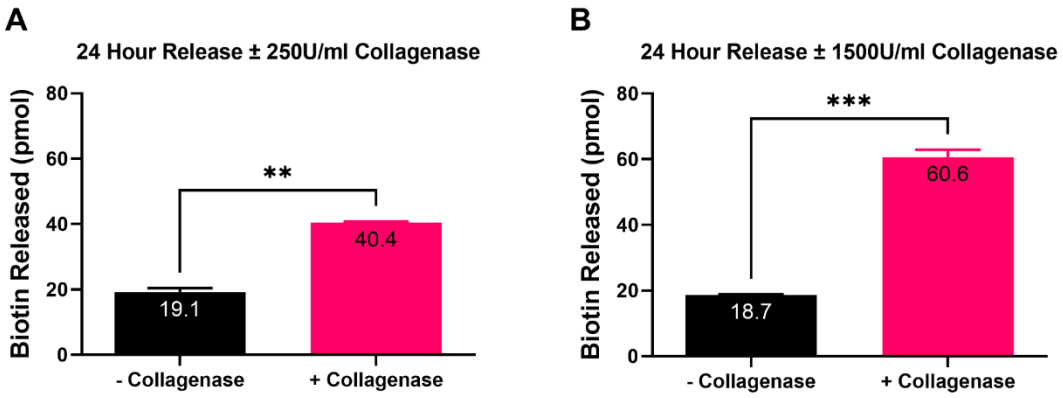

Figure 3.10. Microgel peptide release is dependent on MMP concentration. (A) The amount of biotin released in microgel supernatants was significantly higher in the group receiving 250U/ml collagenase (MMP) enzyme after 24 hours. (B) Microgels release more biotin in 24 hours with more concentrated enzyme present. Mean ± SD, n = 3. **p=0.022 ***p=0.0009

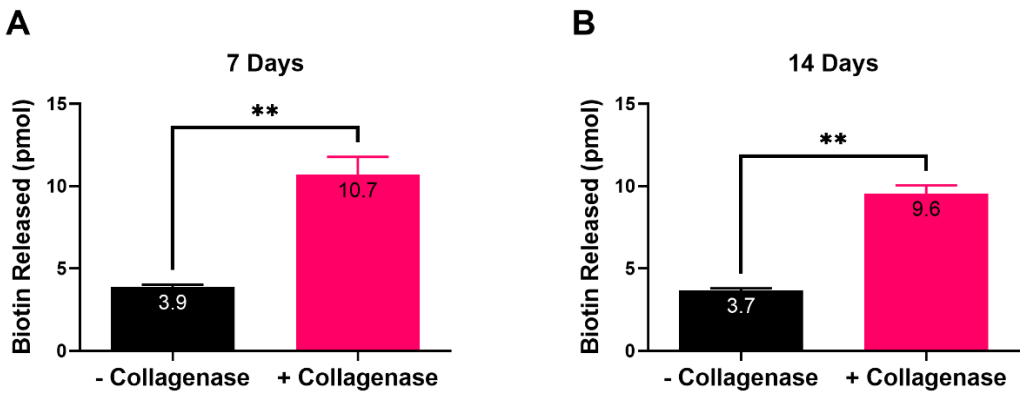

Figure 3.11. MMP sensitivity is retained across 14 days. Microgels show sustained MMP sensitivity upon delayed exposure (day 6 and 13) to collagenase for 24 hours (A; p=0.0067, B; p=0.0013). Mean ± SD, n = 3.

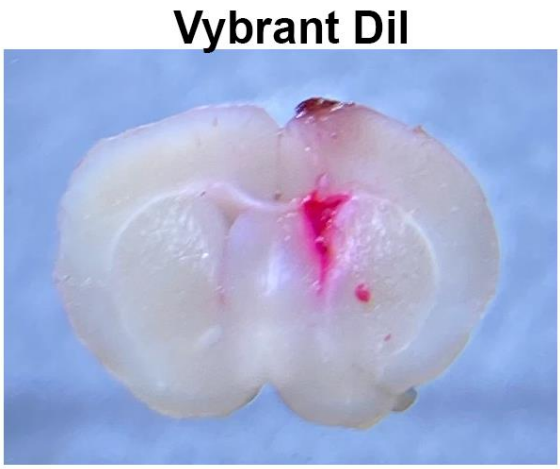

Figure 3.12. Verifying injection location with dil. Representative image of a coronal brain section injected with Vybrant Dil.

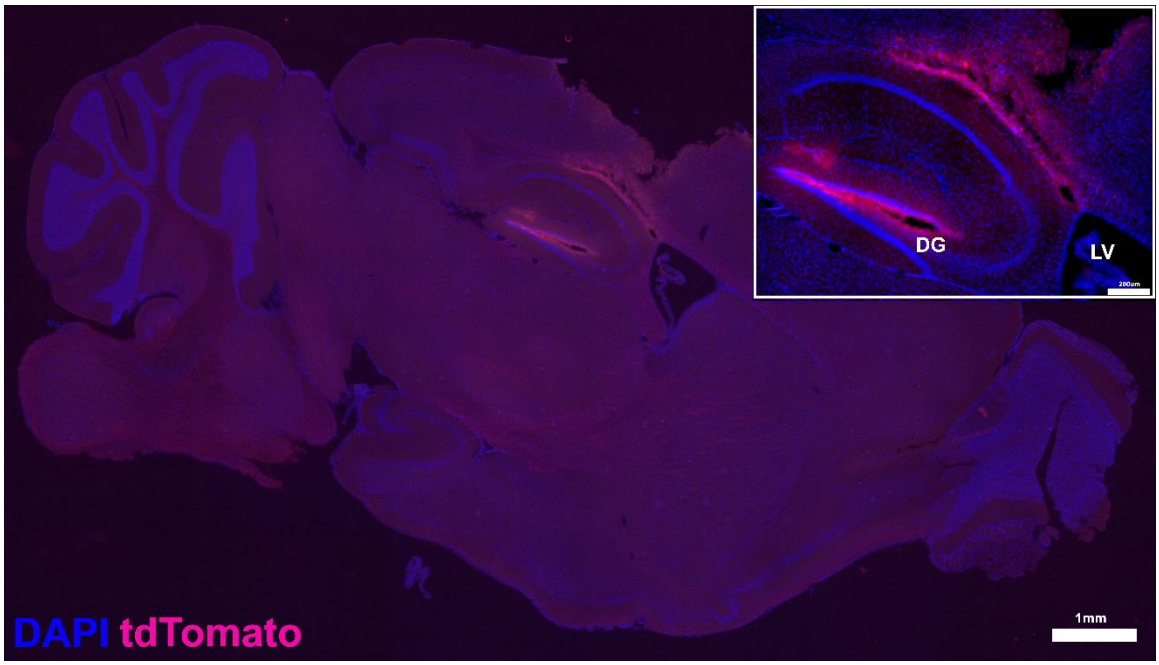

Figure 3.13. Verifying lentiviral particle labeling. Representative image of a saggital brain section injected with tdTomato lentiviral particles where the particles were incorrectly placed into the dentage gyrus (DG) instead of the lateral ventricle (LV).

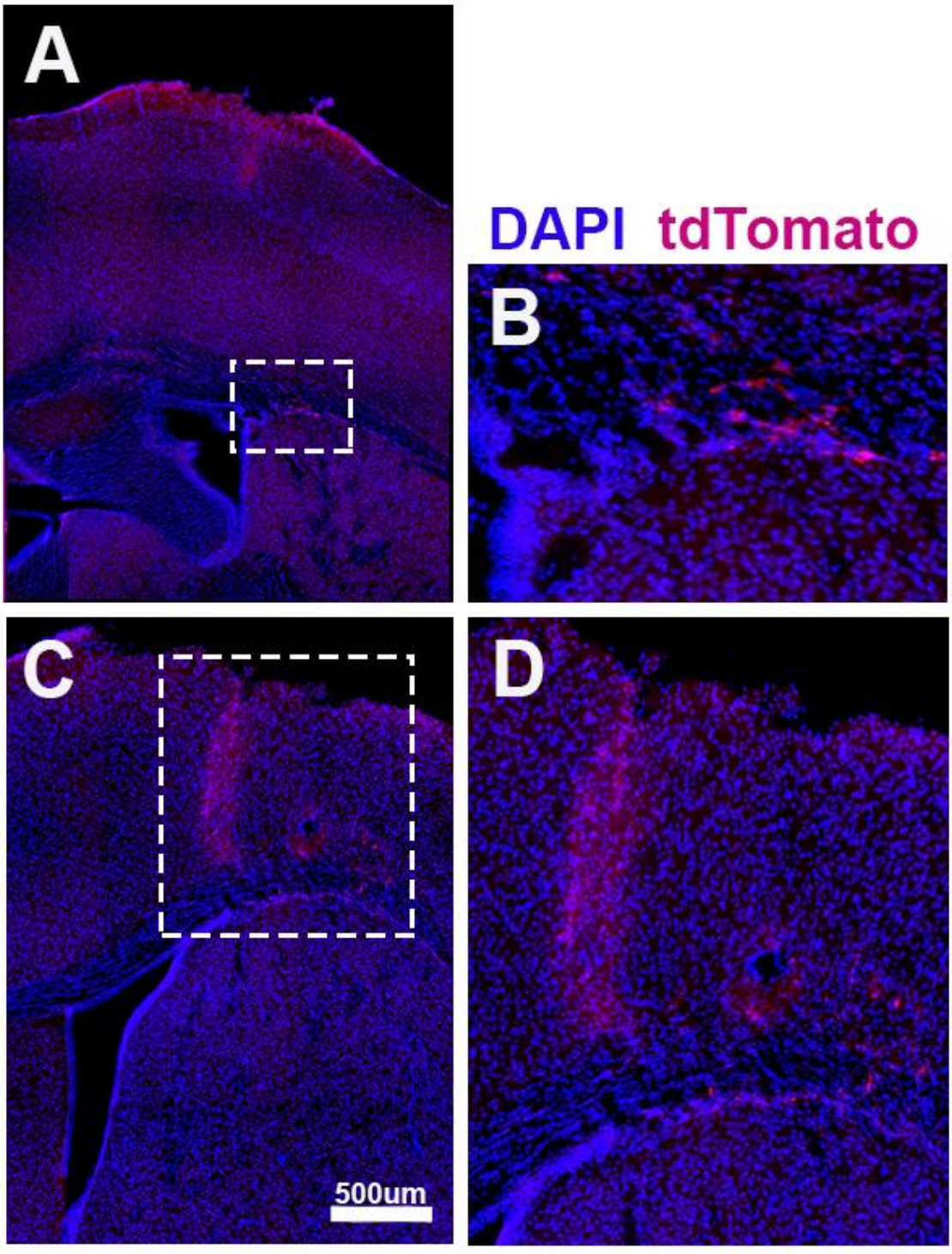

Figure 3.14. Re-assessing lentiviral particle labeling. Representative images of 2 brain coronal sections injected with tdTomato lentiviral particles where the particles. Possible labeling of SVZ derived cells (A, B) and significant labeling of cells local to the injection tract (C, D) are seen.

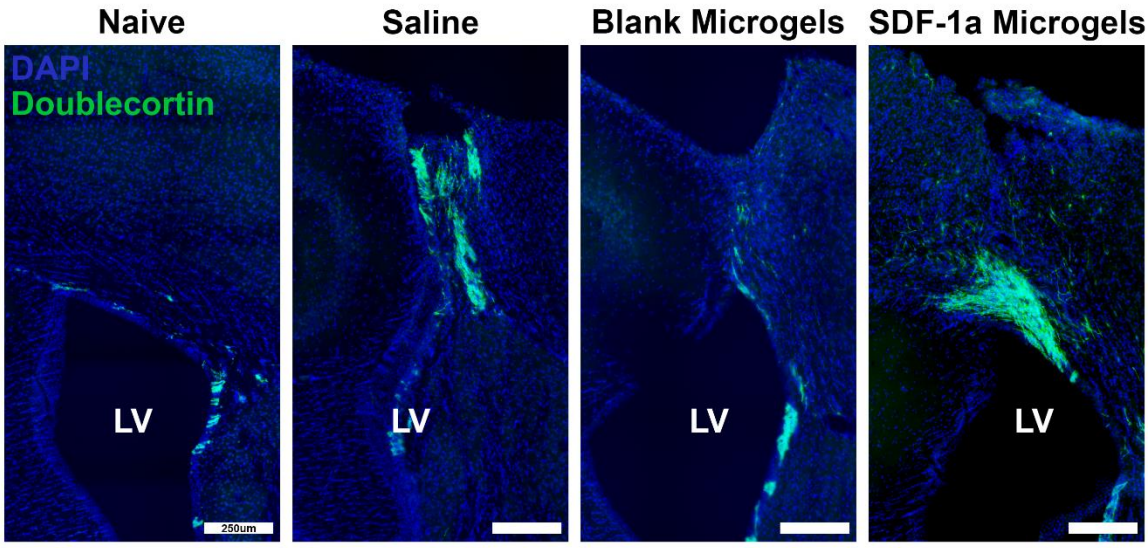

Figure 3.15. Doublecortin presence is found outside of the SVZ following CCI. Representative images of coronal sections from each experimental group. Doublecortin presence is apparent above the lateral ventricle for each of the groups except the naïve. Scale bar = 250μm

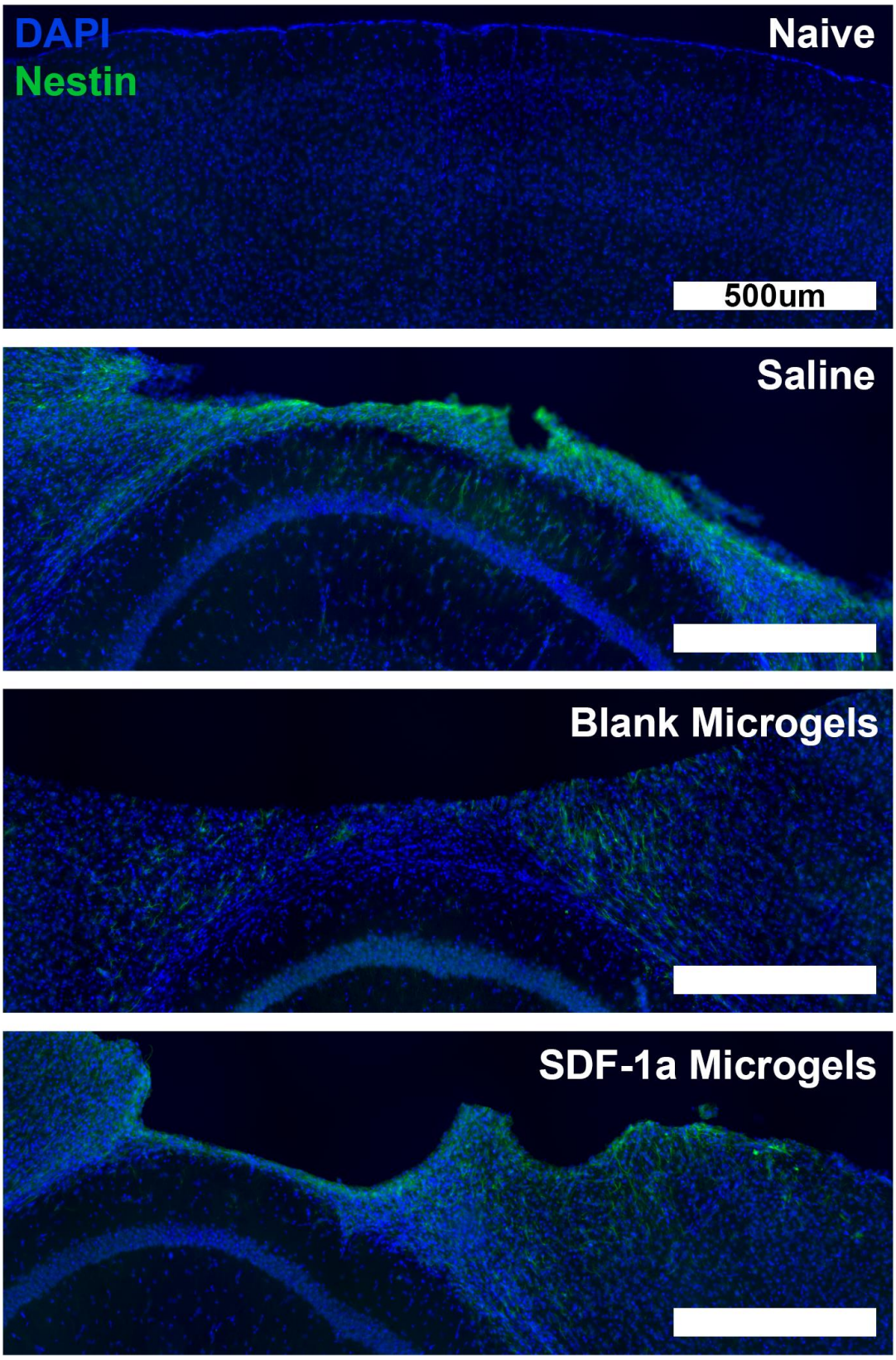
DAPI
Nestin
Naive
500um
Saline
Blank Microgels
SDF-1a Microgels

Figure 3.16. Nestin signal found in corpus callosum and cortex after CCI. Representative images of coronal sections from each experimental group. Nestin presence is found above the hippocampus for each of the groups except the naïve. Scale bar = 500μm.

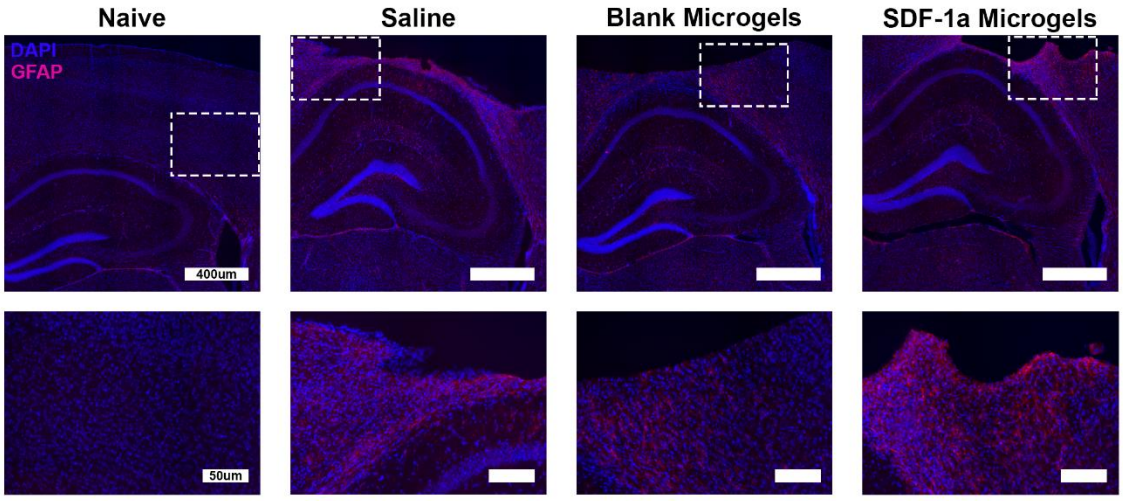

Figure 3.17. Robust GFAP signal found throughout cortex, corpus callosum, and hippocampus after CCI. Representative images of coronal sections from each experimental group. GFAP presence is apparent throughout the cortical tissue for each of the groups except the naïve. Enlargements (bottom) show GFAP signal dispersed throughout tissue for each group. Scale bar = 400μm (top) and 50μm (bottom).

CHAPTER 4

CONCLUSION

Summary of Findings

The potential for adult neurogenesis from the subventricular zone (SVZ) and dentate gyrus to repair neural injuries has been investigated over the last three decades, examining methods to increase neural progenitor cell (NPC) recruitment to injured tissue to reverse cell loss[81, 150, 215]. Current methods to attract more NPCs to the lesioned area include delivery of exogenous chemokine SDF-1a. These methods are limited by lack of understanding the mechanism of SDF-1a driven migration of NPCs to the cortex. The work described in this dissertation expands knowledge of SDF-1a/CXCR4 signaling in the brain by elucidating the contribution of autocrine/paracrine signaling to SDF-1a gradient formation and creates a mathematical model which may be used to test drug delivery strategies for SDF-1a signal propagation. To our knowledge, these are the first studies to suggest SDF-1a/CXCR4 autocrine/paracrine signal propagation across cortical tissue and emphasize its consideration in drug delivery strategies. Traditional drug delivery strategies for NPC recruitment are limited by an overall lack of tunability and variation in the drug carrier itself (i.e., particle size). Moreover, incorporating autocrine/paracrine signal dynamics may require increasingly complex drug release kinetics (i.e., pulsatile). This dissertation addresses the limitations of traditional drug delivery by developing a microfluidic platform that generates monodisperse microgels with tunable release of SDF-1a on demand.

First, we identify that sustained delivery of SDF-1a via PLGA nanoparticles aids in SDF-1a signal propagation *in vivo*. SDF-1a area immunostaining and CXCR4 cell density showed increased spatial and temporal presence following SDF-1a nanoparticle delivery vs. bolus delivery. This suggested that the presentation of exogenous SDF-1a was

key in sustaining SDF-1a levels across cortical tissue. We investigated how these SDF-1a gradients persist across cortical tissue using mathematical models and qPCR. We generated mathematical models that only incorporated SDF-1a diffusion kinetics and found they were not able to match the SDF-1a propagation observed *in vivo*. In contrast, models that included autocrine/paracrine kinetics were able to produce gradients resembling those found *in vivo*. We confirmed that cell types found within brain tissue could participate in SDF-1a/CXCR4 autocrine/paracrine signaling. We found that astrocytes, microglia, and endothelial cells change SDF-1a and CXCR4 expression dynamically over time after exposure to exogenous SDF-1a. These experiments suggested that autocrine/paracrine signaling contributes to SDF-1a gradients in the brain.

Next, we developed a biomaterial delivery platform with tunable properties for delivery of SDF-1a peptide. We generated a microfluidic flow focusing device that produced injectable (<100μm diameter) microgels made of norbornene hyaluronic acid polymer. The mean microgel diameter was 73μm with 88% of the microgel population within a 20μm size range. We investigated the tunability of our system and showed that microgel size could be adjusting by changing the device orifice size and altering the flow rate ratio between the phases of solution entering the device. Microgels produced with a larger orifice device resulted in larger diameter microgels on average than counterparts made in devices with a smaller orifice. A higher flow rate ratio (oil:polymer) resulted in a shift to smaller diameter microgels when using a device with the same orifice size. Microgels exhibited a significant increase in degradation following 24 hours of exposure to hyaluronidase enzyme. This characterized the microgels ability to degrade following exposure to associated enzymes and suggested microgels are capable of degradation *in vivo*.

A SDF-1a peptide was selected for incorporation into the microgels and to examine its impact on NPC migration *in vivo*. Unlike murine SDF-1a, SDF-1a peptide allowed for chemical modification and retained bioactivity. We chose modification of the SDF-1a peptide with a matrix metalloproteinase (MMP) cleavage site to increase SDF-1a stability and extend release from the microgels. The unprocessed form of the peptide significantly increased neurosphere outgrowth in vitro to comparable levels of murine SDF-1a, albeit at higher concentration. Nevertheless, the SDF-1a peptide demonstrated bioactivity. Incorporation of a biotin labeled SDF-1a peptide into the microgels enabled characterization of SDF-1a peptide release. After microgels were incubated in collagenase enzyme for 24 hours, significantly more biotin was quantified. Increasing the concentration of enzyme led to an increase in the amount of biotin released in 24 hours and determined the SDF-1a peptide loading capacity to be 65%. Delaying exposure of collagenase enzyme and administering it to microgels on day 13 of incubation revealed significantly more biotin than without enzyme exposure. This finding demonstrates that microgels generated with this system release SDF-1a peptide on demand and that MMP sensitivity it retained for at least 14 days.

We next investigated the SDF-1a peptide microgels on NPC migration following TBI. We performed a mouse model of TBI (controlled cortical impact) and injected saline, blank microgels, or SDF-1a peptide microgels into the injury periphery 7 days later. We compared these groups against a naïve control that did not receive a TBI. We analyzed tissue 7 days following injections and demonstrated positive signal for cell specific markers. We found robust doublecortin, GFAP, and nestin presence throughout the frontoparietal cortex in all groups except the naïve. This initial finding demonstrates the ability of the TBI alone to stimulate cells that may originate from the SVZ. Further analysis must be completed to conclude differences in the presence of neuroblasts,

astrocytes, and NPCs between experimental groups and to evaluate the complex cell type specific localization following this study.

This work achieved three goals: 1) elucidation of a mechanism of SDF-1a signal propagation in the brain, 2) the development of a biomaterial platform for precise, tunable delivery of SDF-1a peptide and other bioactive molecules, and 3) the preliminary assessment of SDF-1a microgel delivery on NPC migration. These findings emphasize the importance of innate cell signaling mechanics on chemokine delivery strategies and outcomes. Identifying the contribution of SDF-1a autocrine/paracrine signaling in gradient formation provides a new tool for future work to use to maximize delivery strategies and NPC recruitment. The mathematical model allows for testing of these strategies *in silico* and may refine strategies before attempting them *in vivo*. Microgels developed here are relevant not only to our immediate application, but to many regenerative applications needing controlled biomolecule delivery. Due to the tunability of the system generated, microgel stiffness, size, degradation, and molecule release can each be tailored to fit unique scenarios. Overall, the combination of new knowledge on SDF-1a propagation and new platforms to deliver exogenous SDF-1a has the potential to improve chemokine delivery for neural regeneration.

Future Work

High Throughput Microfluidic Flow Focusing Devices

The work described here presented a microfluidic flow focusing device to generate SDF-1a loaded microgels. To build upon this device design, higher microgel output over time would accelerate future application testing. The microgels presented here produce at a rate of 15μL/hour using a dual syringe pump to drive fluid input. Recent advances in microfluidics have proven useful for improved microgel output by incorporating design parallelization within existing devices[216, 217]. For example, a

study incorporating 8 devices in parallel generates similar size microgels at a rate of 600μL/hour[198]. Introducing multiple regions that produce droplets at the same time would require additional development but allow for faster production and testing of microgel batches with distinct features.

Next Generation Microgels for Complex Drug Release

As discussed in this dissertation, autocrine/paracrine signaling dynamics may present a need for complex drug release such as pulsatile release profiles to overcome ligand induced desensitization and receptor downregulation. This dissertation focused on delivering SDF-1a to make use of innate autocrine/paracrine propagation. That is, to delivery enough in a sustained fashion but not necessarily long term (over the course of weeks compared to months). A great opportunity to expand this work would be to examine how pulsatile release impacts SDF-1a propagation through the mathematical model created here and repeated gene expression studies. Limited research has investigated pulsatile release systems on cell migration and particularly NPC migration. Interestingly, one study has examined the effects of pulsatile SDF-1a release on prostate cancer cells *in vitro*[218]. The study found significantly higher cell directionality following pulsatile SDF-1a administration compared to steady release. These findings suggest that there is merit in studying pulsatile release systems for cell recruitment. To pursue this, modification of existing covalent bonds between the MMP cleavage site and SDF-1a peptide could be varied throughout the microgel. Distinct peptides could be generated that incorporate cleavage sites that are paired to enzymes that are expressed at different levels in the injury microenvironment or at different time points following injury. Further mathematical modeling testing and development of alternative microgel release schemes would increase our knowledge of the optimal chemokine delivery strategies for neural regeneration.

Application of Microgels to other Injury Models

Microgels generated in this dissertation were designed and evaluated for use in stimulating NPC migration following TBI. Being composed of native extracellular matrix protein hyaluronic acid and having tunable properties lends this system to be applied to a multitude of alternative applications. There are several ways by which this system can be adjusted. Generally, any biomolecule that can be modified with a thiol group can be coupled to the norbornene backbone of these microgels [219, 220]. Alternatively, these microgels could be produced with varying network properties and encapsulate molecules. In addition, these microgels can be tuned to achieve a desired mechanical stiffness, based upon their degree of crosslinking. Indeed, microgels have been utilized in other systems already, extending from delivery of tumor suppressing molecules to vocal fold regeneration[200, 221].

NPC Tracking

The adult SVZ is a heterogenous niche, comprised of several cells types that exist in multiple states (quiescent, activated). In addition, injury induced changes lead to consequent changes in the protein expression of cells originating from the SVZ[222]. There is no single marker that can identify and track NPCs exclusively[180, 205]. Taking this into consideration, immunohistochemical analysis of NPC migration is limited. Assumptions must be made on the origins of the labeled cells and the time point of assessment is critical to capture cells with distinct markers and phenotype. We attempted lentiviral labeling of the SVZ prior to performing TBI studies to decrease this limitation and found difficulty in accurately labeling the niche. This outcome is valid, considering the SVZ is a mere 5 cells diameters in thickness[223]. Efforts to label the much larger lateral ventricle have proven restricted to label only proximal ependymal cells[224]. Due to the complexity of the SVZ niche and the added changes caused by

neural injuries, improved labeling strategies would bolster NPC migration studies and facilitate quantification of NPCs. Across all possible labeling techniques, each one has pros and cons. For the purposes of this dissertation in particular, increased ability and clarity in counting cells from the SVZ would prove indispensable in drawing conclusions. A transgenic mouse line driven by the nestin gene has been created to aid in labeling cells of the SVZ niche[225]. Although nestin is expressed in multiple cell types of the SVZ and at varying stages, this nestin reporter mouse has a distinct advantage over other labeling methods. The fluorescent molecule driven by the nestin promoter is fused to a nuclear localization signal. This system labels nestin+ cell that is restricted to the nucleus and offers significantly improved enumeration. Additional immunohistochemistry and colocalization analysis would still be necessary to identify specific cell types but would be easier to visualize and assess overall.

REFERENCES

1. Faul M, Xu L, Wald M, Coronado V (2010) Traumatic Brain Injury in the United States: Emergency Department Visits, Hospitalizations and Deaths 2002–2006. Cent Dis Control Prev Natl Cent Inj Prev Control

2. Werner C, Engelhard K (2007) Pathophysiology of traumatic brain injury. Br J Anaesth 99:4–9. https://doi.org/10.1093/bja/aem131

3. Whitnall L, McMillan TM, Murray GD, Teasdale GM (2006) Disability in young people and adults after head injury: 5–7 year follow up of a prospective cohort study. J Neurol Neurosurg Psychiatry 77:640–645. https://doi.org/10.1136/jnnp.2005.078246

4. Kernie SG, Erwin TM, Parada LF Brain remodeling due to neuronal and astrocytic proliferation after controlled cortical injury in mice. J Neurosci Res 66:317–326. https://doi.org/10.1002/jnr.10013

5. Barone FC, Kilgore KS (2006) Role of inflammation and cellular stress in brain injury and central nervous system diseases. Clin Neurosci Res 6:329–356. https://doi.org/10.1016/j.cnr.2006.09.010

6. Itoh T, Satou T, Ishida H, et al (2009) The relationship between SDF-1/CXCR4 and neural stem cells appearing in damaged area after traumatic brain injury in rats. Neurol Res 31:90–102. https://doi.org/10.1179/174313208X332995

7. Sun W, Liu J, Huan Y, Zhang C (2014) Intracranial injection of recombinant stromal-derived factor-1 alpha (SDF-1?) attenuates traumatic brain injury in rats. Inflamm Res 63:287–297. https://doi.org/10.1007/s00011-013-0699-8

8. Itoh T, Imano M, Nishida S, et al (2013) Appearance of neural stem cells around the damaged area following traumatic brain injury in aged rats. J Neural Transm 120:361–374. https://doi.org/10.1007/s00702-012-0895-7

9. Yi X, Jin G, Zhang X, et al (2013) Cortical Endogenic Neural Regeneration of Adult Rat after Traumatic Brain Injury. PLOS ONE 8:e70306. https://doi.org/10.1371/journal.pone.0070306

10. Zamproni LN, Mundim MV, Porcionatto MA, des Rieux A (2017) Injection of SDF-1 loaded nanoparticles following traumatic brain injury stimulates neural stem cell recruitment. Int J Pharm 519:323–331. https://doi.org/10.1016/j.ijpharm.2017.01.036

11. Yu Q, Zhou L, Liu L, et al (2015) Stromal cell-derived factor-1 alpha alleviates hypoxic-ischemic brain damage in mice. Biochem Biophys Res Commun 464:447–452. https://doi.org/10.1016/j.bbrc.2015.06.135

12. Bernat-Peguera A, Simón-Extremera P, da Silva-Diz V, et al (2019) PDGFR-induced autocrine SDF-1 signaling in cancer cells promotes metastasis in advanced skin carcinoma. Oncogene 38:5021–5037. https://doi.org/10.1038/s41388-019-0773-y

13. Miyanishi N, Suzuki Y, Simizu S, et al (2010) Involvement of autocrine CXCL12/CXCR4 system in the regulation of ovarian carcinoma cell invasion. Biochem Biophys Res Commun 403:154–159. https://doi.org/10.1016/j.bbrc.2010.11.007

14. Mueller SG, White JR, Schraw WP, et al (1997) Ligand-induced desensitization of the human CXC chemokine receptor-2 is modulated by multiple serine residues in the carboxyl-terminal domain of the receptor. J Biol Chem 272:8207–8214

15. Park J, Lim E, Back S, et al (2010) Nerve regeneration following spinal cord injury using matrix metalloproteinase-sensitive, hyaluronic acid-based biomimetic hydrogel scaffold containing brain-derived neurotrophic factor. J Biomed Mater Res A 93A:1091–1099. https://doi.org/10.1002/jbm.a.32519

16. Tian WM, Hou SP, Ma J, et al (2005) Hyaluronic Acid–Poly-D-Lysine-Based Three-Dimensional Hydrogel for Traumatic Brain Injury. Tissue Eng 11:513–525. https://doi.org/10.1089/ten.2005.11.513

17. Wang Y, Cooke MJ, Morshead CM, Shoichet MS (2012) Hydrogel delivery of erythropoietin to the brain for endogenous stem cell stimulation after stroke injury. Biomaterials 33:2681–2692. https://doi.org/10.1016/j.biomaterials.2011.12.031

18. Litwiniuk M, Krejner A (2016) Hyaluronic Acid in Inflammation and Tissue Regeneration. 28:12

19. Abdul-Muneer PM, Conte AA, Haldar D, et al (2017) Traumatic brain injury induced matrix metalloproteinase2 cleaves CXCL12α (stromal cell derived factor 1α) and causes neurodegeneration. Brain Behav Immun 59:190–199. https://doi.org/10.1016/j.bbi.2016.09.002

20. Mao W, Yi X, Qin J, et al (2016) CXCL12/CXCR4 Axis Improves Migration of Neuroblasts Along Corpus Callosum by Stimulating MMP-2 Secretion After Traumatic Brain Injury in Rats. Neurochem Res 41:1315–1322. https://doi.org/10.1007/s11064-016-1831-2

21. Filippo TRM, Galindo LT, Barnabe GF, et al (2013) CXCL12 N-terminal end is sufficient to induce chemotaxis and proliferation of neural stem/progenitor cells. Stem Cell Res 11:913–925. https://doi.org/10.1016/j.scr.2013.06.003

22. Hayashi T, Kaneko Y, Yu S, et al (2009) Quantitative analyses of matrix metalloproteinase activity after traumatic brain injury in adult rats. Brain Res 1280:172–177. https://doi.org/10.1016/j.brainres.2009.05.040

23. Leber T (1981) The Origin of Inflammation. The Lancet 1:1446–1448

24. Florio T, Schettini G (2008) Chemokines, their receptors and significance in brain function. NeuroImmune Biol 6:242–273

25. Ubogu EE, Cossoy MB, Ransohoff RM (2006) The expression and function of chemokines involved in CNS inflammation. Trends Pharmacol Sci 27:48–55. https://doi.org/10.1016/j.tips.2005.11.002

26. Balabanian K, Lagane B, Infantino S, et al (2005) The Chemokine SDF-1/CXCL12 Binds to and Signals through the Orphan Receptor RDC1 in T Lymphocytes. J Biol Chem 280:35760–35766. https://doi.org/10.1074/jbc.M508234200

27. Kranich S, Hattermann K, Specht A, et al (2009) VEGFR-3/Flt-4 mediates proliferation and chemotaxis in glial precursor cells. Neurochem Int 55:747–753. https://doi.org/10.1016/j.neuint.2009.07.007

28. Forstreuter F, Lucius R, Mentlein R (2002) Vascular endothelial growth factor induces chemotaxis and proliferation of microglial cells. J Neuroimmunol 132:93–98

29. Garcia Lopez MA, Aguado Martinez A, Lamaze C, et al (2009) Inhibition of dynamin prevents CCL2-mediated endocytosis of CCR2 and activation of ERK1/2. Cell Signal 21:1748–1757. https://doi.org/10.1016/j.cellsig.2009.07.010

30. Zhou P, Porcionatto M, Pilapil M, et al (2007) Polarized Signaling Endosomes Coordinate BDNF-Induced Chemotaxis of Cerebellar Precursors. Neuron 55:53–68. https://doi.org/10.1016/j.neuron.2007.05.030

31. Funamoto S, Meili R, Lee S, et al (2002) Spatial and temporal regulation of 3-phosphoinositides by PI 3-kinase and PTEN mediates chemotaxis. Cell 109:611–623

32. Gardiner EM, Pestonjamasp KN, Bohl BP, et al (2002) Spatial and temporal analysis of Rac activation during live neutrophil chemotaxis. Curr Biol 12:2029–2034

33. Iglesias PA (2016) Dynamics of Gradient Sensing and Chemotaxis. In: Encyclopedia of Cell Biology. Elsevier, pp 4–9

34. Tan W, Martin D, Gutkind JS (2006) The Gα13-Rho Signaling Axis Is Required for SDF-1-induced Migration through CXCR4. J Biol Chem 281:39542–39549. https://doi.org/10.1074/jbc.M609062200

35. Chen L, Iijima M, Tang M, et al (2007) PLA2 and PI3K/PTEN Pathways Act in Parallel to Mediate Chemotaxis. Dev Cell 12:603–614. https://doi.org/10.1016/j.devcel.2007.03.005

36. Kamimura Y, Xiong Y, Iglesias PA, et al (2008) PIP3-Independent Activation of TorC2 and PKB at the Cell's Leading Edge Mediates Chemotaxis. Curr Biol 18:1034–1043. https://doi.org/10.1016/j.cub.2008.06.068

37. Sasaki AT, Firtel RA (2006) Regulation of chemotaxis by the orchestrated activation of Ras, PI3K, and TOR. Eur J Cell Biol 85:873–895. https://doi.org/10.1016/j.ejcb.2006.04.007

38. Sasaki AT, Chun C, Takeda K, Firtel RA (2004) Localized Ras signaling at the leading edge regulates PI3K, cell polarity, and directional cell movement. J Cell Biol 167:505–518. https://doi.org/10.1083/jcb.200406177

39. Ma Q, Jones D, Borghesani PR, et al (1998) Impaired B-lymphopoiesis, myelopoiesis, and derailed cerebellar neuron migration in CXCR4-and SDF-1-deficient mice. Proc Natl Acad Sci 95:9448–9453

40. Reiss K, Mentlein R, Sievers J, Hartmann D (2002) Stromal cell-derived factor 1 is secreted by meningeal cells and acts as chemotactic factor on neuronal stem cells of the cerebellar external granular layer. Neuroscience 115:295–305

41. Borghesani PR, Peyrin JM, Klein R, et al (2002) BDNF stimulates migration of cerebellar granule cells. Development 129:1435–1442

42. Tsai H-H, Frost E, To V, et al (2002) The chemokine receptor CXCR2 controls positioning of oligodendrocyte precursors in developing spinal cord by arresting their migration. Cell 110:373–383

43. Stumm RK, Zhou C, Ara T, et al (2003) CXCR4 regulates interneuron migration in the developing neocortex. J Neurosci 23:5123–5130

44. Gao X, Smith GM, Chen J (2009) Impaired dendritic development and synaptic formation of postnatal-born dentate gyrus granular neurons in the absence of brain-derived neurotrophic factor signaling. Exp Neurol 215:178–190. https://doi.org/10.1016/j.expneurol.2008.10.009

45. Li G, Adesnik H, Li J, et al (2008) Regional Distribution of Cortical Interneurons and Development of Inhibitory Tone Are Regulated by Cxcl12/Cxcr4 Signaling. J Neurosci 28:1085–1098. https://doi.org/10.1523/JNEUROSCI.4602-07.2008

46. Kokubo M, Nishio M, Ribar TJ, et al (2009) BDNF-Mediated Cerebellar Granule Cell Development Is Impaired in Mice Null for CaMKK2 or CaMKIV. J Neurosci 29:8901–8913. https://doi.org/10.1523/JNEUROSCI.0040-09.2009

47. Lois C, Alvarez-Buylla A (1994) Long-Distance Neuronal Migration in the Adult Mammalian Brain. Science 264:1145–1148

48. Wu W, Jin-hui Chen, Zhi-hong Jiang, et al (1999) Directional guidance of neuronal migration in the olfactory system by the protein Slit. Nature 400:331

49. Wittko IM, Schänzer A, Kuzmichev A, et al (2009) VEGFR-1 Regulates Adult Olfactory Bulb Neurogenesis and Migration of Neural Progenitors in the Rostral Migratory Stream In Vivo. J Neurosci 29:8704–8714. https://doi.org/10.1523/JNEUROSCI.5527-08.2009

50. Peng H, Huang Y, Rose J, et al (2004) Stromal cell-derived factor 1-mediated CXCR4 signaling in rat and human cortical neural progenitor cells. J Neurosci Res 76:35–50. https://doi.org/10.1002/jnr.20045

51. Tran PB, Ren D, Veldhouse TJ, Miller RJ (2004) Chemokine receptors are expressed widely by embryonic and adult neural progenitor cells. J Neurosci Res 76:20–34. https://doi.org/10.1002/jnr.20001

52. Faiz M, Acarin L, Villapol S, et al (2008) Substantial migration of SVZ cells to the cortex results in the generation of new neurons in the excitotoxically damaged immature rat brain. Mol Cell Neurosci 38:170–182. https://doi.org/10.1016/j.mcn.2008.02.002

53. Gordon RJ, Tattersfield AS, Vazey EM, et al (2007) Temporal profile of subventricular zone progenitor cell migration following quinolinic acid–induced striatal cell loss. Neuroscience 146:1704–1718. https://doi.org/10.1016/j.neuroscience.2007.03.011

54. Guillemin GJ, Croitoru-Lamoury J, Dormont D, et al (2003) Quinolinic acid upregulates chemokine production and chemokine receptor expression in astrocytes. Glia 41:371–381. https://doi.org/10.1002/glia.10175

55. Saha B, Peron S, Murray K, et al (2013) Cortical lesion stimulates adult subventricular zone neural progenitor cell proliferation and migration to the site of injury. Stem Cell Res 11:965–977. https://doi.org/10.1016/j.scr.2013.06.006

56. Wang Y, Deng Y, Zhou G-Q (2008) SDF-1α/CXCR4-mediated migration of systemically transplanted bone marrow stromal cells towards ischemic brain lesion in a rat model. Brain Res 1195:104–112. https://doi.org/10.1016/j.brainres.2007.11.068

57. Imitola J, Raddassi K, Park KI, et al (2004) Directed migration of neural stem cells to sites of CNS injury by the stromal cell-derived factor 1α/CXC chemokine receptor 4 pathway. Proc Natl Acad Sci 101:18117–18122

58. Yan Y-P, Sailor KA, Lang BT (2007) Monocyte chemoattractant protein-1 plays a critical role in neuroblast migration after focal cerebral ischemia. J Cereb Blood Flow Metab 27:1213–1224

59. Zhang L, Hua Q, Tang K, et al (2016) CXCR4 activation promotes differentiation of human embryonic stem cells to neural stem cells. Neuroscience 337:88–97. https://doi.org/10.1016/j.neuroscience.2016.09.001

60. Ardelt AA, Bhattacharyya BJ, Belmadani A, et al (2013) Stromal derived growth factor-1 (CXCL12) modulates synaptic transmission to immature neurons during post-ischemic cerebral repair. Exp Neurol 248:246–253. https://doi.org/10.1016/j.expneurol.2013.06.017

61. Opatz J, Kury P, Schiwy N, et al (2009) SDF-1 stimulates neurite growth on inhibitory CNS myelin. Mol Cell Neurosci 40:293–300. https://doi.org/10.1016/j.mcn.2008.11.002

62. Liu KKY, Dorovini-Zis K (2009) Regulation of CXCL12 and CXCR4 expression by human brain endothelial cells and their role in CD4+ and CD8+ T cell adhesion

and transendothelial migration. J Neuroimmunol 215:49–64. https://doi.org/10.1016/j.jneuroim.2009.08.003

63. Teng L, Fu H, Deng C, et al (2015) Modulating the SDF-1/CXCL12-induced cancer cell growth and adhesion by sulfated K5 polysaccharides in vitro. Biomed Pharmacother 73:29–34. https://doi.org/10.1016/j.biopha.2015.05.009

64. Belmadani A, Ren D, Bhattacharyya BJ, et al (2015) Identification of a sustained neurogenic zone at the dorsal surface of the adult mouse hippocampus and its regulation by the chemokine SDF-1: SDF-1 Signaling and the Subhippocampal Zone. Hippocampus 25:1224–1241. https://doi.org/10.1002/hipo.22428

65. Gong X, He X, Qi L, et al (2006) Stromal cell derived factor-1 acutely promotes neural progenitor cell proliferation in vitro by a mechanism involving the ERK1/2 and PI-3K signal pathways. Cell Biol Int 30:466–471. https://doi.org/10.1016/j.cellbi.2006.01.007

66. Kokovay E, Goderie S, Wang Y, et al (2010) Adult SVZ Lineage Cells Home to and Leave the Vascular Niche via Differential Responses to SDF1/CXCR4 Signaling. Cell Stem Cell 7:163–173. https://doi.org/10.1016/j.stem.2010.05.019

67. Addington CP, Pauken CM, Caplan MR, Stabenfeldt SE (2014) The role of SDF-1α–ECM crosstalk in determining neural stem cell fate. Biomaterials 35:3263–3272. https://doi.org/10.1016/j.biomaterials.2013.12.102

68. Barkho BZ, Munoz AE, Li X, et al (2008) Endogenous Matrix Metalloproteinase (MMP)-3 and MMP-9 Promote the Differentiation and Migration of Adult Neural Progenitor Cells in Response to Chemokines. Stem Cells Dayt Ohio 26:3139–3149. https://doi.org/10.1634/stemcells.2008-0519

69. Addington CP, Dharmawaj S, Heffernan JM, et al (2017) Hyaluronic acid-laminin hydrogels increase neural stem cell transplant retention and migratory response to SDF-1α. Matrix Biol 60–61:206–216. https://doi.org/10.1016/j.matbio.2016.09.007

70. Hartman NW, Carpentino JE, LaMonica K, et al (2010) CXCL12-Mediated Guidance of Migrating Embryonic Stem Cell-Derived Neural Progenitors Transplanted into the Hippocampus. PLoS ONE 5:e15856. https://doi.org/10.1371/journal.pone.0015856

71. Li S, Wei M, Zhou Z, et al (2012) SDF-1α induces angiogenesis after traumatic brain injury. Brain Res 1444:76–86. https://doi.org/10.1016/j.brainres.2011.12.055

72. Weiss JM, Downie SA, Lyman WD, Berman JW (1998) Astrocyte Derived Monocyte Chemoattractant Protein-1 Directs the Transmigration of Leukocytes Across a Model of the Human Blood-Brain Barrier. J Immunol 161:6896–6903

73. Glabinski AR, Balasingam V, Tani M, et al (1996) Chemokine monocyte chemoattractant protein-1 is expressed by astrocytes after mechanical injury to the brain. J Immunol 156:4363–4368

74. Lee YL, Shih K, Bao P, et al (2000) Cytokine chemokine expression in contused rat spinal cord. Neurochem Int 36:417–425

75. Widera D, Holtkamp W, Entschladen F, et al (2004) MCP-1 induces migration of adult neural stem cells. Eur J Cell Biol 83:381–387

76. Harrison JK, Jiang Y, Chen S, et al (1998) Role for neuronally derived fractalkine in mediating interactions between neurons and CX3CR1-expressing microglia. Proc Natl Acad Sci 95:10896–10901

77. Maciejewski-Lenoir D, Chen S, Feng L, et al (1999) Characterization of fractalkine in rat brain cells: migratory and activation signals for CX3CR-1-expressing microglia. J Immunol 163:1628–1635

78. Liu Y-Z, Wang C, Wang Q, et al (2017) Role of fractalkine/CX3CR1 signaling pathway in the recovery of neurological function after early ischemic stroke in a rat model. Life Sci 184:87–94. https://doi.org/10.1016/j.lfs.2017.06.012

79. Pan Y, Lloyd C (1997) Neurotactin, a membrane-anchored chemokine upregulated in brain inflammation. Nature 387:611

80. Zhu J, Zhou Z, Liu Y, Zheng J (2009) Fractalkine and CX3CR1 are involved in the migration of intravenously grafted human bone marrow stromal cells toward ischemic brain lesion in rats. Brain Res 1287:173–183. https://doi.org/10.1016/j.brainres.2009.06.068

81. Qin W, Li Z, Luo S, et al (2014) Exogenous fractalkine enhances proliferation of endothelial cells, promotes migration of endothelial progenitor cells and improves neurological deficits in a rat model of ischemic stroke. Neurosci Lett 569:80–84. https://doi.org/10.1016/j.neulet.2014.03.052

82. Wang Y-Q, Cui H-R, Yang S-Z, et al (2009) VEGF enhance cortical newborn neurons and their neurite development in adult rat brain after cerebral ischemia. Neurochem Int 55:629–636. https://doi.org/10.1016/j.neuint.2009.06.007

83. Fournier NM, Lee B, Banasr M, et al (2012) Vascular endothelial growth factor regulates adult hippocampal cell proliferation through MEK/ERK- and PI3K/Akt-dependent signaling. Neuropharmacology 63:642–652. https://doi.org/10.1016/j.neuropharm.2012.04.033

84. Jin K, Zhu Y, Sun Y, et al (2002) Vascular endothelial growth factor (VEGF) stimulates neurogenesis in vitro and in vivo. Proc Natl Acad Sci 99:11946–11950

85. Sun Y, Jin K, Xie L, et al (2003) VEGF-induced neuroprotection, neurogenesis, and angiogenesis after focal cerebral ischemia. J Clin Invest 111:1843–1851. https://doi.org/10.1172/JCI200317977

86. Bozoyan L, Khlghatyan J, Saghatelyan A (2012) Astrocytes Control the Development of the Migration-Promoting Vasculature Scaffold in the Postnatal Brain via VEGF Signaling. J Neurosci 32:1687–1704. https://doi.org/10.1523/JNEUROSCI.5531-11.2012

87. Sun J, Sha B, Zhou W, Yang Y (2010) VEGF-mediated angiogenesis stimulates neural stem cell proliferation and differentiation in the premature brain. Biochem Biophys Res Commun 394:146–152. https://doi.org/10.1016/j.bbrc.2010.02.132

88. Thau-Zuchman O, Shohami E, Alexandrovich AG, Leker RR (2010) Vascular endothelial growth factor increases neurogenesis after traumatic brain injury. J Cereb Blood Flow Metab 30:1008–1016

89. Cheng P-L, Song A-H, Wong Y-H, et al (2011) Self-amplifying autocrine actions of BDNF in axon development. Proc Natl Acad Sci 108:18430–18435. https://doi.org/10.1073/pnas.1115907108

90. Wang H, Ward N, Boswell M, Katz DM (2006) Secretion of brain-derived neurotrophic factor from brain microvascular endothelial cells: BDNF release in brain endothelial cells. Eur J Neurosci 23:1665–1670. https://doi.org/10.1111/j.1460-9568.2006.04682.x

91. Bath KG, Mandairon N, Jing D, et al (2008) Variant Brain-Derived Neurotrophic Factor (Val66Met) Alters Adult Olfactory Bulb Neurogenesis and Spontaneous Olfactory Discrimination. J Neurosci 28:2383–2393. https://doi.org/10.1523/JNEUROSCI.4387-07.2008

92. Grade S, Weng YC, Snapyan M, et al (2013) Brain-Derived Neurotrophic Factor Promotes Vasculature-Associated Migration of Neuronal Precursors toward the Ischemic Striatum. PLoS ONE 8:e55039. https://doi.org/10.1371/journal.pone.0055039

93. Cook DJ, Nguyen C, Chun HN, et al (2017) Hydrogel-delivered brain-derived neurotrophic factor promotes tissue repair and recovery after stroke. J Cereb Blood Flow Metab 37:1030–1045. https://doi.org/10.1177/0271678X16649964

94. Wang Y, Cooke MJ, Lapitsky Y, et al (2011) Transport of epidermal growth factor in the stroke-injured brain. J Controlled Release 149:225–235. https://doi.org/10.1016/j.jconrel.2010.10.022

95. Jin Y (2002) Transplants of Fibroblasts Genetically Modified to Express BDNF Promote Axonal Regeneration from Supraspinal Neurons Following Chronic Spinal Cord Injury. Exp Neurol 177:265–275. https://doi.org/10.1006/exnr.2002.7980

96. Cooke MJ, Wang Y, Morshead CM, Shoichet MS (2011) Controlled epi-cortical delivery of epidermal growth factor for the stimulation of endogenous neural stem cell proliferation in stroke-injured brain. Biomaterials 32:5688–5697. https://doi.org/10.1016/j.biomaterials.2011.04.032

97. Adelita T, Stilhano RS, Han SW, et al (2017) Proteolytic processed form of CXCL12 abolishes migration and induces apoptosis in neural stem cells in vitro. Stem Cell Res 22:61–69. https://doi.org/10.1016/j.scr.2017.05.013

98. Dean RA, Cox JH, Bellac CL, et al (2008) Macrophage-specific metalloelastase (MMP-12) truncates and inactivates ELR+ CXC chemokines and generates CCL2, -

7, -8, and -13 antagonists: potential role of the macrophage in terminating polymorphonuclear leukocyte influx. Blood 112:3455–3464. https://doi.org/10.1182/blood-2007-12-129080

99. Luker KE, Steele JM, Mihalko LA, et al (2010) Constitutive and chemokine-dependent internalization and recycling of CXCR7 in breast cancer cells to degrade chemokine ligands. Oncogene 29:4599–4610

100. Emerich DF, Silva E, Ali O, et al (2010) Injectable VEGF Hydrogels Produce Near Complete Neurological and Anatomical Protection following Cerebral Ischemia in Rats. Cell Transplant 19:1063–1071. https://doi.org/10.3727/096368910X498278

101. McQuibban GA, Gong J-H, Wong JP, et al (2002) Matrix metalloproteinase processing of monocyte chemoattractant proteins generates CC chemokine receptor antagonists with anti-inflammatory properties in vivo. Blood 100:1160–1167

102. Guilfoyle MR, Carpenter KLH, Helmy A, et al (2015) Matrix Metalloproteinase Expression in Contusional Traumatic Brain Injury: A Paired Microdialysis Study. J Neurotrauma 32:1553–1559. https://doi.org/10.1089/neu.2014.3764

103. Dong X, Song Y-N, Liu W-G, Guo X-L (2009) MMP-9, a Potential Target for Cerebral Ischemic Treatment. Curr Neuropharmacol 7:269–275. https://doi.org/10.2174/157015909790031157

104. Leppert D, Ford J, Stabler G, Grygar C (1998) Matrix metalloproteinase-9 (gelatinase B) is selectively elevated in CSF during relapses and stable phases of multiple sclerosis. Brain 121:2327–2334

105. Leake A, Morris CM, Whateley J (2000) Brain matrix metalloproteinase 1 levels are elevated in Alzheimer's disease. Neurosci Lett 291:201–203

106. Delgado MB, Clark-Lewis I, Loetscher P, et al (2001) Rapid inactivation of stromal cell-derived factor-1 by cathepsin G associated with lymphocytes. Eur J Immunol 31:699–707. https://doi.org/10.1002/1521-4141(200103)31:3<699::AID-IMMU699>3.0.CO;2-6

107. Padrines M, Wolf M, Walz A, Baggiolini M (1994) Interleukin-8 processing by neutrophil elastase, cathepsin G and proteinase-3. FEBS Lett 352:231–235

108. Starr AE, Dufour A, Maier J, Overall CM (2012) Biochemical Analysis of Matrix Metalloproteinase Activation of Chemokines CCL15 and CCL23 and Increased Glycosaminoglycan Binding of CCL16. J Biol Chem 287:5848–5860. https://doi.org/10.1074/jbc.M111.314609

109. Dutta D, Fauer C, Mulleneux HL, Stabenfeldt SE (2015) Tunable controlled release of bioactive SDF-1α via specific protein interactions within fibrin/nanoparticle composites. J Mater Chem B 3:7963–7973. https://doi.org/10.1039/C5TB00935A

110. Zimmermann N, Conkright JJ, Rothenberg ME (1999) CC Chemokine Receptor-3 Undergoes Prolonged Ligand-induced Internalization. J Biol Chem 274:12611–12618. https://doi.org/10.1074/jbc.274.18.12611

111. Weber M, Blair E, Simpson CV, et al (2004) The Chemokine Receptor D6 Constitutively Traffics to and from the Cell Surface to Internalize and Degrade Chemokines. Mol Biol Cell 15:2492–2508. https://doi.org/10.1091/mbc.E03-09-0634

112. Berchiche YA, Gravel S, Pelletier M-E, et al (2011) Different Effects of the Different Natural CC Chemokine Receptor 2b Ligands on -Arrestin Recruitment, G i Signaling, and Receptor Internalization. Mol Pharmacol 79:488–498. https://doi.org/10.1124/mol.110.068486

113. Meiser A, Mueller A, Wise EL, et al (2008) The Chemokine Receptor CXCR3 is Degraded Following Internalization and is Repelenished at the Cell Surface by De Novo Synthesis of Receptor. J Immunol Baltim Md 1950 180:6713–6724

114. Fan G-H, Lapierre LA, Goldenring JR, Richmond A (2003) Differential regulation of CXCR2 trafficking by Rab GTPases. Blood 101:2115–2124. https://doi.org/10.1182/blood-2002-07-1965

115. Connon CJ, Hamley IW (2014) Hydrogels in Cell-Based Therapies. In: RSC Soft Matter Series. Royal Society of Chemistry, Cambridge, pp P001–P004

116. Raja WK, Gligorijevic B, Wyckoff J, et al (2010) A new chemotaxis device for cell migration studies. Integr Biol Quant Biosci Nano Macro 2:696–706. https://doi.org/10.1039/c0ib00044b

117. Wu Y, Joseph S, Aluru NR (2009) Effect of Cross-Linking on the Diffusion of Water, Ions, and Small Molecules in Hydrogels. J Phys Chem B 113:3512–3520. https://doi.org/10.1021/jp808145x

118. Lim TC, Rokkappanavar S, Toh WS, et al (2013) Chemotactic recruitment of adult neural progenitor cells into multifunctional hydrogels providing sustained SDF-1 release and compatible structural support. FASEB J 27:1023–1033. https://doi.org/10.1096/fj.12-221515

119. Silva EA, Mooney DJ (2007) Spatiotemporal control of vascular endothelial growth factor delivery from injectable hydrogels enhances angiogenesis. J Thromb Haemost 5:590–598. https://doi.org/10.1111/j.1538-7836.2007.02386.x

120. Jain A, Kim Y-T, McKeon RJ, Bellamkonda RV (2006) In situ gelling hydrogels for conformal repair of spinal cord defects, and local delivery of BDNF after spinal cord injury. Biomaterials 27:497–504. https://doi.org/10.1016/j.biomaterials.2005.07.008

121. Gupta D, Tator CH, Shoichet MS (2006) Fast-gelling injectable blend of hyaluronan and methylcellulose for intrathecal, localized delivery to the injured spinal cord. Biomaterials 27:2370–2379. https://doi.org/10.1016/j.biomaterials.2005.11.015

122. Li H, Ham TR, Neill N, et al (2016) A Hydrogel Bridge Incorporating Immobilized Growth Factors and Neural Stem/Progenitor Cells to Treat Spinal Cord Injury. Adv Healthc Mater 5:802–812. https://doi.org/10.1002/adhm.201500810

123. Parker J, Mitrousis N, Shoichet MS (2016) Hydrogel for Simultaneous Tunable Growth Factor Delivery and Enhanced Viability of Encapsulated Cells *in Vitro*. Biomacromolecules 17:476–484. https://doi.org/10.1021/acs.biomac.5b01366

124. Enam SF, Krieger JR, Saxena T, et al (2017) Enrichment of endogenous fractalkine and anti-inflammatory cells via aptamer-functionalized hydrogels. Biomaterials 142:52–61. https://doi.org/10.1016/j.biomaterials.2017.07.013

125. Singh R, Lillard JW (2009) Nanoparticle-based targeted drug delivery. Exp Mol Pathol 86:215–223. https://doi.org/10.1016/j.yexmp.2008.12.004

126. Bharadwaj VN, Lifshitz J, Adelson PD, et al (2016) Temporal assessment of nanoparticle accumulation after experimental brain injury: Effect of particle size. Sci Rep 6:29988

127. Dutta D, Hickey K, Salifu M, et al (2017) Spatiotemporal presentation of exogenous SDF-1 with PLGA nanoparticles modulates SDF-1/CXCR4 signaling axis in the rodent cortex. Biomater Sci 5:1640–1651. https://doi.org/10.1039/C7BM00489C

128. Cao X, Shoichet MS (1999) Delivering neuroactive molecules from biodegradable microspheres for application in central nervous system disorders. Biomaterials 20:329–339

129. Khaing ZZ, Agrawal NK, Park JH, et al (2016) Localized and sustained release of brain-derived neurotrophic factor from injectable hydrogel/microparticle composites fosters spinal learning after spinal cord injury. J Mater Chem B 4:7560–7571. https://doi.org/10.1039/C6TB01602B

130. Baumann MD, Kang CE, Tator CH, Shoichet MS (2010) Intrathecal delivery of a polymeric nanocomposite hydrogel after spinal cord injury. Biomaterials 31:7631–7639. https://doi.org/10.1016/j.biomaterials.2010.07.004

131. Huang Y-C, Liu T-J (2012) Mobilization of mesenchymal stem cells by stromal cell-derived factor-1 released from chitosan/tripolyphosphate/fucoidan nanoparticles. Acta Biomater 8:1048–1056. https://doi.org/10.1016/j.actbio.2011.12.009

132. Popova T, Teunis A, Magni R, et al (2015) Chemokine-Releasing Nanoparticles for Manipulation of the Lymph Node Microenvironment. Nanomaterials 5:298–320. https://doi.org/10.3390/nano5010298

133. Pakulska MM, Tator CH, Shoichet MS (2017) Local delivery of chondroitinase ABC with or without stromal cell-derived factor 1α promotes functional repair in the injured rat spinal cord. Biomaterials 134:13–21. https://doi.org/10.1016/j.biomaterials.2017.04.016

134. Vulic K, Shoichet MS (2014) Affinity-Based Drug Delivery Systems for Tissue Repair and Regeneration. Biomacromolecules 15:3867–3880. https://doi.org/10.1021/bm501084u

135. Skaat H, Ziv-Polat O, Shahar A, Margel S (2011) Enhancement of the Growth and Differentiation of Nasal Olfactory Mucosa Cells by the Conjugation of Growth Factors to Functional Nanoparticles. Bioconjug Chem 22:2600–2610. https://doi.org/10.1021/bc200454k

136. Atterberry PN, Roark TJ, Severt SY, et al (2015) Sustained Delivery of Chemokine CXCL12 from Chemically Modified Silk Hydrogels. Biomacromolecules 16:1582–1589. https://doi.org/10.1021/acs.biomac.5b00144

137. Wang Y, Irvine DJ (2011) Engineering chemoattractant gradients using chemokine-releasing polysaccharide microspheres. Biomaterials 32:4903–4913. https://doi.org/10.1016/j.biomaterials.2011.03.027

138. Gonçalves R, Antunes J, Barbosa M (2012) Mesenchymal stem cell recruitment by stromal derived factor-1-delivery systems based on chitosan/poly(γ-glutamic acid) polyelectrolyte complexes. Eur Cell Mater 23:249–261. https://doi.org/10.22203/eCM.v023a19

139. Thakar D, Dalonneau F, Migliorini E, et al (2017) Binding of the chemokine CXCL12α to its natural extracellular matrix ligand heparan sulfate enables myoblast adhesion and facilitates cell motility. Biomaterials 123:24–38. https://doi.org/10.1016/j.biomaterials.2017.01.022

140. Lee AC, Yu VM, Lowe JB, et al (2003) Controlled release of nerve growth factor enhances sciatic nerve regeneration. Exp Neurol 184:295–303. https://doi.org/10.1016/S0014-4886(03)00258-9

141. Behar TN, Schaffner AE, Tran HT, Barker JL (1994) Correlation of gp140/rk expression and NGF-induced neuroblast chemotaxis in the embryonic rat spinal cord. Brain Res 664:155–166

142. DeLong SA, Moon JJ, West JL (2005) Covalently immobilized gradients of bFGF on hydrogel scaffolds for directed cell migration. Biomaterials 26:3227–3234. https://doi.org/10.1016/j.biomaterials.2004.09.021

143. Wylie RG, Ahsan S, Aizawa Y, et al (2011) Spatially controlled simultaneous patterning of multiple growth factors in three-dimensional hydrogels. Nat Mater 10:799–806. https://doi.org/10.1038/nmat3101

144. Leipzig ND, Wylie RG, Kim H, Shoichet MS (2011) Differentiation of neural stem cells in three-dimensional growth factor-immobilized chitosan hydrogel scaffolds. Biomaterials 32:57–64. https://doi.org/10.1016/j.biomaterials.2010.09.031

145. Benslimane-Ahmim Z, Pereira J, Lokajczyk A, et al (2017) Osteoprotegerin regulates cancer cell migration through SDF-1/CXCR4 axis and promotes tumour development by increasing neovascularization. Cancer Lett 395:11–19. https://doi.org/10.1016/j.canlet.2017.02.032

146. Sun D, Bullock MR, Altememi N, et al (2010) The Effect of Epidermal Growth Factor in the Injured Brain after Trauma in Rats. J Neurotrauma 27:923–938. https://doi.org/10.1089/neu.2009.1209

147. Guaiquil VH, Pan Z, Karagianni N, et al (2014) VEGF-B selectively regenerates injured peripheral neurons and restores sensory and trophic functions. Proc Natl Acad Sci 111:17272–17277. https://doi.org/10.1073/pnas.1407227111

148. Zendedel A, Nobakht M, Bakhtiyari M, et al (2012) Stromal cell-derived factor-1 alpha (SDF-1α) improves neural recovery after spinal cord contusion in rats. Brain Res 1473:214–226. https://doi.org/10.1016/j.brainres.2012.07.037

149. Lian D, He D, Wu J, et al (2016) Exogenous BDNF increases neurogenesis in the hippocampus in experimental Streptococcus pneumoniae meningitis. J Neuroimmunol 294:46–55. https://doi.org/10.1016/j.jneuroim.2016.03.014

150. Fon D, Zhou K, Ercole F, et al (2014) Nanofibrous scaffolds releasing a small molecule BDNF-mimetic for the re-direction of endogenous neuroblast migration in the brain. Biomaterials 35:2692–2712. https://doi.org/10.1016/j.biomaterials.2013.12.016

151. Kim DH, Seo YK, Thambi T, et al (2015) Enhancing neurogenesis and angiogenesis with target delivery of stromal cell derived factor-1α using a dual ionic pH-sensitive copolymer. Biomaterials 61:115–125. https://doi.org/10.1016/j.biomaterials.2015.05.025

152. Dziembowska M, Tham TN, Lau P, et al (2005) A role for CXCR4 signaling in survival and migration of neural and oligodendrocyte precursors. Glia 50:258–269. https://doi.org/10.1002/glia.20170

153. Takeuchi H, Natsume A, Wakabayashi T, et al (2007) Intravenously transplanted human neural stem cells migrate to the injured spinal cord in adult mice in an SDF-1- and HGF-dependent manner. Neurosci Lett 426:69–74. https://doi.org/10.1016/j.neulet.2007.08.048

154. Carbajal KS, Schaumburg C, Strieter R, et al (2010) Migration of engrafted neural stem cells is mediated by CXCL12 signaling through CXCR4 in a viral model of multiple sclerosis. Proc Natl Acad Sci 107:11068–11073. https://doi.org/10.1073/pnas.1006375107

155. Kirkpatrick B, Nguyen L, Kondrikova G, et al (2010) Stability of Human Stromal-Derived Factor-1α (CXCL12α) After Blood Sampling. Ann Clin Lab Sci 40:257–260

156. Gao D, Sun H, Zhu J, et al (2018) CXCL12 induces migration of Schwann cells via p38 MAPK and autocrine of CXCL12 by the CXCR4 receptor. Int J Clin Exp Pathol 11:3119–3125

157. Kang H, Mansel R, Jiang W (2005) Genetic manipulation of stromal cell-derived factor-1 attests the pivotal role of the autocrine SDF-1-CXCR4 pathway in the

aggressiveness of breast cancer cells. Int J Oncol. https://doi.org/10.3892/ijo.26.5.1429

158. Marek R, Caruso M, Rostami A, et al (2008) Magnetic cell sorting: A fast and effective method of concurrent isolation of high purity viable astrocytes and microglia from neonatal mouse brain tissue. J Neurosci Methods 175:108–118. https://doi.org/10.1016/j.jneumeth.2008.08.016

159. Saura J, Tusell JM, Serratosa J (2003) High-yield isolation of murine microglia by mild trypsinization. Glia 44:183–189. https://doi.org/10.1002/glia.10274

160. Pfaffl MW (2001) A new mathematical model for relative quantification in real-time RT–PCR. Nucleic Acids Res 29:e45

161. Shvartsman SY, Wiley HS, Deen WM, Lauffenburger DA (2001) Spatial Range of Autocrine Signaling: Modeling and Computational Analysis. Biophys J 81:1854–1867. https://doi.org/10.1016/S0006-3495(01)75837-7

162. Korsmeyer RW, Gurny R, Doelker E, et al (1983) Mechanisms of solute release from porous hydrophilic polymers. Int J Pharm 15:25–35. https://doi.org/10.1016/0378-5173(83)90064-9

163. Lee K-W, Johnson NR, Gao J, Wang Y (2013) Human progenitor cell recruitment via SDF-1α coacervate-laden PGS vascular grafts. Biomaterials 34:9877–9885. https://doi.org/10.1016/j.biomaterials.2013.08.082

164. Kojima Y, Acar A, Eaton EN, et al Autocrine TGF-β and stromal cell-derived factor-1 (SDF-1) signaling drives the evolution of tumor- promoting mammary stromal myofibroblasts. Med Sci 6

165. Bajetto A, Barbero S, Bonavia R, et al Stromal cell-derived factor-1α induces astrocyte proliferation through the activation of extracellular signal-regulated kinases 1/2 pathway. J Neurochem 77:1226–1236. https://doi.org/10.1046/j.1471-4159.2001.00350.x

166. Bonavia R (2003) Chemokines and their receptors in the CNS: expression of CXCL12/SDF-1 and CXCR4 and their role in astrocyte proliferation. Toxicol Lett 139:181–189. https://doi.org/10.1016/S0378-4274(02)00432-0

167. Mao W, Yi X, Qin J, et al (2020) CXCL12 promotes proliferation of radial glia like cells after traumatic brain injury in rats. Cytokine 125:154771. https://doi.org/10.1016/j.cyto.2019.154771

168. Liu Y, Carson-Walter E, Walter KA (2014) Chemokine Receptor CXCR7 Is a Functional Receptor for CXCL12 in Brain Endothelial Cells. PLoS ONE 9:. https://doi.org/10.1371/journal.pone.0103938

169. Naumann U, Cameroni E, Pruenster M, et al (2010) CXCR7 Functions as a Scavenger for CXCL12 and CXCL11. PLoS ONE 5:. https://doi.org/10.1371/journal.pone.0009175

170. Uto-Konomi A, McKibben B, Wirtz J, et al (2013) CXCR7 agonists inhibit the function of CXCL12 by down-regulation of CXCR4. Biochem Biophys Res Commun 431:772–776. https://doi.org/10.1016/j.bbrc.2013.01.032

171. Signoret N, Oldridge J, Pelchen-Matthews A, et al (1997) Phorbol esters and SDF-1 induce rapid endocytosis and down modulation of the chemokine receptor CXCR4. J Cell Biol 139:651–664

172. Signoret N, Rosenkilde MM, Klasse PJ, et al (1998) Differential regulation of CXCR4 and CCR5 endocytosis. J Cell Sci 111:2819–2830

173. Sigismund S, Algisi V, Nappo G, et al (2013) Threshold-controlled ubiquitination of the EGFR directs receptor fate. EMBO J 32:2140–2157. https://doi.org/10.1038/emboj.2013.149

174. Krieger JR, Ogle ME, McFaline-Figueroa J, et al (2016) Spatially localized recruitment of anti-inflammatory monocytes by SDF-1α-releasing hydrogels enhances microvascular network remodeling. Biomaterials 77:280–290. https://doi.org/10.1016/j.biomaterials.2015.10.045

175. Shen X, Zhang Y, Gu Y, et al (2016) Sequential and sustained release of SDF-1 and BMP-2 from silk fibroin-nanohydroxyapatite scaffold for the enhancement of bone regeneration. Biomaterials 106:205–216. https://doi.org/10.1016/j.biomaterials.2016.08.023

176. Thevenot PT, Nair AM, Shen J, et al (2010) The effect of incorporation of SDF-1α into PLGA scaffolds on stem cell recruitment and the inflammatory response. Biomaterials 31:3997–4008. https://doi.org/10.1016/j.biomaterials.2010.01.144

177. Wang B, Guo Y, Chen X, et al (2018) Nanoparticle-modified chitosan-agarose-gelatin scaffold for sustained release of SDF-1 and BMP-2. Int J Nanomedicine 13:7395–7408. https://doi.org/10.2147/IJN.S180859

178. Jansma AL, Kirkpatrick JP, Hsu AR, et al (2010) NMR Analysis of the Structure, Dynamics, and Unique Oligomerization Properties of the Chemokine CCL27. J Biol Chem 285:14424–14437. https://doi.org/10.1074/jbc.M109.091108

179. Venkatesan S, Rose JJ, Lodge R, et al (2003) Distinct mechanisms of agonist-induced endocytosis for human chemokine receptors CCR5 and CXCR4. Mol Biol Cell 14:3305–3324

180. Ponti G, Obernier K, Guinto C, et al (2013) Cell cycle and lineage progression of neural progenitors in the ventricular-subventricular zones of adult mice. Proc Natl Acad Sci 110:E1045–E1054. https://doi.org/10.1073/pnas.1219563110

181. Faiz M, Sachewsky N, Gascón S, et al (2015) Adult Neural Stem Cells from the Subventricular Zone Give Rise to Reactive Astrocytes in the Cortex after Stroke. Cell Stem Cell 17:624–634. https://doi.org/10.1016/j.stem.2015.08.002

182. Hickey KN, Grassi SM, Caplan MR, Stabenfeldt SE (2020) Stromal Cell-Derived Factor-1a Autocrine/Paracrine Signaling Contributes to Spatiotemporal Gradients in the Brain. Cell Mol Bioeng. https://doi.org/10.1007/s12195-020-00643-y

183. Sun D, Bullock MR, McGinn MJ, et al (2009) Basic fibroblast growth factor-enhanced neurogenesis contributes to cognitive recovery in rats following traumatic brain injury. Exp Neurol 216:56–65. https://doi.org/10.1016/j.expneurol.2008.11.011

184. Kleindienst A, McGinn MJ, Harvey HB, et al (2005) Enhanced Hippocampal Neurogenesis by Intraventricular S100B Infusion Is Associated with Improved Cognitive Recovery after Traumatic Brain Injury. J Neurotrauma 22:645–655. https://doi.org/10.1089/neu.2005.22.645

185. Lu D, Mahmood A, Qu C, et al (2005) Erythropoietin Enhances Neurogenesis and Restores Spatial Memory in Rats after Traumatic Brain Injury. 22:7

186. Yamashita T, Ninomiya M, Acosta PH, et al (2006) Subventricular Zone-Derived Neuroblasts Migrate and Differentiate into Mature Neurons in the Post-Stroke Adult Striatum. J Neurosci 26:6627–6636. https://doi.org/10.1523/JNEUROSCI.0149-06.2006

187. Lai B, Mao XO, Xie L, et al (2008) Electrophysiological neurodifferentiation of subventricular zone-derived precursor cells following stroke. Neurosci Lett 442:305–308. https://doi.org/10.1016/j.neulet.2008.07.032

188. Xu Y, Kim C-S, Saylor DM, Koo D (2017) Polymer degradation and drug delivery in PLGA-based drug-polymer applications: A review of experiments and theories: REVIEW ON BIODEGRADATION AND DRUG DELIVERY FROM PLGA POLYMERS. J Biomed Mater Res B Appl Biomater 105:1692–1716. https://doi.org/10.1002/jbm.b.33648

189. Highley CB, Prestwich GD, Burdick JA (2016) Recent advances in hyaluronic acid hydrogels for biomedical applications. Curr Opin Biotechnol 40:35–40. https://doi.org/10.1016/j.copbio.2016.02.008

190. Foster GA, Headen DM, González-García C, et al (2017) Protease-degradable microgels for protein delivery for vascularization. Biomaterials 113:170–175. https://doi.org/10.1016/j.biomaterials.2016.10.044

191. Vigen M, Ceccarelli J, Putnam AJ (2014) Protease-Sensitive PEG Hydrogels Regulate Vascularization In Vitro and In Vivo. Macromol Biosci 14:1368–1379. https://doi.org/10.1002/mabi.201400161

192. Veldhuizen J, Cutts J, Brafman DA, et al (2020) Engineering anisotropic human stem cell-derived three-dimensional cardiac tissue on-a-chip. Biomaterials 256:120195. https://doi.org/10.1016/j.biomaterials.2020.120195

193. Truong D, Puleo J, Llave A, et al (2016) Breast Cancer Cell Invasion into a Three Dimensional Tumor-Stroma Microenvironment. Sci Rep 6:. https://doi.org/10.1038/srep34094

194. Gramlich WM, Kim IL, Burdick JA (2013) Synthesis and orthogonal photopatterning of hyaluronic acid hydrogels with thiol-norbornene chemistry. Biomaterials 34:9803–9811. https://doi.org/10.1016/j.biomaterials.2013.08.089

195. Azari H, Sharififar S, Rahman M, et al (2011) Establishing Embryonic Mouse Neural Stem Cell Culture Using the Neurosphere Assay. J Vis Exp. https://doi.org/10.3791/2457

196. Dang T-D, Kim YH, Kim HG, Kim GM (2012) Preparation of monodisperse PEG hydrogel microparticles using a microfluidic flow-focusing device. J Ind Eng Chem 18:1308–1313. https://doi.org/10.1016/j.jiec.2012.01.028

197. Lashkaripour A, Rodriguez C, Ortiz L, Densmore D (2019) Performance tuning of microfluidic flow-focusing droplet generators. Lab Chip 19:1041–1053. https://doi.org/10.1039/C8LC01253A

198. Mealy JE, Chung JJ, Jeong H-H, et al (2018) Injectable Granular Hydrogels with Multifunctional Properties for Biomedical Applications. Adv Mater 1705912. https://doi.org/10.1002/adma.201705912

199. Sideris E, Griffin DR, Ding Y, et al (2016) Particle Hydrogels Based on Hyaluronic Acid Building Blocks. ACS Biomater Sci Eng 2:2034–2041. https://doi.org/10.1021/acsbiomaterials.6b00444

200. Chen J, Huang K, Chen Q, et al (2018) Tailor-Making Fluorescent Hyaluronic Acid Microgels via Combining Microfluidics and Photoclick Chemistry for Sustained and Localized Delivery of Herceptin in Tumors. ACS Appl Mater Interfaces 10:3929–3937. https://doi.org/10.1021/acsami.7b15832

201. Chau M, Deveau TC, Song M, et al (2017) Transplantation of iPS cell-derived neural progenitors overexpressing SDF-1α increases regeneration and functional recovery after ischemic stroke. Oncotarget 8:97537–97553. https://doi.org/10.18632/oncotarget.22180

202. Lee S-T, Chu K, Jung K-H, et al (2008) Anti-inflammatory mechanism of intravascular neural stem cell transplantation in haemorrhagic stroke. Brain 131:616–629. https://doi.org/10.1093/brain/awm306

203. Hagan M (2003) Neuroprotection by human neural progenitor cells after experimental contusion in rats. Neurosci Lett. https://doi.org/10.1016/S0304-3940(03)00944-3

204. Bacigaluppi M, Pluchino S, Jametti LP, et al (2009) Delayed post-ischaemic neuroprotection following systemic neural stem cell transplantation involves multiple mechanisms. Brain 132:2239–2251. https://doi.org/10.1093/brain/awp174

205. Obernier K, Alvarez-Buylla A (2019) Neural stem cells: origin, heterogeneity and regulation in the adult mammalian brain. Dev Camb Engl 146:. https://doi.org/10.1242/dev.156059

206. Salman H, Ghosh P, Kernie SG (2004) Subventricular Zone Neural Stem Cells Remodel the Brain following Traumatic Injury in Adult Mice. J Neurotrauma 21:283–292. https://doi.org/10.1089/089771504322972077

207. Zamproni LN, Mundim MTVV, Porcionatto MA (2021) Neurorepair and Regeneration of the Brain: A Decade of Bioscaffolds and Engineered Microtissue. Front Cell Dev Biol 9:649891. https://doi.org/10.3389/fcell.2021.649891

208. Li Y, Chang S, Li W, et al (2018) cxcl12-engineered endothelial progenitor cells enhance neurogenesis and angiogenesis after ischemic brain injury in mice. Stem Cell Res Ther 9:. https://doi.org/10.1186/s13287-018-0865-6

209. Lazarini F, Tham TN, Casanova P, et al (2003) Role of the α-chemokine stromal cell-derived factor (SDF-1) in the developing and mature central nervous system. Glia 42:139–148. https://doi.org/10.1002/glia.10139

210. Guyon A (2014) CXCL12 chemokine and its receptors as major players in the interactions between immune and nervous systems. Front Cell Neurosci 8:. https://doi.org/10.3389/fncel.2014.00065

211. Simon DW, McGeachy M, Bayır H, et al (2017) Neuroinflammation in the Evolution of Secondary Injury, Repair, and Chronic Neurodegeneration after Traumatic Brain Injury. Nat Rev Neurol 13:171–191. https://doi.org/10.1038/nrneurol.2017.13

212. Herzog C, Pons Garcia L, Keatinge M, et al (2019) Rapid clearance of cellular debris by microglia limits secondary neuronal cell death after brain injury in vivo. Development 146:. https://doi.org/10.1242/dev.174698

213. Scherbel U, Raghupathi R, Nakamura M, et al (1999) Differential acute and chronic responses of tumor necrosis factor-deficient mice to experimental brain injury. Proc Natl Acad Sci U S A 96:8721–8726

214. Kumar A, Loane DJ (2012) Neuroinflammation after traumatic brain injury: Opportunities for therapeutic intervention. Brain Behav Immun 26:1191–1201. https://doi.org/10.1016/j.bbi.2012.06.008

215. Wang Z, Zheng Y, Zheng M, et al (2020) Neurogenic Niche Conversion Strategy Induces Migration and Functional Neuronal Differentiation of Neural Precursor Cells Following Brain Injury. Stem Cells Dev 29:235–248. https://doi.org/10.1089/scd.2019.0147

216. Amstad E, Chen X, Eggersdorfer M, et al (2017) Parallelization of microfluidic flow-focusing devices. Phys Rev E 95:. https://doi.org/10.1103/PhysRevE.95.043105

217. Headen DM, García JR, García AJ (2018) Parallel droplet microfluidics for high throughput cell encapsulation and synthetic microgel generation. Microsyst Nanoeng 4:17076. https://doi.org/10.1038/micronano.2017.76

218. Microfluidic studies of pulsatile CXCL12 stimulation on prostate cancer cells - ProQuest. https://www.proquest.com/openview/94a8304f775cffd5bbcf2438e1f2eaef/1?pq-origsite=gscholar&cbl=18750. Accessed 25 Oct 2021

219. Kharkar PM, Rehmann MS, Skeens KM, et al (2016) Thiol–ene click hydrogels for therapeutic delivery. ACS Biomater Sci Eng 2:165–179. https://doi.org/10.1021/acsbiomaterials.5b00420

220. Lin C-C, Ki CS, Shih H (2015) Thiol-norbornene photo-click hydrogels for tissue engineering applications. J Appl Polym Sci 132:. https://doi.org/10.1002/app.41563

221. Jia X, Yeo Y, Clifton RJ, et al (2006) Hyaluronic Acid-Based Microgels and Microgel Networks for Vocal Fold Regeneration. Biomacromolecules 7:3336–3344. https://doi.org/10.1021/bm0604956

222. Holmin S, Almqvist P, Lendahl U, Mathiesen T (1997) Adult nestin-expressing subependymal cells differentiate to astrocytes in response to brain injury. Eur J Neurosci 9:65–75

223. Luo J, Daniels SB, Lennington JB, et al (2006) The aging neurogenic subventricular zone. Aging Cell 5:139–152. https://doi.org/10.1111/j.1474-9726.2006.00197.x

224. Consiglio A, Gritti A, Dolcetta D, et al (2004) Robust in vivo gene transfer into adult mammalian neural stem cells by lentiviral vectors. Proc Natl Acad Sci 101:14835–14840. https://doi.org/10.1073/pnas.0404180101

225. Encinas JM, Vaahtokari A, Enikolopov G (2006) Fluoxetine targets early progenitor cells in the adult brain. Proc Natl Acad Sci U S A 103:8233–8238. https://doi.org/10.1073/pnas.0601992103

APPENDIX A

ANIMAL SUBJECTS

Research involving the use of animals conducted under the auspices of Arizona State University is reviewed by the University Institutional Animal Care & Use Committee (IACUC, approval #17-1593R and #20-1793R), Institutional Biosafety Committee (IBC, approval #20-955), and in compliance with federal regulations.